Spatial and Stochastic Modeling of TrkB Mediated Signaling Pathways Involved in Long Term Potentation in the Dendritic Spine

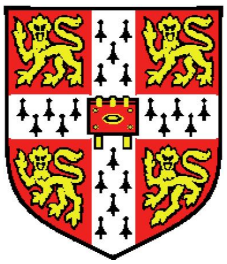

Christine Seeliger
Wolfson College
University of Cambridge

A thesis submitted for the degree of

Doctor of Philosophy

1 January 2014

Spatial and Stochastic Modeling of TrkB Mediated Signaling Pathways Involved in Long Term Potentiation in the Dendritic Spine

- Summary -

Christine Seeliger

Long Term Potentiation (LTP) is thought to be one of the main molecular mechanisms underlying the processes of memory and learning in the brain. One of the most studied mechanisms is the synaptic potentiation mediated by glutamate and its receptors resulting in conductance changes of the post-synaptic membrane. Brain-derived neurotrophic factor and its receptor TrkB, first identified as an important growth factor for neuronal survival and growth, appears to be a crucial modulator of LTP at glutamatergic synapses. The small size of the synapses and their highly structured spatial appearance gives rise to signaling properties that have to be accounted for by using stochastic and spatial simulation methods.

This thesis implements a computational model and its stochastic evaluation to explicitly study the influence of the spatial location of signaling components on the signal output itself as defined by its duration, amplitude and spatial extent. Furthermore, a geometrically accurate model of the spine is developed together with a biochemical representation of the TrkB signaling pathway and its influence on membrane conductance changes. This work focuses on the interactions of the involved kinases and phosphatases and their dynamic behavior in time and space. An extension of the simulation environment Smoldyn is proposed to allow explicit modeling of the molecular behavior based on the membrane environment to account for different submembrane compartments such as the synaptic membrane. The influence of different spatial and biochemical modifications of the TrkB signaling pathways and the different levels of integration down to its influence on membrane receptor trafficking are addressed. The results demonstrate the importance of the spatial layout of the signaling systems for the created signal and the possibilities of fine-tuning it based on spatial properties.

To my family

Elke, Friedrich Wilhelm, Martin and Ulrich Seeliger

Declaration

This dissertation is the result of my own work and includes nothing which is the outcome of work done in collaboration except where specifically indicated in the text.
This thesis does not exceed the specified length limit of 60.000 words as defined by the Biology Degree Committee.
This thesis has been typeset in 12pt font using Latex according to the specifications defined by the Board of Graduate Studies and the Biology Degree Committee.

Acknowledgements

Many thanks to my supervisor Dr. Nicolas LeNovere for the opportunity to work and write my PhD thesis in his lab and my TAC members to join in for the yearly discussion of intermediate results: Dr. Julio Saez-Rodriguez, Dr. Carsten Schulz and Dr. Llewellyn Roderick. Along with this, I'd like to thank all fellow CompNeurians, especially Melanie Stefan, Jean-Baptiste Petit, Lu Li, Michele Mattioni, Benedetta Frida Baldi and Massimo Lai. The shared laughter, flying animals and other lab equipment and sometimes advise and discussions were very valuable especially during the first phases of this journey.

Massive thanks and hugs for keeping me sane during times of intense rowing and work and sharing the odd bowl of midnight porridge every now and then to my flatmates Nenad Bartonicek and Sander Timmer - keeping the Wiggle Mansion Spirit high! The same for my PhD twin and buddy in crime - Benedetta Frida Baldi. Without our endless discussions in the smoking corner from PhD related topics to general life issues, I would have probably tried to run away. Oh... wait... Zagreb was an awesome experience and probably made the otherwise daunting period of writing up and excellent adventure in itself as part of our amazing trio including Nenad.

Thanks to the EBI PreDoc community for pub nights, PhD lunches, trips and all things social and in general being an awesome bunch as much as all the people I have rowed with during my time in Cambridge as a member of Wolfson College Boatclub (WCBC) and Cambridge University Women's Boatclub (CUWBC). Special thanks to the Friends of WCBC and Wolfson College for supporting my rowing ventures also financially and welcoming me back to college rowing every year for May Bumps.

Kudos to all my proofreaders Nenad Bartonicek, Melanie Stefan, Michele Mattioni, Benedetta Frida Baldi, Dr. Nicolas LeNovere and John Coadwell that spend time reading this manuscript and provided valuable feedback on structure, figures, legends and last but not least the English language. Special

thanks to Nenad Bartonicek for being the only person except for John who made it through the entire manuscript and providing additional supervision along the way.
However, without the support of my family at home I would have never made it. My eternal gratitude and love is with them and most of all my parents Elke and Friedrich Wilhelm that stood by my side especially during the hard, non-PhD related events during my early months in Cambridge, always supporting my decisions and wanting the best for me and my life.

Contents

List of Figures

List of Tables

List of Symbols

AC	Adenyl Cyclase
AMPAR	α-amino-3-hydroxy-5-methyl-isoxazolepropionic receptor
AP	Action Potential
AP-1	Activator Protein 1 - transcription factor
BDNF	Brain-derived neurotrophic factor
C/EBP	CCAAT/Enhancer-Binding-Protein - transcription factor
CaMKII	Ca2+ /calmodulin-dependent protein kinase II
CME	Chemical Master Equation
CNS	Central Nervous System
Copasi	The COmplex PAthway SImulator
CREB	cAMP response element-binding protein - transcription factor
CSR	Complete Spatial Randomness
DAG	Diacylgycerol
DAGK	Diacylglycerol Kinase
EGF	Epidermal Growth Factor

EPSP	Excitatory Postsynaptic Potential
Fyn	Tyrosinekinase
GluR1-4	AMPAR subunits
GPI	Glycosylphosphatidylinositol
IP3	Inositol-1,4,5-triphosphat
IP3R	IP3 Receptor
LTD	Long Term Depression
LTP	Long Term Potentiation
MAL	Mass action law
MAPK	Mitogen-activated protein kinase
MCA	Metabolic Control Analysis
NGF	Nerve growth factor
NMDAR	N-methyl-D-aspartate receptor
NR1/2	NMDAR subunits
NT-3/4	Neurotrophin-3/4
ODE	Ordinary Differential Equation
PA	Phosphatidic Acid
PCF	Pair correlation function
PDE	Partial Differential Equation
PH domain	Pleckstrin homology domain
PI3K	Phosphatidylinositol-3-kinase
PIP2	Phosphatidylinositol-4,5-diphosphat

PIP3	Phosphatidylinositol (3,4,5)-triphosphate
PKB	Proteinkinase B - Akt
PKC	Proteinkinase C
PLC	Phospholipase C
PNS	Peripheral Nervous System
PSD	Post Synaptic Density
PSD95	Postsynaptic Density Protein 95 - PSD Scaffold Protein
SBML	Systems Biology Markup Language
SER	Smooth Endoplasmic Reticulum
SER	Smooth Endoplasmic Reticulum
Smoldyn	Spatial and stochastic single molecule simulator
Stargazin	PSD Scaffolding Protein
TrkB	Tropomyocin receptor kinase
TRPC	transient receptor potential cation channels
VCell	The Virtual Cell Simulation Environment

1 Introduction

Learning and memory, the acquisition of knowledge and skills and the ability to remember the experienced and learned are some of the most profound and stunning capabilities of the brain. They shape human behavior and define the interactions of humans with themselves and their environment.

The scientific advances in the fields of molecular and cellular biology over the last century greatly improved our knowledge of the brain. It is unlikely that there is a single scientific discipline that did not contribute to the wide field of Neuroscience but we are still far away from understanding how the brain works and how the activities of single cells joined in a complex network are able to create complex behavior, the sensation of consciousness or feelings. In addition, severe illnesses like Alzheimer's or Parkinson's disease and psychological disorders like Schizophrenia or drug addiction have their origin in malfunctions of the brain. Other conditions such as headaches, brain injuries or infections belong to the group of neurological disorders that affect over 1 billion people worldwide creating an immense burden, not only financial but also social (World Health Organization, 2007).

One of the first scientists to deliver a description of the nervous system was the anatomist Andreas Vesalius. He also recognized that sensations are transmitted via nerves that are connected to the brain and not to the heart which was frequently believed in the 15th century (Van Laere, 1993). Other scientists of the time, such as Leonardo DaVinci, studied and contributed to the early understanding of brain anatomy (Pevsner, 2002).

It was not until the late 19th century with the invention of Golgi staining by

Camillo Golgi that the cellular nature of the nervous system was discovered (Fuxe et al., 2007). Figure 1 shows examples of the early work done by Ramon y Cajal. It shows micrographs of a mouse hippocampal preparation (top) and dendritic spines (bottom) and Cajals illustration of them.

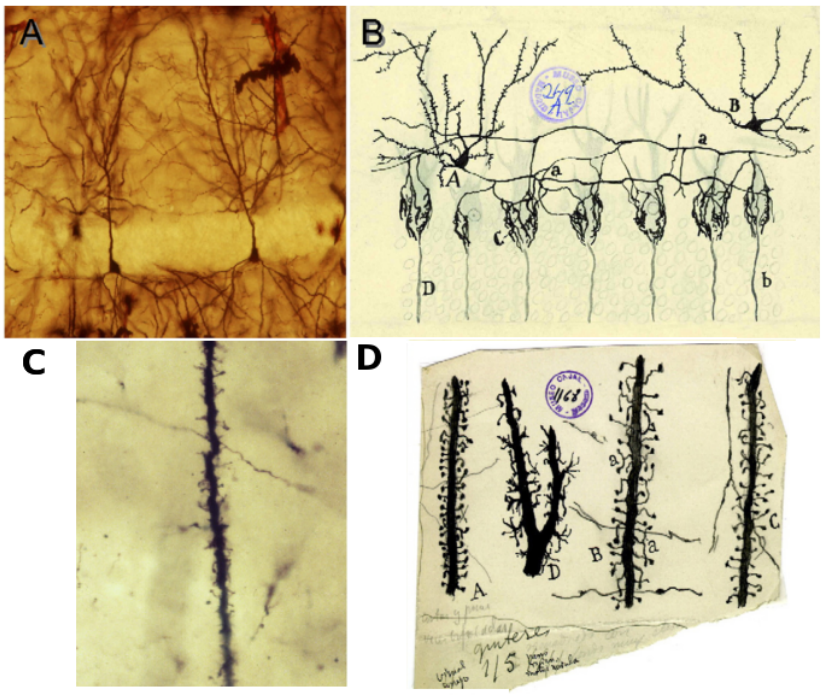

Figure 1: Examples of early micrographs showing the cellular nature of the nervous system and dendritic spines
Ramon y Cayal and Camillo Golgi were awarded the Nobel Prize in 1906 for their work on the nervous system.
a) A micrograph of a mouse hippocampal preparation done by Fuxe et al. (2007) using Golgi's staining method.
b) Reproduction of an original drawing done by Cayal illustrates a transverse section of cerebellar lamellae. The cellular structure is clearly visible.
c) A photomicrograph of an original preparation showing dendritic spines done by Cayal and
d) his illustration of them.
All pictures taken from (Fuxe et al., 2007).

About a decade later, Charles Scott Sherrington coined the term synapsis for the connection between two neurons in his work on the "Integrative action of the nervous system" (Sherrington, 1906). The early 20th century was characterized by the discovery of the biochemical nature of neurotransmission and the identification of chemical neurotransmitters such as noradrenaline and acetylcholine. Henry Hallet Dale and Otto Loewi received the Nobel Prize in 1936 for their major work on the chemical transmission of nerve impulses.
From then on, technological advances in experimental and imaging techniques drove the neurobiological discoveries shaping the picture of how the brain functions and the molecular theories about learning and memory that we have today (see López-Muñoz and Alamo (2009) for a comprehensive review).
The following section of this introduction explains the current molecular theory that is thought to underlie the processes of learning and memory. The key players are described in more detail and the usage of computational models to study signaling pathways is motivated to gain further insights into the complex interplay of the biochemical signaling pathways involved. Finally, the choice of computational modeling paradigms used in this thesis is argued.

1 The molecular basis of learning and memory

The brain is a complex network of interconnected and communicating neurons. During the life of an individual, this network is able to acquire, process, and store information. Neurons are the main electrically excitable cell type. They are capable of conducting electric signals in the form of membrane depolarizations called action potentials (AP). Neurons communicate with other neurons through special cell-cell contacts, the synapses. The strength of a synapse, the synaptic weight, can change depending on its activity. This capability of modifying the communication between neurons is called synaptic plasticity. The weight of a synapse can either be reduced causing Long Term Depression (LTD) or increased resulting in Long Term Potentiation (LTP). LTD and LTP are thought to be two of the underlying molecular processes of learning and memory in the brain and depend on the presynaptic signal (Hebb, 1949; Lynch, 2004; Whitlock et al., 2006).
Chemical synapses as opposed to electrical ones transmit signals from one

neuron to another by transforming the action potential arriving at the presynaptic side into a chemical signal that is transmitted to the postsynaptic side. The depolarization of the membrane during an AP mediated by Sodium and Potassium currents (Hodgkin and Huxley, 1952) triggers the release of neurotransmitters into the synaptic cleft. The neurotransmitters bind to receptors on the postsynaptic side and potentially trigger another AP.
One of the most common neurotransmitters at excitatory synapses in the central nervous system of mammals is glutamate (Niciu et al., 2012). It was known for a long time that glutamate is ubiquitously present in the central nervous system (CNS) before its importance in synaptic signal transmission became apparent (Fonnum, 1984). Glutamate binding to its receptors at the postsynaptic side causes the depolarization of the postsynaptic membrane by opening postsynaptic ion channels. This depolarization, the excitatory postsynaptic potential (EPSP), renders the neuron more likely to fire itself. The amplitude of the EPSP is the direct equivalent of synapse strength (Sayer et al., 1990). Subsequently, biochemical signaling pathways are triggered and eventually gene transcription is altered in addition to the changes in the permeability of the postsynaptic membrane. These alterations are able to modify the amplitude of future EPSPs resulting in potentiation of the synapse (Niciu et al., 2012).
In the following sections, the glutamatergic synapse is described in more detail as well as the molecular processes thought to be involved in short- and long term changes of synaptic strength.

1.1 The glutamatergic synapse

Glutamatergic synapses are composed of an axonal presynaptic and a postsynaptic terminal (see figure 2).

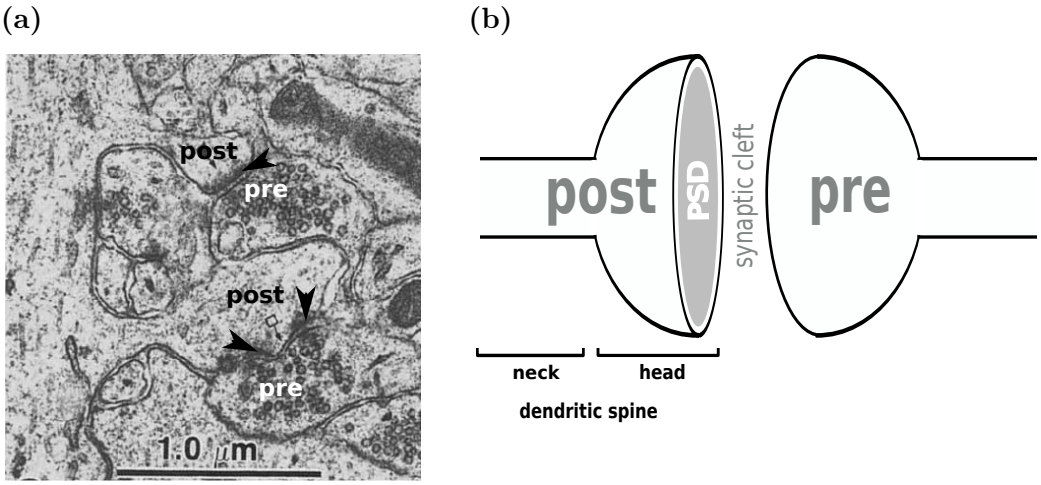

Figure 2: The morphology of the neuronal synapse
This figure illustrates the morphology of a neuronal synapse. a) The image is an electron micrograph of a thin-section showing two adjacent spines, modified from Harris and Landis (1986). The picture shows a smaller spine (upper) with a continuous and a larger one (lower) with a discontinuous postsynaptic density (PSD). The PSDs (arrows) are easily visible as electron dense areas. Post- and presynaptic sides are labeled accordingly.
b) Schematic illustration of a neuronal synapse consisting of a pre- and postsynaptic terminal separated by the synaptic cleft. The postsynaptic density is located on the spine head opposite of the presynaptic terminal.

The postsynaptic sides are located on dendritic protrusions called spines. The pre- and postsynaptic side are separated by a cleft. This section of the introduction focuses on the description of postsynaptic structures and events in accordance with the work presented in this thesis.
Dendritic spines come in different sizes and shapes. Their morphology is usually divided into thin, stubby, and mushroom shaped spines according to Peters and Kaiserman-Abramof (1970). Spines are frequently depicted as mushroom shaped structures but most spines appear to be of intermediate morphology (Spacek and Hartmann, 1983; Harris et al., 1992; Arellano et al., 2007). Spines are exceptionally adapted to their functions as signal receiving and processing side of the synapse. Their morphology is characterized by the correlation between spine head volume and the area of the post synaptic density (PSD) located opposite of the presynaptic terminal on a spines head. Spine neck lengths correspond to their capabilities in isolating the spine

electrically (Araya et al., 2006) and biochemically by creating a diffusion bottleneck (Svoboda et al., 1996; Hugel et al., 2009). These findings underline the importance of spines and the relation between their morphology and their regulatory function in postsynaptic signal transmission.

The PSD was first characterized as a visible electron dense area in electron micrographs (Gray, 1959) (see figure 2a). Its position opposite of the presynaptic neurotransmitter release site suggests an important role in signal transmission at the synapse. It is composed of structural scaffold elements and contains the key players in synaptic transmission and the molecular processes of plasticity. (Cheng et al., 2006; Bayés et al., 2011).

Two of those key players in synaptic transmission in the spine are the ionotropic glutamate receptors α-amino-3-hydroxy-5-methyl-isoxazolepropionic receptor (AMPAR) and N-methyl-D-aspartate receptor (NMDAR) .

AMPARs are cation channels permeable to Sodium and Potassium. Some AMPAR are permeable to Calcium as well depending on their subunit composition (Liu and Zukin, 2007). AMPARs consist of four subunits usually organized as a dimer of dimers (Rosenmund, 1998; Mansour et al., 2001; Sobolevsky et al., 2009). There are four different types of subunits (GluR1-GluR4) and those different subunits give different properties to the receptor such as its trafficking (Shi et al., 2001) and gating behavior (Sommer et al., 1991). The composition itself varies with developmental stage and depends on the area of the brain (Catania et al., 1995) as well as their location within the synapse (Bernard et al., 1997). GluR1/GluR2 are the major AMPAR heteromers found in the hippocampus (Lu et al., 2009).

The cationic NMDAR receptors are tetrameric structures as well. They are composed of two NR1 subunits and two NR2 subunits. The NR2 subunits are expressed based on the tissue (Watanabe et al., 1994) and developmental stage (Watanabe et al., 1992) and have the glutamate ligand binding site. NMDAR receptors are permeable to Calcium, Sodium and Potassium and their channel is blocked by Magnesium ions at resting potential. The depolarization due to the opening of AMPAR after glutamate binding causes the release of the Magnesium block. This allows the NMDAR to open as well and contribute to the depolarization of the spine. This way, NMDAR receptors couple the detection of depolarization with presynaptic glutamate release. In addition,

the Calcium influx through NMDAR contributes as second messenger to the signaling pathways that are involved in synaptic plasticity (see figure 3).

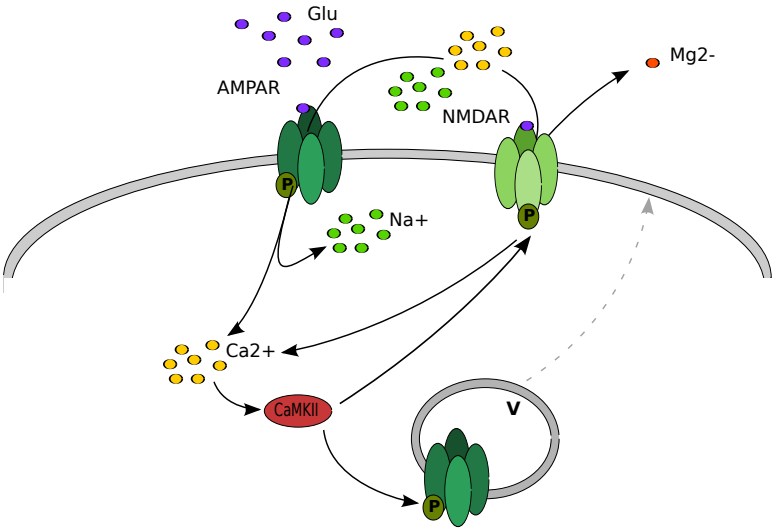

Figure 3: Synaptic transmission and NMDAR dependent Long Term Potentiation This scheme illustrates the main processes during synaptic transmission and long term potentiation
Glutamate (purple) binds to its receptors (green) on the postsynaptic side upon its release into the synaptic cleft. The opening of AMPAR (dark green) causes the depolarization of the postsynaptic membrane as a result of the ionic currents (primarily Sodium). The depolarization releases the Magnesium (orange) block of NMDAR (light green) and NMDAR mediated currents in addition to the AMPAR ones. Biochemical alterations triggered by activated signaling pathways, for example the activation of the kinase CaMKII (red), trigger changes that are able to increase the responsiveness of the synapse to further stimulation. This process is called potentiation.

1.2 Synaptic plasticity

Synaptic plasticity, the alteration of the efficiency with which a signal is transmitted over a synapse, changes the connectivity of neurons. Transmission can either be enhanced or weakened depending on the presynaptic activity resulting in potentiation or depression. The outcome depends on the pattern, the frequency, and the strength of stimulation (Hebb, 1949; Citri and Malenka, 2008). The processes are divided into short-term and long-term

plasticity depending on their duration. Short-term processes are lasting for a maximum of seconds (Zucker and Regehr, 2002). They are frequently related to the transiently facilitated release (potentiation) or depletion (depression) of transmitters on the presynaptic side (Zucker and Regehr, 2002). Long-term processes on the other hand can last up to hours. While LTP is mainly a postsynaptic process, retrograde signaling mechanisms and presynaptic involvement in LTP are under discussion (Yang and Calakos, 2013). LTP occurs in various forms throughout the brain however, most knowledge and evidence today comes from studies on the hippocampal Schaffer collateral-CA1 synapses and is NMDAR dependent (Szirmai et al., 2012).

The electrical manifestation of long-term potentiation (LTP) as enhanced excitatory postsynaptic potential of neuronal groups in response to presynaptic activity was first described by Lomo (1966) and Bliss and Lomo (1973). The molecular players of LTP induction such as NMDAR (Collingridge et al., 1983; Bliss and Collingridge, 1993) and the critical influx of Calcium ions (Lynch et al., 1983; Malenka et al., 1988) were subsequently identified. However, the direct evidence that LTP is specific at the single spine level was demonstrated much later (Matsuzaki et al., 2004; Zhang et al., 2008).

The triggered LTP signaling pathways modulate AMPAR activity and change their trafficking behavior. More AMPARs are inserted into the PSD as a result (Derkach et al., 2007) therefore contributing to the increased glutamate sensitivity of the postsynaptic side (see figure 4).

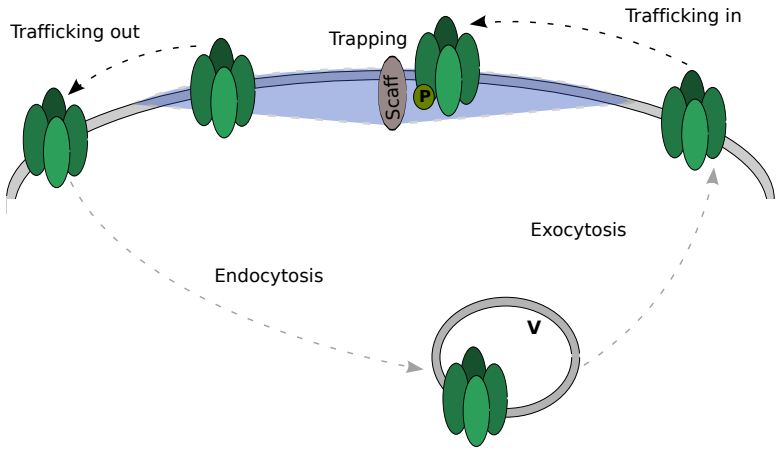

Figure 4: AMPAR trafficking at the postsynaptic side
AMPAR (green) trafficking at the postsynaptic side is characterized by three main processes: Endo/exocytosis of new receptors, diffusion into and out of the synaptic membrane at the PSD (blue), and the trapping of AMPAR at the PSD by scaffold binding.

AMPARs appear to be recruited mainly from existing perisynaptic pools (Patterson et al., 2010) during the early stage of LTP (E-LTP). Later phases of LTP (L-LTP) show changes in protein synthesis and gene expression that goes along with morphological changes such as an increase in spine size, spine numbers, and increased exocytosis of AMPAR (Makino and Malinow, 2009). Crucial transcription factors like CREB , C/EBP or AP-1 where shown to be activated during the course of LTP.
An important mediator between the Calcium influx and the observed changes in AMPAR distribution is the dodecameric enzyme Ca2+ /calmodulin-dependent protein kinase II (CaMKII) that is activated upon LTP induction. Its increased activity and autophosphorylation are observed during LTP induction (Fukunaga et al., 1993; Fukunaga et al., 1995). An inhibition of CaMKII (Otmakhov et al., 1997) as well as mutations (Silva et al., 1992) lead to LTP deficiency. Calmodulin, a CaMKII cofactor, is one of the fastest Calcium buffering molecules in the spine (Faas et al., 2011). Activated CaMKII translocates to the PSD facilitated by its binding to other molecules present in the PSD, most notably the NR2B subunit of NMDAR receptors (Leonard et al., 1999; Strack, 1998). This recruitment to the synapse facilitates the

phosphorylation of the AMPAR subunit GluR1 by CaMKII (Roche et al., 1996; Barria et al., 1997; Lu et al., 2010). The main effect of these phosphorylations appear to be an increase in AMPAR conductance. Phosphorylation of the scaffolding proteins Stargazin and PSD95 are involved in trapping AMPAR at the PSD (Tsui and Malenka, 2006). NMDAR receptors themselves appear to have a role as binding scaffold for CaMKII and position the kinase at a key location to exert its role in LTP via AMPAR conductance changes and anchoring of AMPAR at the synapse. These early events depend strongly on CaMKII activity, this is less clear for LTP maintenance (Chen et al., 2001; Sanhueza et al., 2007).
Other kinases and pathways as well as receptors appear to be involved in LTP. One of them, the tropomyosin-related kinase B (TrkB) and its ligand brain-derived neurotrophic factor (BDNF) is described in the following section.

1.3 Growth factor signaling in long term potentiation

Brain-derived neurotrophic factor (BDNF) was discovered in the 1980s as a neuronal growth factor for the survival and fibre growth of chick sensory neurons (Barde et al., 1982). The cloning of the molecule by Leibrock et al. (1989) and the discovery of its receptor tropomyosin-related kinase B (TrkB) (Klein et al., 1989; Klein et al., 1991) paved the way for the in-depth study of the growth factor and its induced signaling pathways. The Trk family of receptors itself consists of three receptor tyrosine kinases TrkA, TrkB and TrkC. They bind the neurotrophins nerve growth factor (NGF) , neurotrophin-3/4 (NT-3/4) , and BDNF with different affinities. TrkB, the main receptor for BDNF (Squinto et al., 1991), is expressed throughout the central and peripheral nervous system (CNS and PNS) (Zhou et al., 1993; Pruunsild et al., 2007). TrkB also binds to NT-3 but with lower affinity. TrkB's binding of neurotrophins is mediated by a leucine-rich repeat motif (Windisch et al., 1995).
Levine et al. (1995) were amongst the first who observed and studied an increase of synaptic transmission in hippocampal neurones after treatment with BDNF. This increase was manifested in the spontaneous firing rate and the amplitude of postsynpatic currents. The higher frequency was of

presynaptic origin while the change in amplitude of the postsynaptic currents was due to a postsynaptic signaling cascade triggered by the tyrosine kinase TrkB (Li et al., 1998; Levine et al., 1995).
Malfunctioning of the BDNF/TrkB signaling pathway have been associated with a plethora of diseases. The loss of striatal neurons in Parkinson's and Huntingdon's disease is attributed to lack of BDNF in its neuroprotective role (Hyman et al., 1991; Strand et al., 2007). It has been suggested that the early memory dysfunction occurring in Alzheimer's disease is a result of the observed downregulation of BDNF/TrkB expression (Allen et al., 2011). Outside of the CNS, BDNF/TrkB are involved in the control of food intake with implications in obesity usually together with developmental disorders (Yeo et al., 2004; Bariohay et al., 2009).
BDNF is released on the presynaptic side in an activity dependent manner (Balkowiec and Katz, 2000; Balkowiec and Katz, 2002). Its presynaptic effects are positive changes in glutamate release (Li et al., 1998). Presynaptic BDNF release itself depends on both, intra- (Balkowiec and Katz, 2002) and extracellular (Hartmann et al., 2001) Calcium signaling. Especially the observed increase in BDNF induced quantal transmitter release was shown to be dependent on Calcium influx through transient receptor potential cation channels (TRPC) channels (Amaral and Pozzo-Miller, 2007b; Amaral and Pozzo-Miller, 2012).
Inhibition of TrkB signaling on the postsynaptic side by gene knockouts or introduction of non-functional competitors, were shown to impair LTP and learning depending on the type of stimulation (Kang et al., 1997; Minichiello et al., 1999; Saarelainen et al., 2000).
TrkB activates three major canonical pathways: The phospholipase C (PLC) , mitogen-activated protein kinase (MAPK), and phosphatidylinositol-3-kinase (PI3K) pathways (Minichiello, 2009). All pathways seem to be involved in LTP, however the MAPK pathway more towards late-phase and the PLC pathway towards early-LTP (Horwood et al., 2006). PLC catalyses the hydrolysis of Phosphatidylinositol-4,5-biphosphate (PIP2) to Diacylglycerol (DAG) and Inositol-1,4,5-triphosphate (IP3). The latter opens Calcium channels in the Smooth Endoplasmic Reticulum (SER). Calcium and DAG are needed for the activation and recruitment of other important kinases such as members of the

proteinkinase C (PKC) family (Minichiello, 2009). The Calcium influx links TrkB Signaling to the activation of CaMKII and Calmodulin, key players in LTP (Stefan et al., 2008). Changes in intracellular Calcium influence a lot of other nodes in the signaling network, like the IP3 receptor on the SER membrane itself. Furthermore, intracellular Calcium and DAG activate transient receptor potential canonical subfamily channel 3/6 (TRPC) that amplify Calcium transients that are important during spine formation (Li et al., 2005; Amaral and Pozzo-Miller, 2007a). Calcium-induced activation of adenylyl cyclase (AC) is important in spine formation (Ji et al., 2005) and ultimately leads to the activation of cAMP responsive element (CREB) activation and transcription (Nguyen et al., 1994). CREB is also one of the main targets of the induced MAPK cascade (Shaywitz and Greenberg, 1999). Other targets of the MAPK cascade regulate translation, thus making this cascade one of the main regulatory cascades in late phase LTP (Kelleher et al., 2004). Other signaling lipids such as phosphatidic acid (PA), which is produced by diacylglycerol kinase (DAGK) from DAG are implicated especially in morphological changes in the spine (Kim et al., 2009). In addition, PA is known to be an allosteric modifier of PLCγ itself (Jones and Carpenter, 1993).

Signaling through PI3K involves the production of Phosphatidylinositol (3,4,5)-triphosphate (PIP3) and activation of the Akt/PKB signaling pathway. PIP3 itself is important in maintaining the AMPAR distribution in the postsynaptic membrane (Arendt et al., 2010). In general, PIP3 and PIP2 are major regulators of cytoskeleton organisation (Insall and Weiner, 2001). This links TrkB Signaling to morphological changes of the spine happening during LTP and to changes in mechanisms that mediate trafficking of vesicles and proteins within as well as towards active spines.

TrkB also exerts some direct interactions with ion channels with direct influences on the membrane potential. It interacts with the tetrodoxin insensitive Sodium channel $Na_V1.9$ (Blum et al., 2002) and thereby activates Calcium influx through voltage gated Calcium channels. Interactions with the NMDAR receptor presumably via the tyrosine kinase Fyn seem to increase NMDAR opening probability (Kovalchuk et al., 2004).

The integration of major activating signaling pathways of BDNF/TrkB signal-

ing with NMDAR dependent LTP on the postsynaptic side that is the subject of this study is illustrated in figure 5.

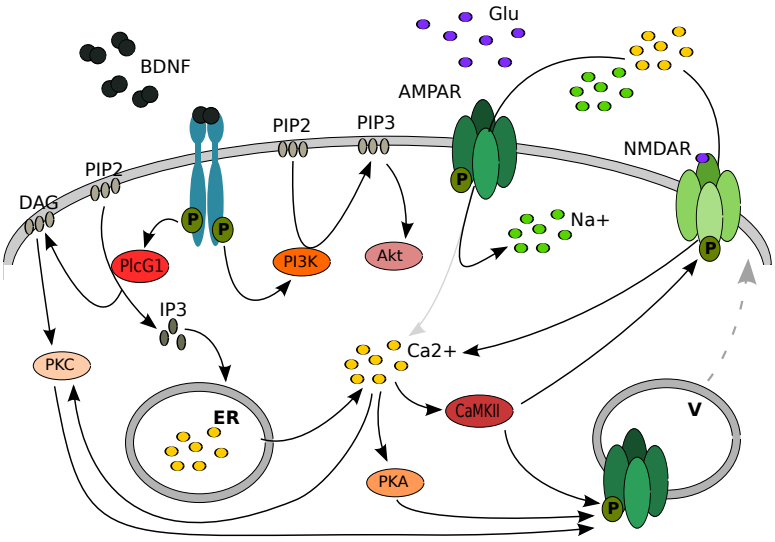

Figure 5: TrkB Receptor Signaling at the postsynaptic site
This figure illustrates the signaling pathways invoked by binding of BDNF(black) to its receptor TrkB(blue) and their integration with NMDAR dependent long term potentiation.
The signaling pathways activated by TrkB signaling result in the production of several small second messengers such as IP3, DAG or PIP3 and Calcium release from internal stores (endoplasmic reticulum, ER). Different downstream kinases such as PKC(pink), PKA(orange) or CaMKII act together to change the trafficking behavior of AMPAR (green) and their conductance resulting in potentiation of the synapse.

The plethora of different possible interactions and modulations that TrkB signaling could exert in the context of long-term plasticity is difficult to grasp with conventional biochemical methods. TrkB signaling happens across several different spatial compartments from small membrane molecules diffusing and signaling in two dimensions to the activation of cytoplasmic kinases that are recruited to the membrane upon activation therefore changing from three dimensional signaling compartments to a two dimensional one. Computational modeling can provide the necessary tools to integrate the available information and address characteristic properties of growth factor signaling

in learning and memory within the explicit context of the dendritic spine. In addition, the spine itself is a structure close to the current resolution limit of microscopic techniques that allow live visualization of molecular movement. Computational modeling can aid the development of hypotheses with regards to likely spatial locations and configurations of molecules involved in signaling. The following section provides an overview over current state-of-the-art modeling techniques and available simulation environments. At the end, the choice of the simulation environment used in this thesis is explained.

2 Computational modeling in biology

Mathematical modeling has a long history in describing and understanding biological systems and their dynamics. Amongst the most famous ones are the models proposed by Lotka (1925) and Volterra (1927) describing the dynamics between predator and prey populations using systems of non-linear differential equations. Interestingly, despite its fame in population dynamics, Lotkas derivation of the model developed from studies on biochemical systems (Lotka, 1909; Lotka, 1920). The late work of Alan Turing, one of the pioneers of computer science, focused on the description and analysis of pattern formation in nature. Turing studied reaction-diffusion systems describing the interactions of "morphogens" in space explaining how a simple reaction diffusion process could give rise to branching in plant structures, gastrulation, or patterns on animal skins (Turing, 1952). Although some of the theories of his work are falsified by now, others such as diffusion-driven instability or the existence of "morphogens" were shown to be true. Turings work demonstrates how the mathematical formulation of a problem guides the development of new theories and hypotheses even before the detailed biology was known possibly making Turing one of the first systems biologists (Maini, 2004).
1952 also saw the publication of one of the major biophysical models in neuroscience: The description of the propagation of action potentials in the giant squid axon by Hodgkin A L and Huxley (1952), again based on non-linear differential equations. Some of the mentioned models and others lead to hypotheses valid after decades and their extensions and further developments are still in use today demonstrating the importance and insights gained from

theoretical systematic descriptions and evaluation of biological systems.
The first computational models explicitly dealing with the biochemical analysis of networks were developed as early as the 1950. An early review by Garfinkel et al. (1970) gives a comprehensive overview of computational studies and the first attempts to develop standartized languages for the use in metabolic pathway analysis such as SAAM (Simulation Analysis And Modeling) (Berman et al., 1962b; Berman et al., 1962a) and the efforts of Garfinkel (1968) Garfinkels software allowed the input of biochemical reactions in the form chemical reaction equations and was able to translate those into differential equations and solve them under the provided initial conditions. Other advances, for example in the field of metabolic control analysis (MCA) paved the way for modeling and computation as valuable tools to understand the behavior of systems as a whole (Westerhoff and Palsson, 2004).
Finally, the vast increase in the amount of available biological data and information in recent years led to an even further increase in the complexity of the models used to describe and analyze biological systems (Ochs, 2010). As of today (2013), BioModels Database (Le Novère et al., 2006) contains almost 500 curated and validated models. Some of the oldest stored biochemical models address the interplay of enzymes in glycolysis and respiration (Chance et al., 1960) and oscillations in biochemical systems (Field, 1974).
The dynamics of systems comprising large numbers of interacting species are difficult to grasp using pen and paper and laboratory experiments are usually focused on a small excerpt of reality. When simple components and their behavior are plugged together, new properties and behavior emerge following the statement: "A system is more than its parts" (Materi and Wishart, 2007; Bakker et al., 2010).
Advances in computing technology today provide powerful means to track a plethora of different species and their interactions and numerically solve (simulate) even extreme complex models. This provides insights into their interactions and the emergence of synergistic dynamic behavior of the system itself with some of the most ambitious projects aiming to simulate entire cells, simple organisms or organs like The Virtual Brain Project (Ritter et al., 2013).
Computational models help to validate or falsify hypotheses. They can high-

light important gaps in the current knowledge of the studied systems and advise experiments to fill those. Model predictions can lead to the development of new hypotheses and guide experimental approaches to verify them in turn. This approach can yield real monetary gain by focusing experiments onto certain aspects and by optimizing experimental setups before they are conducted in the more expensive environment of an experimental laboratory. Lastly, computational models allow the experimenter to modify and vary parameters that might (not yet) be accessible in real experimental setups and derive hypotheses concerning their importance, role, and influence (Meier-Schellersheim et al., 2009).
In the past years, several different modeling and simulation approaches were developed that are implemented in different combinations by many available simulation environments for biochemical systems. The following section briefly describes the central properties of principles in common modeling frameworks. Afterwards, a few concrete examples of simulation environments are given that implement different subsets of those principles.

2.1 Different modeling approaches

Many modeling frameworks can fundamentally be differentiated by their inclusion of probability, their treatment of molecular entities, and whether or not space and its influence on the encoded processes is explicitly considered.

2.1.1 Deterministic versus stochastic approaches

The classical definition of a deterministic system is that its future states are determined by the knowledge of the set of states the system was in before. From this follows, that a deterministic system will always produce the same output for the same set of initial starting conditions or states. The dynamics of deterministic systems are frequently described as a set of ordinary differential equations (ODEs). In case of biochemical reaction networks, these equations encapsulate the development of molecular concentrations over time. The examples given in the previous section are deterministic descriptions of biological processes including many of the models deposited in the online model repository BioModels Database (Le Novère et al., 2006).

Although all of these models have been proven to provide valuable insights into the behavior of systems, the underlying assumption that molecular species in large numbers are evenly distributed in space and well mixed is frequently not true in biological reality (Halling, 1989). Low molecule numbers, spatial heterogeneity and the property of biochemical reactions being discrete events in time and space give rise to stochastic effects that cannot be accounted for in ODE based modeling frameworks (Rao et al., 2002). Although noise and random behavior appears to be an effect bound to be minimized in biological systems, it is in fact frequently found as an important component. Gene expression noise provides means for populations to react to their environment (Wolf et al., 2005; Fraser and Kaern, 2009) and stochastic noise in biochemical reaction networks can have beneficial effects such as the enhancement of sensitivity of intracellular regulation (Paulsson et al., 2000) or by simplifying biochemical networks needed for complex responses (Govern and Chakraborty, 2013). Thus, stochastic behavior provides means of evolution and flexibility and can be considered as one of the main characteristics of signaling networks (Shahrezaei and Swain, 2008).

A famous stochastic process studied in the literature is the switch of the bacteriophage λ between the lytic and lysogenic stage (Arkin et al., 1998). This stochastic switch enables a population of bacteriophages to show different phenotypes across a population even if the individuals are genetically identical. The Gillespie Algorithm (Gillespie, 1977) applied in that study is frequently used to describe and analyze stochastic systems. One simulation run of Gillespie's Algorithm reproduces a realization of the Chemical Master Equation (CME). The CME is a differential equation describing states of a system and the transition probabilities from one state to another. The systems states are described by discrete molecular numbers. The probabilities are deducible from macroscopic rate constants. However, the CME state space explodes exponentially with the number of involved reacting species and renders the CME itself very difficult to solve directly. Gillespie's Algorithm generates one path through the CME state space by determining the amount of time that passes until the next reaction happens and which reaction that is. The result is an accurate representation of the CME if simulations are performed. (Andrews, 2009). Although the usage of the CME and Gillespie account for

the stochastic nature of processes, they are still based on the description of spatially homogeneous pools of molecules.

2.1.2 Single compartment versus spatial approaches

As stated before, the assumption that molecules are evenly distributed in space and present in large numbers does not stand for many realistic biological problems. The well-mixed reactor assumption essentially resembles the situation found in common laboratory test-tube experiments.
Live cellular systems on the contrary are characterized by well defined and structured signaling compartments separated by membranes. Organizational elements such as scaffolds or lipid domains within membranes and the formation of macromolecular complexes creates such a diversified spatial and special environment even within compartments that the well-mixed reactor assumption fails to represent accurately. Moreover, the influence of spatial structure on signaling outcomes cannot be neglected. Molecular complexes, scaffolds and compartments increase local concentrations of molecules and reduce the amount of copy numbers needed for efficient signaling, they enhance the specificity of signaling pathways by preventing unwanted interactions and they increase the likelihood for the wanted interactions to happen (Round et al., 2005; Shaw and Filbert, 2009).
Multi-compartmental models are the first step towards a more diversified representation of spatial heterogeneity. Each compartment that is considered in the model contains its own representation of a signaling network consisting of molecular pools and a set of reactions. The latter can be described using a deterministic or stochastic framework as described before. Compartments do not necessarily correspond to cellular compartments but can represent any segregation of space. Modeling of membrane environments for example can be accomplished by representing the membrane as a compartment in its own right within this framework. The compartmental approach requires explicit modeling of transport processes between compartments to allow certain molecules to cross between them. In addition, molecular pools within each compartment are still assumed to be continuous and well-mixed. This could potentially result in a shift of the associated problem to even smaller subelements of the model where molecular quantities are likely to be even

smaller and stochastic effects and the discreteness of signaling events are even more important.

Developing the multi-compartmental approach further allows the modeler to address more detailed properties of heterogeneous space. The reaction diffusion master equation for example separates space into finite small subvolumes (F. Baras, 1997). Diffusion is assumed to be fast enough to homogenize molecular populations within each of these subvolumes. Reactions depend on the molecular concentration in each subvolume and diffusion is modeled by "jump" first order reactions from one subvolume into the next (Hattne et al., 2005a). Similar to the CME, the amount of different states a model can be in increases exponentially with the amount of molecular species involved requiring Monte Carlo based sampling methods to approximate the solution (Elf and Ehrenberg, 2004).

Partial differential equations (PDEs) can be used to describe the dependence of a systems state not only with regards to time but also space. Within the context of biology, the term reaction-diffusion systems is frequently used as for example in case of the pattern studies conducted by Turing mentioned earlier. Under certain circumstances, PDE systems can be solved analytically providing the means of a detailed analysis of the modeled system. In most cases however, similar to ODEs, numerical integration is needed to approximate the solution and implementations exists for common mathematical software environments such as MatLab or Octave. PDEs are in the same way as ODEs deterministic descriptions of systems. Stochastic effects due to small reaction volumes, low molecule numbers and the discrete nature of biochemical reactions cannot be considered.

Analysis of whole cell proteomes suggests that especially proteins conducting posttranslational modifications such as glycosylation or phosphorylations which are mostly involved in signal transduction, regulation, and cell communication are present in very low copy numbers even in whole cells (Beck et al., 2011). It is no surprise that especially small, highly structured, and specialized organelles like the dendritic spine are characterized by extremely low numbers of important regulators. Estimates for the number of NMDAR receptors in the PSD yield values of between 1-10 molecules per PSD complex while numbers for AMPAR and scaffolding proteins are around 10 - 20

times higher (Sugiyama et al., 2005; Shinohara, 2012). Considering this, it is reasonable to move the focus from a population centered view to one where particles are explicitly represented. In this framework, reactions are treated as events happening to molecules upon encountering other elements instead of modifying abundances of molecular pools in dependence of each other.
Single-particle methods use an explicit representation of space that can be either continuous or discrete. A molecule has a distinct position within this space at each time step. Explicit modeling of movement in space can aid the understanding of effects such as molecular crowding, confinement, and increased local concentrations on signaling properties (Zhou et al., 2008). Movement is usually assumed to follow a random walk and single molecule trajectories in time and space are simulated using Brownian dynamics algorithms (Andrews and Bray, 2004).

2.2 Examples of different simulation environments

The amount of different software packages implementing different types of modeling frameworks and simulation methods is growing. However, some simulators are more widely used than others and are a standard within their application domain. Three major simulators are briefly described in the following that implement a certain subset of the modeling paradigms discussed above. All of them have been applied to a range of modeling problems in the literature and have an established user community.

2.2.1 The COmplex PAthway SImulator - COPASI

Copasi is a comprehensive modeling and simulation environment (Hoops et al., 2006). It comes with a graphical user interface (GUI) that allows easy editing and development of biochemical models. Routines for plotting of results and exporting models into standardized formats such as the Systems Biology Markup Language (SBML) are implemented. A useful set of methods for parameter estimation, optimization, and model analysis such as time course experiments are available. Copasis strength is its flexibility in the definition of ODE based models in addition to its useful set of tools and its ease of use. Users can define virtually any equation to represent the desired

kinetics. Copasi implements different algorithms to simulate pathway models. It implements a deterministic and a stochastic solver. If stochastic simulation is required, Copasi provides routines to help with the conversion of the models into mass action law based ones. A deterministic stochastic hybrid simulation method allows speed optimized simulation. Copasi decides based on particle numbers in the system which parts have to be simulated stochastically and which ones can be solved using numeric ODE integration. Copasi is capable of simulating multi-compartmental models to account for spatially segregated reaction containers. It does not provide methods for the simulation of real spatial properties within a realistic three-dimensional model geometry. Copasi has been used for example to model the biochemical module of transforming growth factor signaling and expression in the context of the human epidermis (Adra et al., 2010). Copasi is also frequently found as the validation simulator of choice for models that are deposited in BioModels Database (Le Novère et al., 2006).

2.2.2 The Virtual Cell - VCell

VCell is a client-based simulation environment (Moraru et al., 2008; Resasco et al., 2008). Users download the graphical user interface instead of providing the entire program. This GUI allows the definition and analysis of models. The analysis and simulations themselves are submitted to a computing center based at the University of Connecticut. Similar to Copasi, VCell provides routines to import and export models from and into common standards and databases. The main simulation framework and strength of VCell is the modeling and simulation of PDE based models. VCell provides tools to import and design three-dimensional realistic geometries based on microscopy data. In addition to its PDE solvers, VCell implements standard ODE solvers and a stochastic simulation frameworks. However, if those are used, the models are reduced to non-spatial ones. In recent versions, VCell adopts methods from other simulators to increase its repertoire such as Copasis parameter estimation and the algorithms of Smoldyn as spatial and stochastic solver. Studies using the VCell environment include phosophoinositide turnover (Xu et al., 2003) and combined biochemical and electrophysiological models of Purkinje neurons (Brown et al., 2011).

2.2.3 Smoldyn

Smoldyn is a simulation environment that models single point-like molecules with their trajectories in time and space (Andrews and Bray, 2004; Andrews et al., 2010). Stochastic behavior arises due to representation of molecular movement as Brownian motion and the evaluation of molecular interactions and molecule - surface interactions based on probabilities. Smoldyn allows the construction of arbitrary three-dimensional surface geometries. Molecules can be attached to these surfaces or interact in various ways with them. The only visual output Smoldyn provides is a representation of the currently running simulation. Models are implemented in a Smoldyn specific configuration file format. The different output formats of Smoldyn allow the tracking of molecule numbers and positions over time and in different spatial locations and compartments. The lack of tools for model development suggests that a combination of Smoldyn with other tools such as the simulators described before is a good choice to aid model development. However, this limitation is common between different stochastic spatial simulation environments. Common mathematical and statistical tools such as the statistical scripting language R are necessary to evaluate the outcome of simulations.
Smoldyn was successfully used to study biological phenomena such as bacterial chemotaxis and the distribution and diffusion of the involved proteins (Lipkow, 2006; Lipkow and Odde, 2008), spatiotemporal segregation of CaMKII in dendritic spines (Khan et al., 2011; Khan et al., 2012).

Other spatial stochastic simulation environments were considered at the beginning of this project in addition to Smoldyn. Some of them were excluded due to their lack of support for diffusion and reactions in two and three dimensions such as StochSim (Morton-Firth and Bray, 1998) and STEPS (Wils and De Schutter, 2009). StochSim supported spatial modeling but only in two dimensions, while STEPS, although developed with molecular neurobiology in mind, did not support membrane diffusion of molecules.
Another lattice/subvolume based simulation environment similar to STEPS is MesoRD (Hattne et al., 2005b). MesoRDs method was not designed to implement diffusion and reactions on surfaces. More recent versions of MesoRD are capable of reducing subvolumes to about molecular reaction radii which

enables the user to implement surfaces as compartments (Fange et al., 2010). However, the usage of constructive solid geometries to define a systems spatial geometry from very basic volumetric shapes instead of simple planar ones made the definition of more complex geometries such as the dendritic spine difficult.

MCell is another simulator with its origins in neurobiology (Stiles et al., 1996; Kerr et al., 2008). In contrast to the simulators mentioned before, MCell simulates single volumeless particles in continuous space and allows the definition of arbitrary geometries quite similar to Smoldyn. Smoldyn simulations were easier and more intuitive to configure and faster to run in the authors experience. The latter is confirmed by a benchmark test undertaken by Andrews et al. (2010).

Table 1: Characteristic properties of established simulation environments
This table provides a summary of the introduced established simulation environments with regards to the discussed properties of simulation methods, the treatment of molecular entities and the possible inclusion of space.

	simulation	molecular entities	inclusion of space
Copasi	deterministic	continuous	multi-compartment
	stochastic	discrete	multi-compartment
VCell	deterministic	continuous	complex 3D geometries
	stochastic	discrete	multi-compartment
Smoldyn	stochastic	single molecule	complex 3D geometries

2.3 Modeling long-term potentiation in the dendritic spine

An increasing amount of computational studies improved the knowledge of postsynaptic signaling pathways and their role in long-term potentation over the last 10 years. In 2010, more than 117 different models addressing properties of postsynaptic signal transduction were published. Manninen et al. (2010) group them into three categories: The first group consists of models of single signaling pathways. Many of these models focus on the mechanisms of CaMKII and Calmodulin activation. So far, they helped to understand the switch-like behavior of CaMKII (Lisman, 1985) and its importance in

long-term storage of information (Miller et al., 2005). An allosteric model of Calmodlin by Stefan et al. (2008) explains in detail how different Calcium concentrations result in differential activation of CaMKII and Calcineurin causing positive or negative effects on long-term potentiation.
The second group deals with the properties of Calcium signaling addressing a wide range of questions from the influence of the stimulation frequency (Franks et al., 2001; Li et al., 2012) to Calcium compartimentalization in spines (Zador et al., 1990) and the influence of spine geometry on signaling outputs (Volfovsky et al., 1999; Schmidt and Eilers, 2009).
Group three is the most interesting one within the context of this thesis. It contains models of more complex signaling networks to study the integration of signaling pathways involved in potentation at the postsynaptic side.. Most of them are extensions of preexisting models of CaMKII, however newer studies focus more and more on different interactions as well. Bhalla and Iyengar (1999), Bhalla (2002) and Bhalla (2004) address general properties of signaling networks within the context of plasticity. Amongst the signaling pathways that have been addressed so far are those containing MAPK(Smolen et al., 2008; Bhalla, 2002), ERK (Ajay and Bhalla, 2007), PKA (Kötter, 1994) and PKC (Bhalla, 2002), DARP32 (Fernandez et al., 2006) and others. More recent models extend the studies to incorporate protein transcription and translation control to investigate further in the late stages of LTP (Smolen et al., 2008; Aslam et al., 2009; Jain and Bhalla, 2009).
No computation model of postsynaptic TrkB signaling has been proposed so far except for the model by Jain and Bhalla (2009). Their study focuses on the integration of Calcium, BDNF and the MAPK to regulate L-LTP protein synthesis. The model is deterministic and non-spatial. It is structured into different modules. The TrkB module contains the BDNF induced receptor activation and the downstream pathways down to PI3K and PLCγ activation. This module could be useful within the context of this work. It could be utilized as upstream receptor component if it is ported into a spatial and stochastic context.

2.3.1 Choosing a modeling framework for growth factor signaling in the dendritic spine

Some essential key features of signaling events in the dendritic spine determine the choice for a suitable simulation environment.

1. The signaling space of the spine is a highly organized and heterogeneous environment. The examples of AMPAR diffusion and trafficking behavior during LTP give clear examples of the influence of spatial location on the overall behavior of the molecules. Explicit representation of the membrane environment as two-dimensional space, separated into the synaptic membrane associated with the PSD and the extrasynaptic membrane are necessary.

2. Molecular numbers of key signaling elements in the spine are small, estimates for the amount of TrkB receptors within the synaptic membrane yield approximately 10-20 molecules. Kinases and phosphatases are represented in numbers of around 20-30. Stochastic effects are likely to influence the signaling outcome.

3. The possibility of tracking individual molecules in time and space could provide the means of addressing signaling properties arising from molecular distributions as an important parameter of signaling itself. This shifts the focus from an entirely biochemical one towards a more integrated modeling approach putting the otherwise isolated biochemical components back into a realistic context.

Altogether, a spatial and stochastic simulation environment providing the possibility of tracking individual entities is needed. The simulator Smoldyn will be used in this work, due to the required level of details. However, the usage of Smoldyn (V2.16 at the beginning of this project) required the implementation of a software modification to explicitly model different diffusion areas within a membrane environment to explicitly represent the synaptic membrane at the PSD. Copasi and VCell are useful to aid model design and development due to the set of tools they provide as Smoldyn comes without any. The analysis of Smoldyn results requires the development of spatial statistical pipelines to adequately analyze and interpret simulation results on a larger scale.

3 Objectives

This work develops and analyzes a spatial and stochastic computational model of the growth factor BDNF evoked signaling pathways that are modulating long term potentiation responses at glutamatergic synapses. Spatial localization is a key aspect of signaling cascades and the first results chapter demonstrates by means of a less complex sub model how the signal of a small and fast diffusing molecule can be focused to a very restricted area in space, the PSD, over time. Together with this, analysis pipelines and routines are developed to allow the statistical analysis of larger spatial and stochastic simulation datasets produced by Smoldyn.
The second part describes the entire BDNF signaling model and its implementation. The analysis focuses on different levels of signal integration after stimulation with different amounts of BDNF: The competition between PI3K and Plcγ for the same substrate PIP2 and the contribution of two different PKC isoforms on two important AMPAR modifications. These modifications are direct manifestations of LTP on the level of AMPAR since they modulate AMPAR abundance and conductance.
In addition, two modifications of the model address the potential influence of molecular trapping and the results of an inhibitory effect of the PI3K pathway on Plcγ.
The last section describes and validates a modification of Smoldyn that was implemented within this work and used in in the previous chapters. This modification allows to explicitly model different diffusion environments within membranes to simulate diffusive effects, such as trapping of molecules at the PSD.

It's a dangerous business, Frodo, going out your door. You step onto the road, and if you don't keep your feet, there's no knowing where you might be swept off to.

- Bilbo -

2

Significance of the kinase and phosphatase localization on the formation of lipid signaling domains in dendritic spines

1 Introduction

The fluid mosaic model of cell membranes describes them as a layer composed of lipids and proteins that are moving more or less freely and at random. Already by the time the model was proposed by Singer and Nicolson (1972) it was suspected, that membranes are not homogeneous and randomly organized (Siekevitz, 1972). More experiments and confirmations followed, leading to the proposal of lipid domains forming within the membrane (Stier and Sackmann, 1973; Karnovsky et al., 1982). Since then, different models and theories were developed to explain the formation of signaling domains. The lipid raft theory explains the lateral formation of domains by self-associative properties of certain lipids such as cholesterol and sphingolipids. Their organizational properties as signaling platforms are mediated by interactions with trans membrane domains, Glycosylphosphatidylinositol-anchors (GPI-anchors) or acyl-chains of proteins (Simons and Ikonen, 1997; Simons and Sampaio, 2011). Other mechanisms governing lateral membrane structure are interactions with the cytoskeleton (especially actin) and of course other protein-protein interactions (Kusumi et al., 2012).

Together with this development more and more lipids themselves, such as the inositide phospholipids, were discovered to play central roles in signaling path-

ways. Lipid-modifying proteins such as Phosphatidylinositide 3-kinase (PI3K) (Whitman et al., 1988; Stephens et al., 1991) and Phosphatase and Tensin homolog (PTEN) (Maehama, 1998; Myers et al., 1998) and lipid-binding protein domains like the pleckstrin homology (PH) domain (Harlan et al., 1994) and their pathways were discovered as well. Signaling studies moved away from the previously protein centered view of the field.

Today it is accepted that biological membranes show quite distinct spatial organizations and take part in signaling pathways themselves. They form a unique structured signaling compartment in their own right. Examples for the segregation and clustering of signaling elements in distinct regions of this special signaling space are frequently observed:

Spatial segregation of Phosphatidylinositol 4,5-bisphosphate (PIP2) and Phosphatidylinositol (3,4,5)-triphosphate (PIP3) is already observed in unstimulated cells (PC12) as reported by Wang and Richards (2012). However, a lot of signaling processes, especially those involved with cell growth and migration show precisely localized and timed spikes of PIP3 in the membrane. PIP3 micro domains were shown to colocalize with F-actin accumulation in axonal filopodia growth (Ketschek and Gallo, 2010; König et al., 2008). The protruding end of moving cells is associated with PIP3 patches and colocalizes with actin polymerization at the front end of the moving cell (Gerisch et al., 2012). PIP2 might play a role in actin polymerisation as well by permitting the reaction to take place at the plasma membrane, while PIP3 coordinates time and location (Insall and Weiner, 2001). Evidence suggests that PIP3 is also important during LTP to maintain the necessary α-amino-3-hydroxy-5-methyl-4-isoxazolepropionic acid receptor (AMPAR) distribution at the post synaptic density (PSD) in the spine (Arendt et al., 2010) as well as being involved in many signaling pathways related to neuronal outgrowth and survival (Ménager et al., 2004; Kakumoto and Nakata, 2013)

Computational models containing phospholipid messengers in their context of a signaling pathway exist frequently in the context of growth factor receptor signaling pathways (Birtwistle et al., 2007; Borisov et al., 2009). Xu et al. (2003) explicitly studied phosphoinositide turnover in neuroblastoma cells using a compartmental approach (see section 1).

None of these models consider some main characteristics of the plasma mem-

brane as a signaling environment. The plasma membrane is a two dimensional environment, restricting the movement of molecules to the plane instead of a volume. In addition, molecules might move differently or could even be fixed to specific regions to exert their specific function.

1.1 Objectives

A simple "proof of concept" model of a kinase phosphatase system is implemented and analyzed in this chapter. The analysis should provide insights into the variability of a signaling system solely based on its spatial properties when molecule numbers and kinetic properties are fixed. How does the spatial setup influence aspects of the time course of a reaction (such as speed and amplitude of the signal) and its spatial structure (dispersity and accuracy)? This model shows how to focus the quickly diffusing signal of a small molecule to a specific area of the membrane enabling a very localized signal to be established. It highlights how important it is to consider spatial properties in signaling studies. The analysis also provides a set of tools to aid in the analysis of larger subsequent models.

2 Methods

This section provides the background information on the modeling and analysis methods used within this chapter.

2.1 Modeling and simulation

Smoldyn (Andrews and Bray, 2004; Andrews et al., 2010) is a spatial and stochastic single molecule simulation environment. Smoldyn uses a Brownian Dynamics Algorithm (Edelstein and Agmon, 1993) to move molecules represented by points in space. Smoldyn simulates zeroth-order, unimolecular and bimolecular reactions, and requires model reactions to be described according to mass action law (MAL). Reaction probabilities for each molecule at each time step are calculated in case of zeroth order and uni molecular reactions. The outcome of bimolecular reactions is approximated using Smoluchowski's

theory of coagulation (Smoluchowski, 1917). This theory is used to estimate binding radii for the molecules based on their diffusion constants and the reaction rate. The binding radius determines whether or not molecules are close enough to react with each other.
The simulations were run on the European Bioinformatics Institute computing farm using Smoldyn V2.22 [1]. The cluster nodes are 64-bit Intel based cores running under Redhat Linux 6.1 or later. Currently, there is no parallelized version supporting all Smoldyn functionality. Each simulation was run using one core only.

2.2 Modeling reactions and parameters

Smoldyn restricts modeling of chemical reactions to those that are MAL compliant. Catalytic reactions are therefore represented according to the following scheme:

$$S + E \underset{k_{\text{off}}}{\overset{k_{\text{on}}}{\leftrightarrow}} SE \xrightarrow{k_{\text{cat}}} S + P$$

k_{on}, and k_{off} can be estimated from the Michaelis-Menten (MM) parameters k_{cat} and K_{m} according to Bhalla (2000), if only Michaelis-Menten paramters are found in the literature:

$$\begin{aligned} k_{\text{off}} &= 4k_{\text{cat}} \\ k_{\text{on}} &= \frac{k_{\text{off}} + k_{\text{cat}}}{K_{\text{m}}} \end{aligned}$$

All rate parameters were extracted from the public model repository BioModels Database (Le Novère et al., 2006). The actual values of parameters used in this study are given later in section 3.

[1] can be obtained via http://www.smoldyn.org/archive.html

2.3 Geometry and diffusion

The models presented in this chapter contain three spatial dimensions. The modeled reactions take place at an identifiable position in space and the possible locations of the molecules and their diffusive paths are constrained by the surface area of the neuronal spine. Smoldyn provides a collection of shapes such as rectangles, triangles, and spheres that can be used as panels to build the necessary surfaces in space. Triangles are the most common shapes used in computer animations to construct complex surface geometries. Tools, such as Blender[2] or MeshLab[3] can be used to create triangulated surfaces and store them in the generic Wavefront format. Those can be converted into Smoldyn's surface format.
Smoldyn's Brownian Dynamics algorithm uses Fick's second law (Berg, 1993; Andrews and Bray, 2004) to compute a random displacement for each molecule at each time step with the distance determined by the diffusion coefficient D for that molecule. I estimated the diffusion coefficients for my models if they were not available in the literature. The estimates are based on an empirical relation between diffusion coefficients and the molal volume of proteins proposed by Young et al. (1980):

$$D = 8.34 * 10^{-8} * T/(\eta * M^{1/3})$$

The temperature was set to T=310 K and the viscosity of the cytoplasm η to 2.5 mPa s^{-1} (Mastro et al., 1984). The molecular weight M in Dalton was retrieved from UniProt (The UniProt Consortium, 2012).

2.4 Analysis

Smoldyn does not come with integrated methods to analyze simulation outcomes in contrast to some of the popular deterministic simulation environments (e.g. VCell[4], Copasi[5]). However, Smoldyn provides several different raw data output formats. Two different ones are utilized to analyze the simulation

[2] http://www.blender.org
[3] http://meshlab.sourceforge.net/
[4] http://www.nrcam.uchc.edu/
[5] http://www.copasi.org/tiki-view_articles.php

results with regards to two different aspects. The first records the total molecule numbers for each molecular species at each time step. Such a time course is illustrated in figure 6a. The other gives the molecular coordinates for each single molecule currently present in the simulation. This data provides the information needed to analyze spatial properties of the system, such as molecular densities - illustrated in figure 6b.

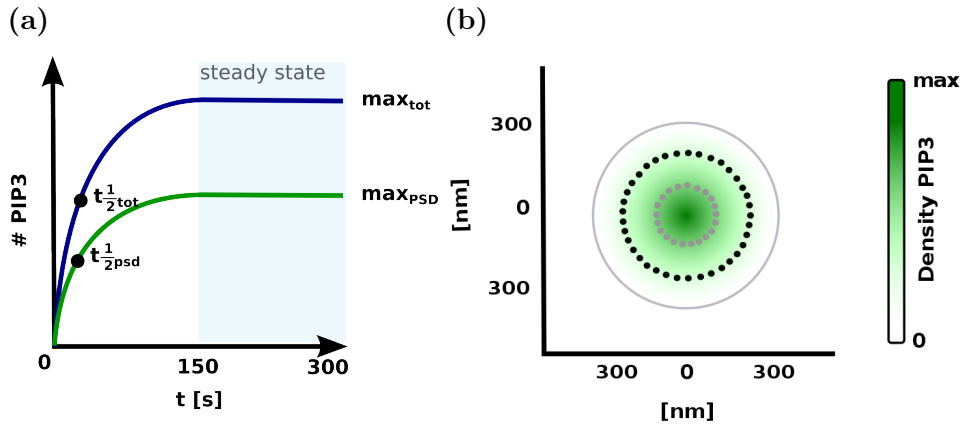

Figure 6: Illustration of different simulation result types
(a) Example of a simulation time course illustrating the PIP3 molecule production during one simulation run on the PSD (green) and overall (blue)
(b) Example of a density plot illustrating the PIP3 distribution at the PSD at a specific time point during the simulation. Grey and black dots indicate the position of PI3K and PTEN respectively. The grey lines mark the boundaries of the PSD. Spatial information gathered from time frame based analysis is condensed to yield information about an entire simulation run.

2.4.1 Time course analysis

Time course analysis is carried out by characterizing two aspects of the modeled system. Firstly, the levels of PIP3 molecules present during steady state give the amplitude of the PIP3 signal. This can be done for the overall spine surface or specifically for the PSD having the neuronal spine as signaling environment in mind (see figure 6a: $\max_{\text{tot}}$, $\max_{\text{psd}}$).
Secondly, the halftime the system needs to reach steady state gives an indication of the apparent reaction speed. Again, these values can be compared for

the overall spine surface or just the PSD (figure 6a: $t_{\frac{1}{2}tot}$, $t_{\frac{1}{2}psd}$).
Time course analysis is carried out using the standard statistic methods provided by the R statistical package itself and the package ggplot2[6].

2.4.2 Spatial analysis

The Smoldyn output provides the positions of molecules in space for each time step of the simulation. This type of data, spatial point patterns, is encountered in other disciplines such as astrophysics and geography. Geography and its discipline geostatistics provide a vast collection of methods to analyze spatial point patterns. One of the most versatile and comprehensive geostatistic R packages is SpatStat[7] (Adrian Baddeley, 2005). Methods provided by SpatStat are used to analyze the data per time step. The different results are collected during steady state and summarized to characterize aspects such as randomness of point distributions.
The following list provides an overview of the main SpatStat methods used and how they are utilized in the following analysis.

Molecular densities The estimate of molecular densities on the PSD allows both, the visual inspection of signal formation and the application of extended analysis functions.
The default density function for point patterns provided by SpatStat uses an isotropic Gaussian kernel whose bandwidth is estimated based on the data sample. It also provides the possibility to correct the estimated density for edge effect bias. The edge effect occurs at the boundaries of the observation window (here the PSD) in which the intensity is estimated. The boundary separates the area of known point density from an unknown one resulting in an underestimate of the intensity at the boundary. This underestimate is corrected following Diggle's approach (Diggle, 1985; Adrian Baddeley, 2005).

Testing for complete spatial randomness: CSR Testing for complete spatial randomness (CSR) of the signal distribution is carried out with SpatStat's CSR test (Adrian Baddeley, 2005). The test separates the sample

[6] http://ggplot2.org/
[7] http://www.spatstat.org/

area into quadrants. Theχ^2 statistic for the quadrant count for each tile is compared to that of generated point patterns under CSR (default: 1999 simulations sampled from a Poisson distribution) determining the p-value for a time frame. If not stated differently, H_0 is rejected for $p<0.05$. One-sided tests are performed for individual time frames with H_0="The points are randomly distributed" and H_A="The points are clustered".

Pair-correlation function: PCF The pair correlation function (PCF) is a second-order summary characteristic of a spatial point pattern and related to Ripley's K-function (Illian et al., 2008) in the following way (for a radius $r\geq 0$):

$$pcf(r) = \frac{K'(r)}{2\pi r}$$

The K-function (K) gives the average number of points expected in the pattern at distances r from each point. K itself is a cumulative function. K' is its first derivative. The PCF gives the probability that another point can be found at distance (r) to any point in the pattern ($p(r) = \lambda \cdot pcf(r)$). Here, the PCF is used as it provides essentially the same information in a more accessible way (Illian et al., 2008). Depending on pcf(r) being smaller than, equal to, or larger than 1, the result of the function indicates a uniform distribution, standard Poisson process or aggregation. A function to estimate the PCF based on the data point distribution per time frame is available in SpatStat (Adrian Baddeley, 2005)

3 Results

3.1 Model parameters

The biochemical components of the model presented in this chapter are the key components of the PI3K - PTEN kinase - phosphatase system put into the spatial context of a dendritic spine. Each of the two following catalytic reactions depicted in figure 7a are modeled as three MAL conform reactions according to the description in section 2.2:

$$\begin{array}{lllllllll} \text{R1:} & \text{PI3K} & + & \text{PIP2} & \rightarrow & \text{PI3K} & + & \text{PIP3} \\ \text{R2:} & \text{PTEN} & + & \text{PIP3} & \rightarrow & \text{PTEN} & + & \text{PIP2} \end{array}$$

(a) Biochemical Signaling Network **(b)** Geometry

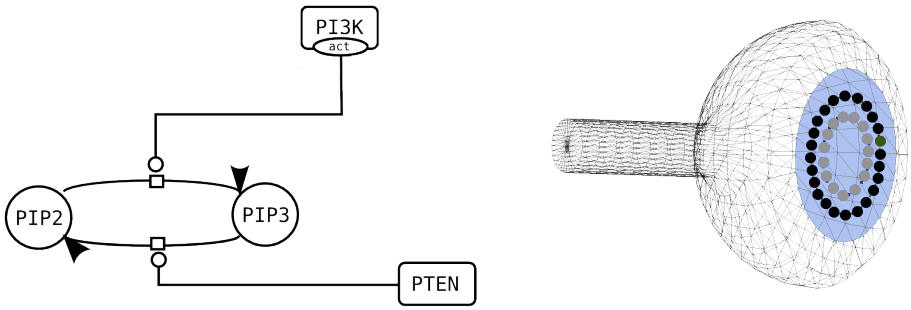

Figure 7: Biochemical and spatial illustration of the implemented signaling system
SBGN process description (Le Novère et al., 2009) of the implemented biochemical signaling pathway in (a) and an illustration of the underlying spatial geometry in (b). Light blue denotes the area of the PSD while grey and black dots represent positions of kinase and phosphatase molecules.

All reaction parameters and their source are listed in table 2. Initial molecule numbers are listed as well. The diffusion coefficients for each molecule are given in table 2.

Table 2: Parameters of biochemical reactions
MM: Michaelis-Menten Kinetics, estimated according to (Bhalla, 2000)

Rate Constants		
R1: $PI3K + PIP2 \rightarrow PI3K + PIP3$		
R1 kf	8302889 moleculesnm^{-3} s^{-1}	(Jain and Bhalla, 2009)
R1 kb	16 s^{-1}	estimated
R1 kcat	4 s^{-1}	from MM
R2: $PTEN + PIP3 \rightarrow PTEN + PIP2$		
R2 kf	8302889 molecules nm^{-3} s^{-1}	(Yong et al., 2008)
R2 kb	0.5 s^{-1}	estimated
R2 kcat	5 s^{-1}	from MM
Initial molecule numbers		
PI3K	31	(Jain and Bhalla, 2009)
PTEN	80	(Jain and Bhalla, 2009)
PIP2	2107	(Jain and Bhalla, 2009)
height PIP3	0	-

The spine surface is modeled based on Byrne et al. (2010) using 1214 triangles (see figure 7b). Spine sizes and shapes vary depending on their developmental state and plasticity (Park et al., 2006), brain region and observational angle (Arellano et al., 2007). The size of the PSD is correlated with the spines head volume and membrane area (Wilson and Linder, 1983; Arellano et al., 2007; Heck et al., 2012) as well as the distribution and number of AMPAR (Matsuzaki et al., 2001; Nusser et al., 1998). The chosen dimensions reflect the ratios found in the literature. The implemented geometry attempts to represent an average sized mushroom-shaped spine as present in the mature excitatory glutamatergic synapses of the CNS (Arellano et al., 2007; Izeddin et al., 2011; Takasaki et al., 2013). The dimensions are given in table 3.

Metric dimensions		
spine volume	0.5 µm^3	
spine head volume	0.11µm^3	
spine surface area	3.7 µm^2	
PSD area	0.28 µm^2	
PSD radius	0.37µm	
neck length	0.75µm	
neck diameter	0.2 µm	
Diffusion Coefficients D		
PI3K	17000 nm^2 s^{-1}	(Young et al., 1980)
PTEN	28000 nm^2 s^{-1}	(Young et al., 1980)
PIP2	80000 nm^2 s^{-1}	(Xu et al., 2003)
PIP3	80000 nm^2 s^{-1}	(Xu et al., 2003)

Table 3: Spatial parameters of the spine

3.2 Simulation setup

The biochemical reaction rates and initial molecule numbers were identical for all simulations. Diffusion constants of lipids were independent of time or their current surface location and the same in all simulations. All lipids present at t=0 s are PIP2 molecules that are randomly distributed over the whole spine surface. The initial positions of phosphatases and kinases were varied between simulations (see figure 8). Circular configurations were chosen because TrkB receptors and their associated signaling apparatus (containing PI3K) line up on the outer borders of the the PSD resembling an enclosure (Drake et al., 1999; Petralia et al., 2005). Kinases and phosphatases in circular setups are not allowed to diffuse and keep their position for the duration of the simulation. This resembles molecules being attached to cytoskeletal features. Different radii were chosen for these ring shaped configurations, the biggest radius being r=370 nm just outside of the PSD. The others were placed evenly spaced between a hypothetical r=0 nm and this outer circle. The simulations with molecules placed at r=0 nm were considered but decided to be irrelevant because it is impossible to place more than one molecule at exactly the same physical position.

Simulations with random initial placement of kinase or phosphatase while keeping their position fixed for the duration of the simulation is the first step

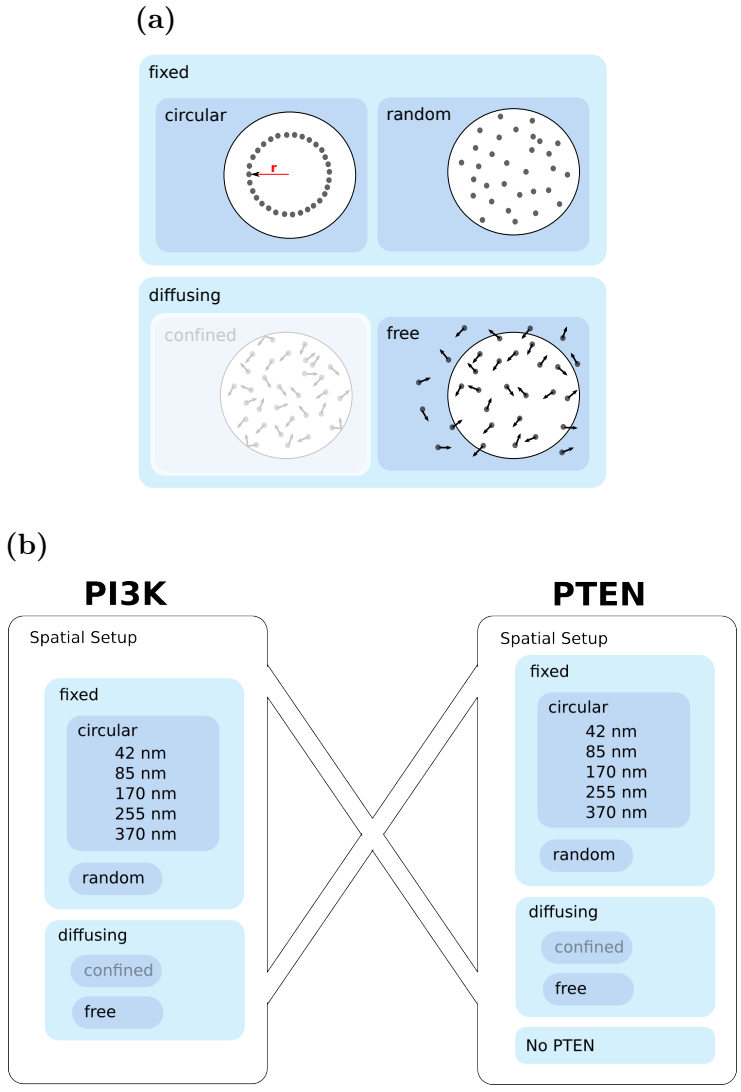

Figure 8: Spatial Simulation Scenarios
(a) The schematic illustration explains the different initial spatial setups for PI3K or PTEN placement in simulations. Setups are differentiated in "fixed" - the respective molecule stays at that position during the whole simulation - and "diffusing" - the respective molecules are diffusing with a constant diffusion coefficient. "Fixed" setups are either circular - the respective molecules are fixed on circles with a given radius r - or random. In "diffusing" setups molecules are either confined within the boundaries of the PSD or they are allowed to leave the PSD and diffuse along the whole spine surface. However, the confined scenario could not be implemented accurately as explained later in section 3.3.2 and is therefore shaded in this figure. (b)The full spatial setup for a simulation combines one such PI3K setup and one PTEN setup. However, the "confined" scenario could not be implemented accurately in Smoldyn V2.21 as indicated by the grey colored label and explained in section 3.3.2

in relaxing the circular constraints and increasing the random properties of the system ("fixed" settings). Those random properties are further increased in another set of simulations where kinase and phosphatase positions are randomly initialized at the PSD and the molecules are allowed to diffuse (keeping the same diffusion constant during the whole simulation and between simulations). Molecules in confined setups were not supposed to diffuse out of the PSD area, while those in random settings are allowed to leave the PSD and diffuse over the whole spine surface thus representing the most random simulation scenario. However, the confined scenario could not be implemented accurately due to technical limitations as described subsequently in section 3.3.2. Its description was kept (but shaded) in the illustration of simulation scenarios as it is a logical intermediate between random fixed positions and freely diffusing molecules.
Each possible kinase scenario is combined with every phosphatase scenario as figure 8 indicates. This generates a total of 56 different spatial scenarios. Each simulation ran with simulation time steps of 0.001 s for 300 s at which the system appears to be in steady state. The system is considered to be in steady state when the average number of the observed molecular species over time does not change anymore (it can however fluctuate due to the stochastic nature of the simulations). Each spatial scenario is simulated 5 times[8].

3.3 Technical constraints

Two main technical difficulties were encountered while using Smoldyn for simulations. First, simulations on complex geometries can exhibit a trapping behavior for diffusing molecules. Second, trapping molecules in a confined area of the surface by implementing a second perpendicular surface as "wall" is not possible. Both issues are addressed in the following section.

3.3.1 The surface partitioning influences the simulation results

The mesh representing the spine surface in simulations was adapted from Byrne et al. (2010). The triangulation of the surface was kept the same while

[8]The Smoldyn configuration files are availabe at https://github.com/yetime/SmoldynConfigs.git

the volumetric properties and the dimensions were adjusted. This triangulation represents the circular area of the PSD as a wedged faces structure comprising a central high valence vertex as shown in figure 9. Initial sim-

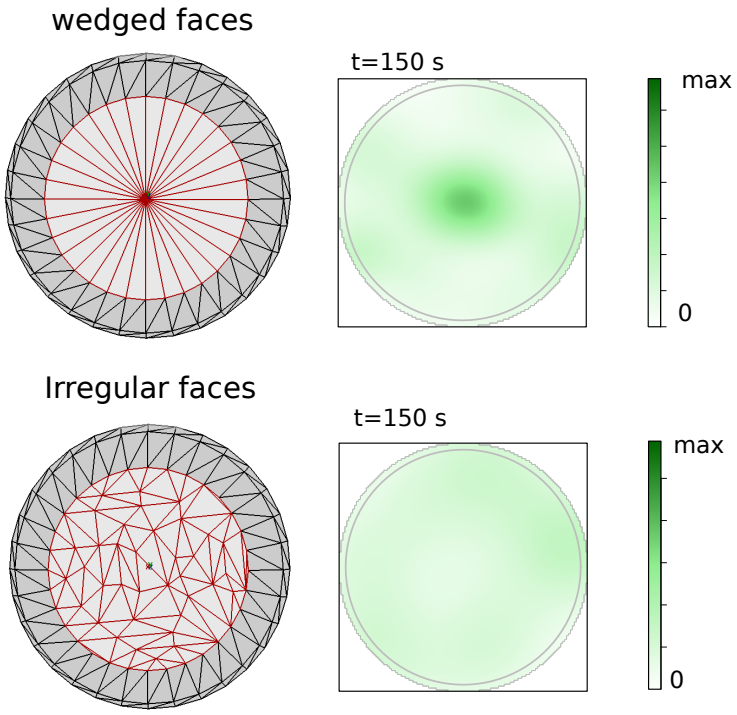

Figure 9: The surface tessellation influences the simulation results
Two different triangular PSD surface tessellations are illustrated in the first column. The PSD area is colored light grey. Column 2 gives the corresponding PIP3 density for a randomly moving PIP3 molecules at time t=150 s.

ulations without PTEN being present were performed on this surface and showed a central accumulation of molecules at the location of this central vertex. This accumulation also appeared in cases where PI3K was allowed to diffuse randomly. It did not disappear over time due to dilution effects once all PIP2 was converted to PIP3. Control simulations monitoring the diffusion of PIP3 alone gave a similar peak of molecule concentration in the center (figure 9, upper row) suggesting that the cause is an artifact of the surface tiling.

A new surface tiling for the PSD surface was designed by tiling the PSD into triangles based on the size of those surrounding the PSD. The edge valence of this tiling is six. The number of tiles was reduced afterwards using the polygon reduction algorithm implemented in Maya (Melax, 1998), keeping

the vertex valence at an average of six compared to the valence of 32 for the central vertex in the wedged tiling.
The PIP3 only simulations performed on this surface have a random appearance (figure 9, bottom row) compared to those run on the wedged surface (figure 9, upper row).
Four simulations with different numbers of PIP3 molecules n(PIP3)={350, 700, 1400, 2100} were performed on both surfaces to further compare the two different tilings with regard to their influence on simulating random diffusion. Each simulation was analyzed by testing for complete spatial randomness (CSR) at every simulation time point. The p-values for these tests are illustrated in figure 10.

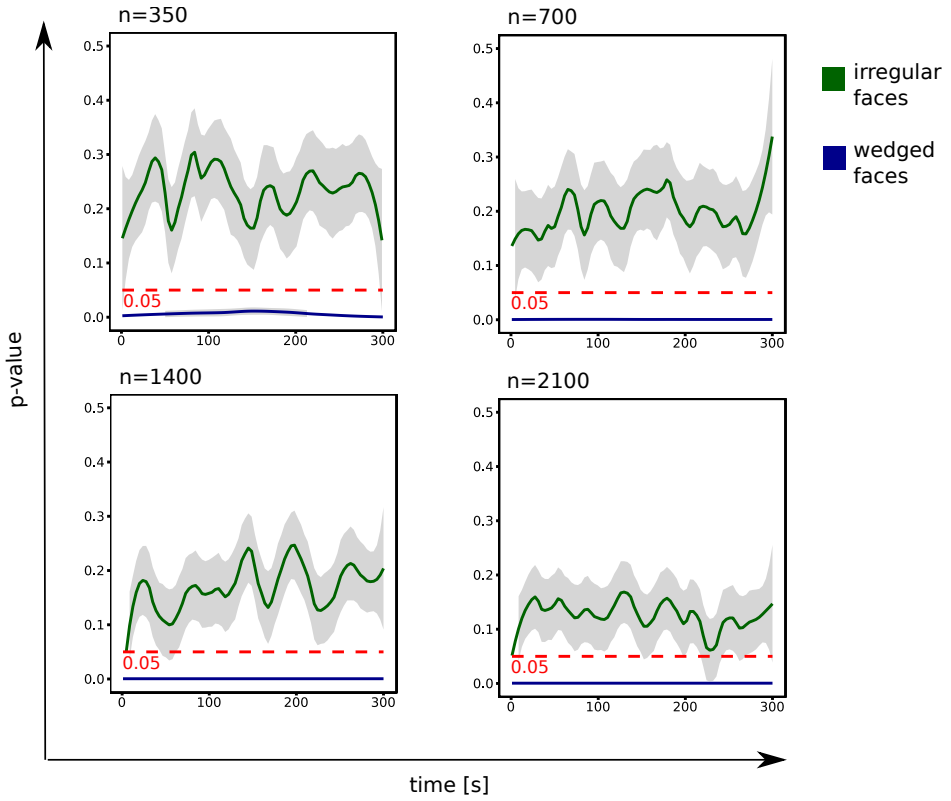

Figure 10: Reducing the valence of edges enables random diffusion
Testing for CSR (Complete Spatial Randomness) was performed for every time step of PIP3 only simulations on both PSD surfaces (wedged:blue and irregular:green, the blue and green line are smoothed using the a local loess fitting, confidence interval (95%):grey). The amount of PIP3 was varied, with n(PIP3)=350, 700, 1400, 2100. The plots compare the corresponding p-values over time for simulations done with the same amount of PIP3. The red dashed line marks the significance threshold of p=0.05.

Each figure compares the test results of the wedged surface simulation (blue) with the results of the corresponding (by means of PIP3 molecule numbers) irregular tiling (green). P-values below the significance threshold of 0.05 reject the hypothesis of a random distribution of molecules on the surface. The fraction of time points with p-value test results below the threshold are given in table 4.

Table 4: Fraction of time points below the p-value significance threshold CSR tests were performed for every simulation time point. The given fractions are the number of tests with p-values below the threshold over the total amount of tested time points for that simulation. The simulations contained only PIP3 molecules in different quantities n(PIP3) and were performed on differently tiled surfaces (wedged, irregular)

n(PIP3)	wedged	irregular
350	0.97	0.08
700	1	0.11
1400	1	0.23
2100	1	0.35

The results clearly show that the diffusion on the wedged surface does not behave randomly in contrast to the irregular surface. The increasing number of time points that appear to be clustered on the irregular surface are due to the increasing probability of molecules being close to each other when the overall molecule numbers increase.

3.3.2 Surface interaction during surface diffusion appears to be leaky

Spatial scenarios that involve at least one species to be confined to the PSD involve the implementation of a surface boundary that is reflective for the respective species but allows other molecule types to pass at the same time. Smoldyn provides the functionality of surface interactions for surface diffusing molecules since version V2.19.

A cylindrical surface boundary was implemented as shown in figure 11 to trap molecules on the PSD surface by reflecting them upon interaction. However, this boundary seems to allow PI3K and PTEN molecules to leave the PSD

area. PSD molecule counts between boundary-free scenarios and boundary-containing scenarios where compared for both PI3K and PTEN to quantify this leak (see figure 11).

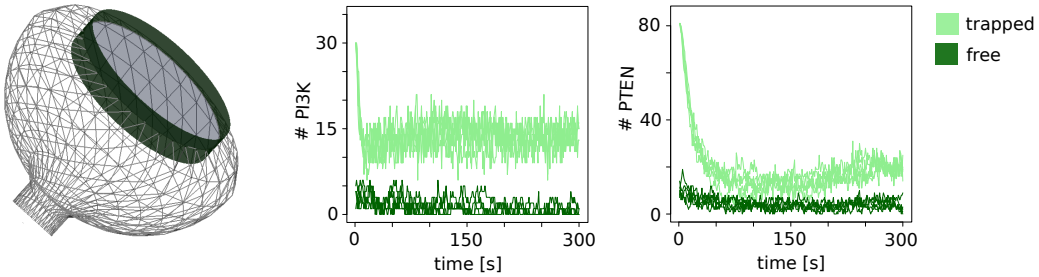

Figure 11: Surface interaction during surface diffusion is leaky
An illustration of the implemented cylindrical PSD boundaries shown on the left. The time courses of PI3K molecules (middle) and PTEN molecules (right) show the fluctuations in molecule numbers on the PSD surface. Dark green depicts the molecule number development on the PSD if the respective molecules are allowed to move freely (no boundaries), light green illustrates scenarios, where the molecules are supposed to be confined by a cylindrical boundary. 5 simulation runs are shown in each case.

Approximately ten times more PI3K and six times more PTEN molecules are present at the PSD, if it is surrounded by the reflecting cylinder than in the random case rendering the confined scenarios less stringent as intended. Unfortunately, the whole behavior of the system changes over time from most of the molecules being confined at the PSD to a quite substantial loss of molecules. Because of this, the results are not directly comparable to the other spatial setups where the properties and distribution of molecules does not change over time and were excluded from the following comparative analysis. They were kept in the figures of the previous section 3.2 to illustrate that confined diffusion would have been a valuable intermediate step between a fixed and an entirely free moving setup.

3.3.3 Summary

A surface geometry could be implemented that allows random diffusion of molecules on the surface. The implementation of an intermediate spatial scenario between fixing molecules at random positions at the PSD and letting them diffuse randomly over the whole surface could not be implemented.

3.4 Development of membrane PIP3 levels over time depends on the spatial scenario

This section compares different spatial scenarios with regards to the PIP3 signal they produce. Characteristic simulation runs are chosen to illustrate the main features of a signal: its amplitude, speed, spatial extent and shape are addressed and quantified. In most cases the discussion starts with circular setups and progresses to increasingly unordered ones.

3.4.1 Circular spatial setups can focus the signal to the PSD

The different circular scenarios can be separated into two groups based on whether PI3K or PTEN form the inner circle. Both groups are expected to show fundamental differences with regards to the PIP3 distribution they are producing in the PSD.
Figure 12 illustrates the results of simulation runs where an inner circle of PI3K molecules is surrounded by a circle of PTEN. This setup focuses the signal effectively to the PSD area which can be seen from the density plots. The upper row shows the surface density of PIP3 at t=0, during steady state and at $t_{1/2}$ (the time needed to reach half of the steady state PIP3 numbers on the PSD). The time course given underneath illustrates the PIP3 levels in the PSD and in total. The proximity of both lines, the PSD PIP3 molecule numbers and the total number of PIP3, is also highly important. It indicates a low amount of leakage of PIP3 to the peripheral space around the PSD thus creating an efficient and focused signal.

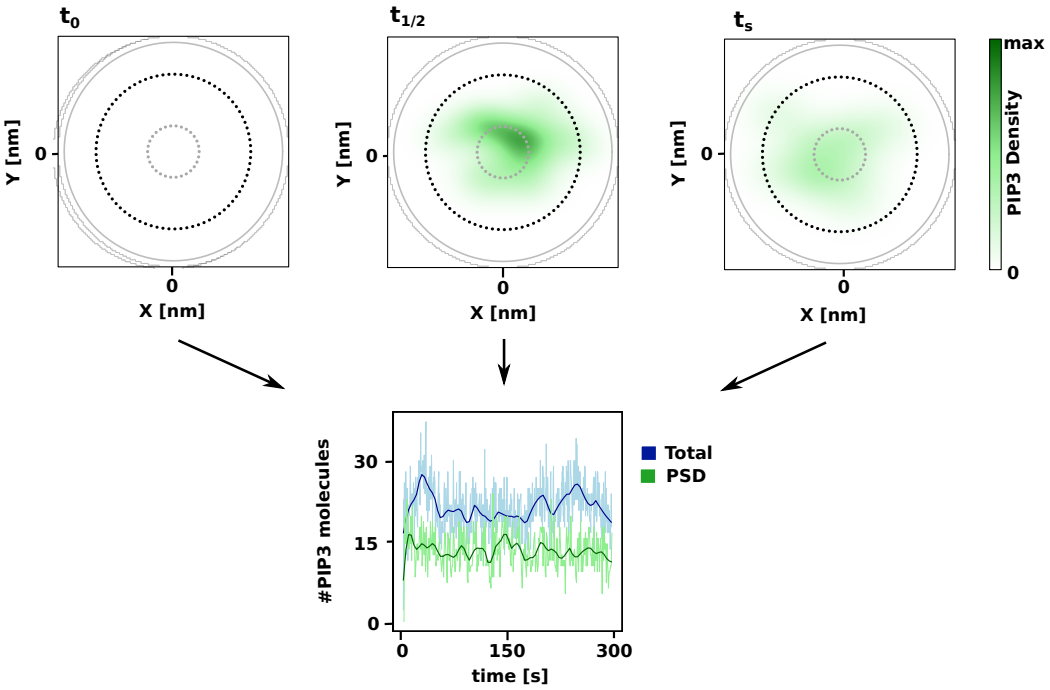

Figure 12: Arranging PI3K molecules on an inner ring surrounded by PTEN creates a focused PIP3 signal at the PSD

Typical simulation result for PIP3 development on the spine membrane for circular spatial setups where $r_{PTEN} > r_{PI3K}$ are shown. $r_{PTEN} = 255$nm, $r_{PI3K} = 85$nm The top row illustrates the PIP3 density as green gradient. The darkest shade gives the maximum PIP3 reached over the whole simulation run. PI3K and PTEN positions are indicated by grey and black dots respectively. Density plots for three different time points are shown to illustrate the development over time. t_0 represents the start of the simulation, $t_{\frac{1}{2}}$ represents that point in time when half of the steady state amount of PIP3 is reached and t_S illustrates the steady state.

A time course of PIP3 molecule numbers on the surface is shown on the bottom. Blue: Smoothed PIP3 molecule count over the whole surface; Green: Smoothed PIP3 molecule count on the PSD. Smoothed functions are loess curves (local regression) to illustrate the trend.

A signaling peak or ring - depending on the radius of the PI3K ring - might transiently form at the beginning of simulation runs in those spatial settings that do not contain PTEN. However, it is short lived. The signal is lost due to diffusion and overproduction of PIP3 within one to two seconds, see example in figure 44.

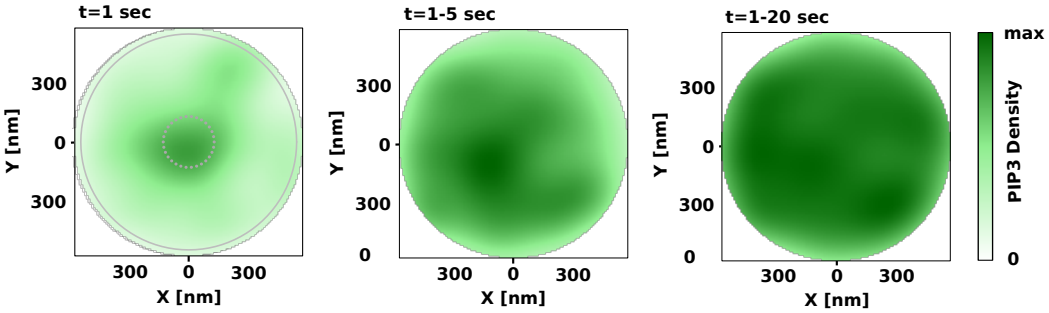

Figure 13: A transient center signaling peak might form in beginning of simulating spatial setups without PTEN
The figure shows density plots of a single time frame at t=1 sec. In the middle and on the right, the average density of 5 (middle) and 20 (right) time frames is shown to highlight an accumulating effect in the beginning (left and middle) and dispersion afterwards (right).

If the order of the two rings is swapped - PTEN on the inside and PI3K on the outside - the system creates an exclusion zone in the center of the PSD (see figure 14). PIP3 accumulates on the overall spine surface but is dephosphorylated to PIP2 if it reaches the circle of PTEN. This is reflected in the time course in figure 14 by the bigger difference between total and PSD PIP3 molecule numbers. The PTEN ring has to be close to the outer PSD boundaries if PIP3 is supposed to be totally excluded from the PSD.

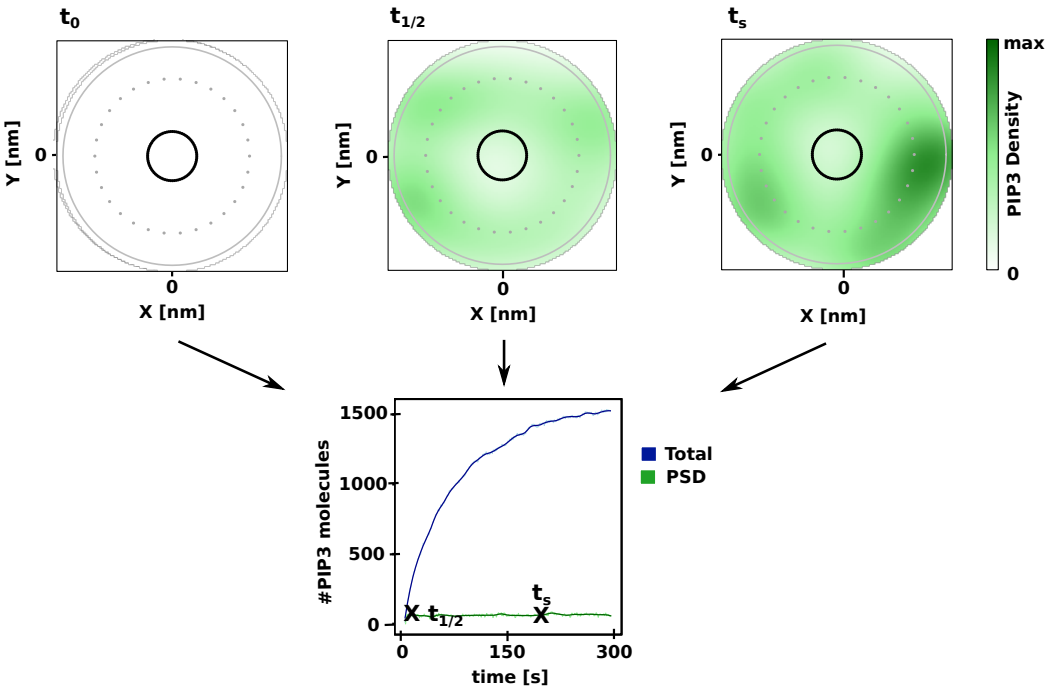

Figure 14: Arranging PI3K molecules on an outer ring surrounding PTEN creates an exclusion zone for the PIP3 signal at the PSD
Typical simulation result for PIP3 development on the spine membrane for circular spatial setups where $r_{PTEN} < r_{PI3K}$ are shown. $R_{PTEN} = 85$nm, $R_{PI3K} = 255$nm (see figure 12).

3.4.2 The magnitude of the PIP3 signal and the PSD/Total PIP3 ratio are the major parameters influenced by changes in the spatial scenario

Further examples of PSD PIP3 densities and time courses are given in figure 15. The scenarios contain PI3K and/or PTEN in the random diffusing or random fixed configuration (a)-(d) and (e)-(f) respectively.
Changing PTEN from a random fixed position to randomly diffusing results in an overall signal increase in the system and increases the PSD/Total PIP3 ratio (compare (a) and (b)). Swapping the configurations of PI3K and PTEN (compare (a) and (c)) decreases the ratio, but increases the overall amount of PIP3 in the system. This is further amplified by changing the PI3K configuration to randomly diffusing (compare (c) and (d)). The formation of a clear exclusion zone or a central signaling peak is much less pronounced or absent in comparison to the double circular scenarios in figure 12 and 14. An exclusion zone can partly be observed in time frames of (d): Circular PTEN configuration and random diffusing PI3K. A partial ring shaped peak forms in b): Circular PI3K and random diffusing PTEN. The random fixed contribution in (a) and (c) is too strong to allow either of the two distribution patterns to form. Scenarios (e) and (f) combine both molecule types in random configurations. Both scenarios fail to produce a clear pattern on the PSD. Changing the PI3K configuration from fixed to random diffusing decreases the overall signal and the PSD/Total ratio.

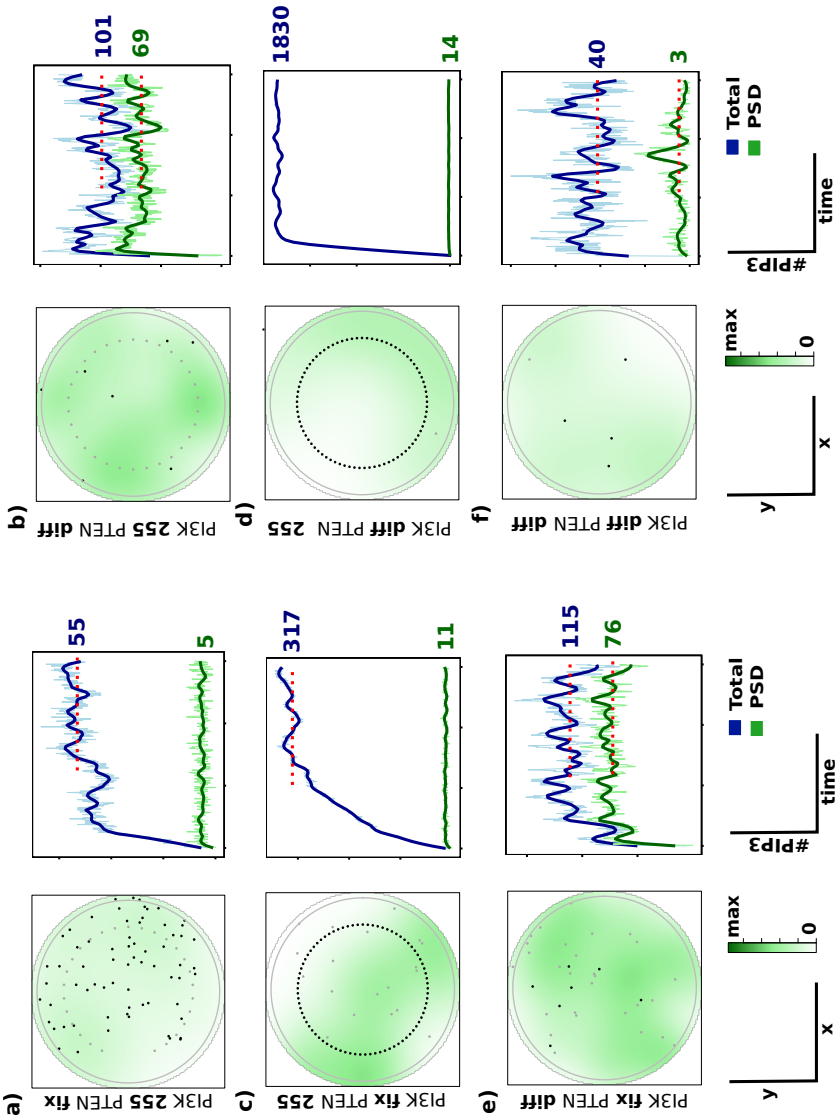

Figure 15: The spatial scenario influences the PIP3 signal level and the PSD/Total PIP3 ratio
This figure gives 6 further examples of PIP3 densities (left) and the corresponding time course (right). At least one of the systems components (PI3K or PTEN) are arranged in a random fixed or randomly diffusing order. The time courses are given for the whole simulation time of 300s. Numbers indicate the average steady PIP3 level over the whole spine surface (blue) and the PSD (green). The average taken is indicated by the red dotted line.

3.4.3 Spatial scenarios with r(PI3K) < r(PTEN) are most efficient in focusing the signal to the PSD

If the purpose of a signaling system is to focus a signal to a certain location in space, it appears to be favorable to reduce the leakage of signal to the surrounding environment and maximize the signal in the desired area. This area in case of the spine is the PSD. Figure 16 shows the average PIP3 levels at steady state for the different spatial scenarios. Subfigure (a) gives the total amount of PIP3 present at the PSD while figure (b) gives the ratio: $PIP3_{PSD}/PIP3_{total}$ (see Appendix for mean values and their standard deviation).

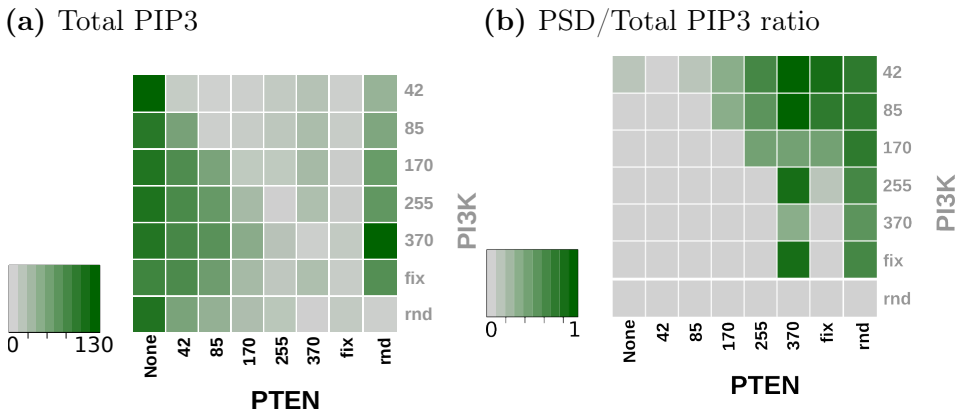

Figure 16: Spatial scenarios that yield the overall highest level of PIP3 at steady state are not the most efficient ones
(a) The heatmap shows the overall PIP3 levels developing on the PSD surface at steady state in the different simulated scenarios. Grey (very low), dark green (very high: All PIP2 converted to PIP3). The highest levels of steady state PIP3 are observed in scenarios where PTEN is restricted to the PSD, the radius of the PTEN circle is small and inside of the PI3K one.
(b) The heatmap gives the ratio of PSD/Total PIP3 in the system. This indicates the efficiency of the system by means of focusing the signal to the PSD. Grey (inefficient), dark green (very efficient: PSD/Total ≈ 1)
Each square represents the mean over 5 simulation runs (means and their standard deviation are given in table 8, Appendix).

The ratios for PI3K configurations without PTEN reflect the ratio of PSD area to total surface area of 0.076. Although this produces the highest amount of overall PIP3, the signal is distributed evenly over the whole surface instead

of being focused.
The highest amount of overall steady state PIP3 is present in scenarios that restrict PTEN to the area of the PSD and surrounds PTEN by PI3K. Comparing this to figure (b) shows, that these signals are inefficient as well and leak a high percentage of PIP3 to the PSD surrounding areas. These are the scenarios that effectively create an exclusion zone in the center of the PSD. If the PTEN circle is small, this exclusion zone is small as well and there is PIP3 on the PSD. Increasing the PTEN circle diameter clarifies this exclusion effect.
The most efficient spatial settings in restricting signaling to the PSD are the circular configurations with PI3K on the inner ring and PTEN on the outer. The $\mathrm{PIP3_{PSD}/PIP3_{total}}$ ratio for $\mathrm{PI3K}_{r42}$ and $\mathrm{PI3K}_{r85}$ with PTEN_{r370} is 0.95 indicating that almost all of the produced PIP3 is located at the PSD and almost no leakage to the surrounding surface occurs. The signal amplitude in these settings can be increased sixfold, just by changing the spatial configuration (comparing the setting with the lowest and the highest amount of PIP3 on the PSD during steady state).

3.4.4 The maximum steady state PIP3 levels at the PSD depend on the radii of the circles and the average distance between PI3K and PTEN molecules

Looking at figure 16a suggests a relation between the radius of the kinase or phosphatase circle and the maximum PIP3 observed at the PSD in cases where the other enzyme is randomly diffusing over the whole spine surface. This relation can be fitted with a cubic polynomial as shown in figure 17: Figure (a) shows data for the spatial setups of random PIP3 production over the different circular PTEN settings, while (b) shows the inverse, random PIP3 dephosphorylation over circular PIP3 production by PI3K. While increasing r(PI3K) has an increasing effect on the PSD PIP3 levels in these scenarios, the opposite is true for r(PTEN).

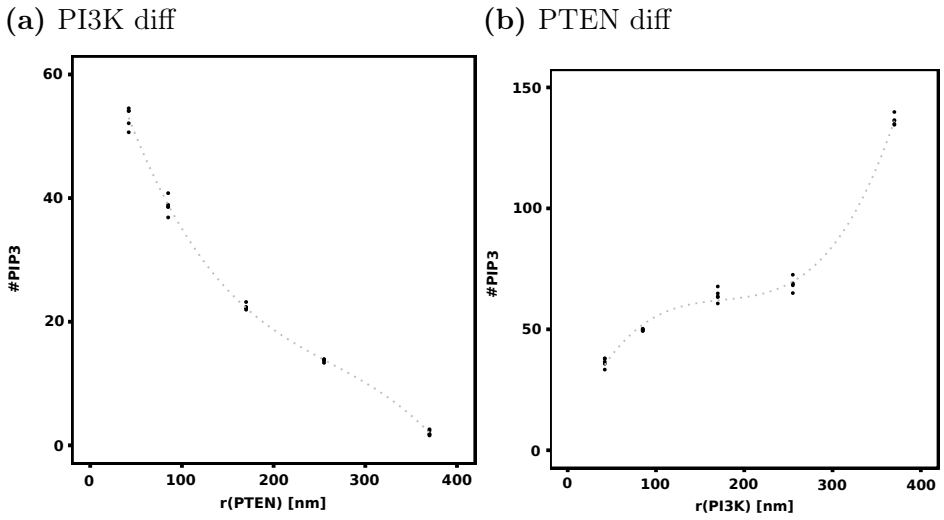

Figure 17: The steady state PIP3 level at the PSD in presence of random PIP3 phosphorylation or dephosphorylation depends on the radius of enzyme distribution
(a) Dependency of the steady state PIP3 level at the PSD on r(PTEN) for random PIP3 production
(b) Dependency of the steady state PIP3 level at the PSD on r(PI3K) for random PIP3 dephosphorylation
Each point represents the steady state PIP3 level of a single simulation run. The cubic fit is significant (parameters given in table 11, Appendix).

A relation between the steady state PIP3 levels and the spatial configuration is more difficult to quantify for the other spatial setups because the order of the PI3K and PTEN rings dramatically change the quality of the PIP3 signal: From central peaks to exclusion zones. The analysis is therefore restricted to those setups that keep the order of rings. The distance between rings is given as the average pairwise distance between PI3K and PTEN molecules:

$$D = \frac{1}{n_{ts}} \sum_{ts=1}^{n_{ts}} \left(\frac{1}{n_{kin} \cdot n_{phos}} \sum_{\substack{i=1 \\ j=1}}^{\substack{n_{kin} \\ n_{phos}}} d(p_{Ki}, p_{Pj}) \right) \tag{2.1}$$

Figure 18 depicts all those circular spatial configurations where r(PI3K) $<$ r(PTEN). Subfigures (a) and (b) show the same dataset. While (a) is colored according to the PI3K setting, (b) is marked according to the PTEN setting. Every point represents the mean steady state PIP3 level of one simulation (means and standard deviation are given in table 8,Appendix). The overall tendency is clearly an increase in steady state PIP3 levels with increasing distances between PI3K and PTEN molecules. Comparing the different color schemes in (a) and (b), this difference seems to be manifested in the increasing distance with regards to PTEN, not PI3K. Keeping r(PI3K)=42 nm and increasing r(PTEN) from 85 nm to 370 nm seems to follow a power law relation as shown in more detail in figure 18c (see table 10, Appendix, for fitting details). Keeping r(PTEN)=370 nm and looking at the results for different kinase radii looks different. While increasing r(PI3K) in this case shows an increase in PIP3 levels for r(PI3K)=$\{42,85,170\}$ nm it drops r(PI3K)=255 nm indicating an optimum for PI3K and PTEN spacing and the overall dispersity of the system.

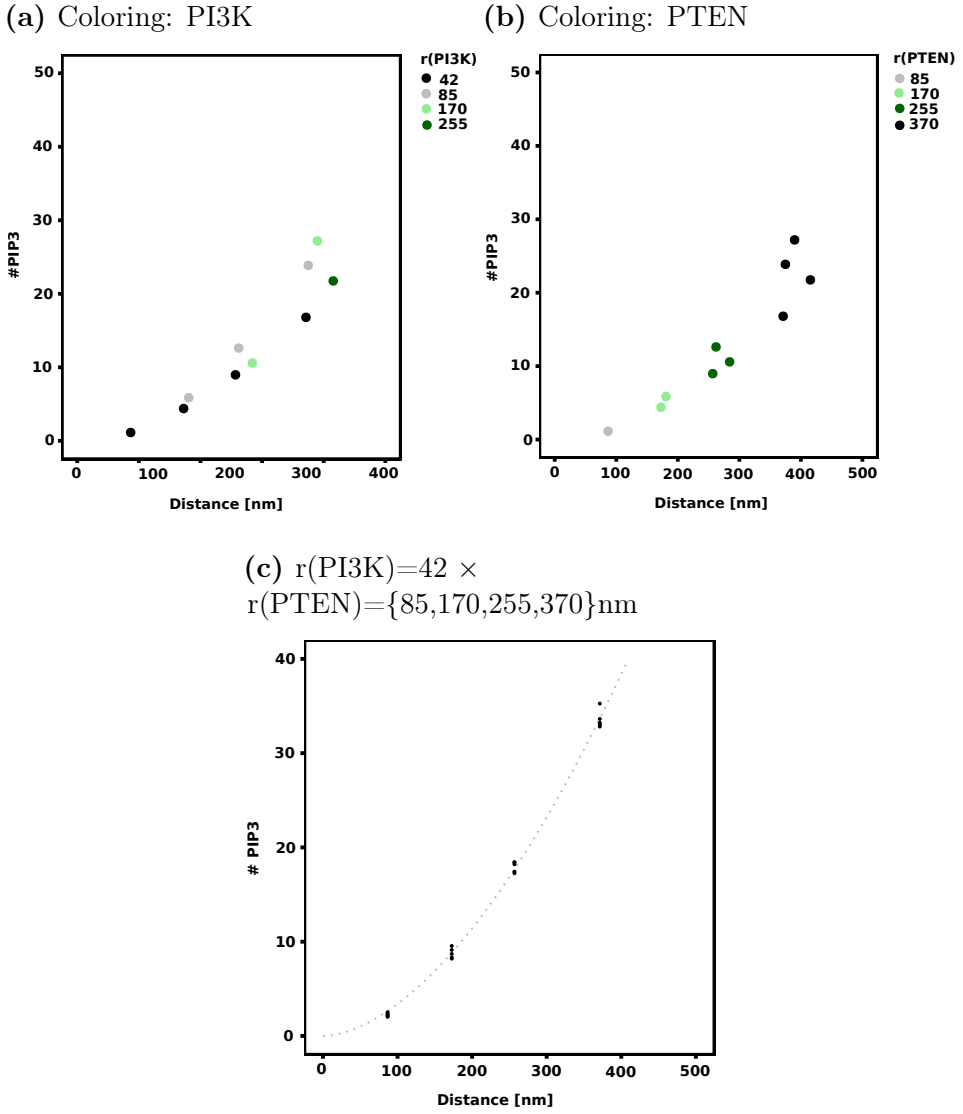

Figure 18: Increasing the distance between kinase and phosphatases increases PSD PIP3 levels

Figure (a) and (b) illustrate the same dataset consisting of all circular setups with r(PI3K) < r(PTEN). While (a) is colored according to the r(PI3K), (b) shows the corresponding r(PTEN) coloring. Figure (c) shows a power law fit of r(PI3K)=42 × r(PTEN)={85,170,255,370} nm spatial setups.
(a)-(b) Dots represent average steady state PIP3 over 5 simulation runs
(c) A dot represents the steady state PIP3 level for one simulation run.
The distance is the average pairwise distance calculated according to equation 2.1

3.4.5 The overall reaction speed is similar between different spatial scenarios

As seen before, different spatial scenarios produce different levels of PIP3 in the system. The time that is needed to reach steady state gives an indication if the spatial setting has an influence on the speed of the reaction.
The halftimes that characterize the absolute time in seconds needed to reach steady state are shown in figure 19a. The diagonal r(PI3K)=r(PTEN) appears to split the results in two separating the PSD exclusion scenarios from those that focus the signal to a center peak at the PSD. However, the overall PIP3 levels in the system are much higher in the PSD exclusion scenarios.
The ratio of the time needed to reach steady state and the steady state PIP3 level in the system is shown in figure 19b. This figure indicates that the apparent speed of PIP3 production in seconds/molecule to reach steady state is similar in most spatial scenarios, except for those close to the diagonal r(PI3K)=r(PTEN) where the overall PIP3 levels are extremely low, resulting in slow speed.

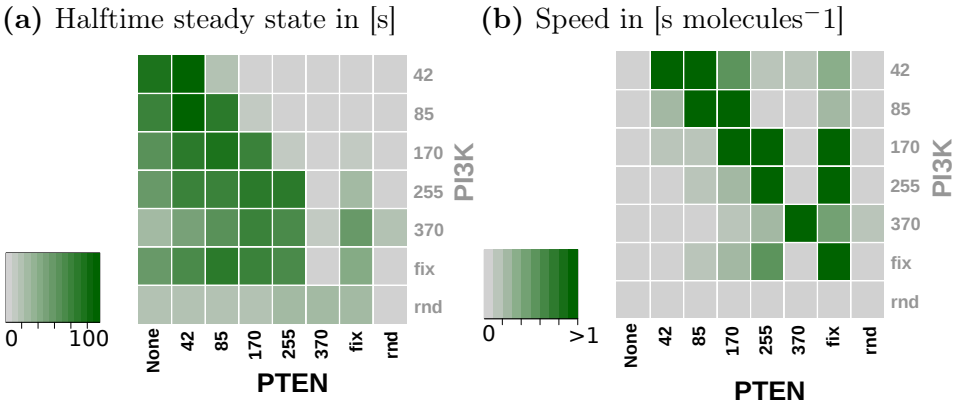

Figure 19: The overall reaction speed is similar between different spatial scenarios
The figure illustrates the absolute halftime (a) and the speed in [sec/molecule] (b) needed to reach steady state.
(a) The heatmap shows $t_{1/2}$: The halftime needed to reach steady state PIP3 levels in the system based on the spatial setting. Grey (short), dark green (long).
(b) This heatmap depicts the ratio of the time when steady state is reached over the total steady state PIP3 levels in the different simulated scenarios. This can be interpreted as speed in time per molecule. Grey (fast), dark green (slow).

3.4.6 Statistical testing for complete spatial randomness (CSR) identifies scenarios producing signaling peaks

An apparent property of those spatial scenarios that either appear to create a center peak or an exclusion zone in the area of the PSD is the obviously non-random distribution of molecules. Tests for complete spatial randomness (CSR) asses this property and provides a possibility to quickly distinguish those potentially interesting settings from the rest (see section 2.4 for CSR). The CSR testing procedure for a whole time series is illustrated in figure 20. The CSR test itself is carried out on the PIP3 distribution pattern present at a single time step. Two different approaches are used to summarize the CSR test results over the entire set of simulation runs. This analysis is sketched in figure 20. The first approach calculates the fraction of time frames for which H_0 was rejected (based on $p<0.05$): The percentage non-random time frames. The mean of these fractions over all simulation runs of a certain setting is taken. The second approach collects all p-values of all steady state time frames. It determines the most prevalent one. Based on this, the fraction of total simulation runs for which H_0 was rejected is given (based on $p<0.05$).

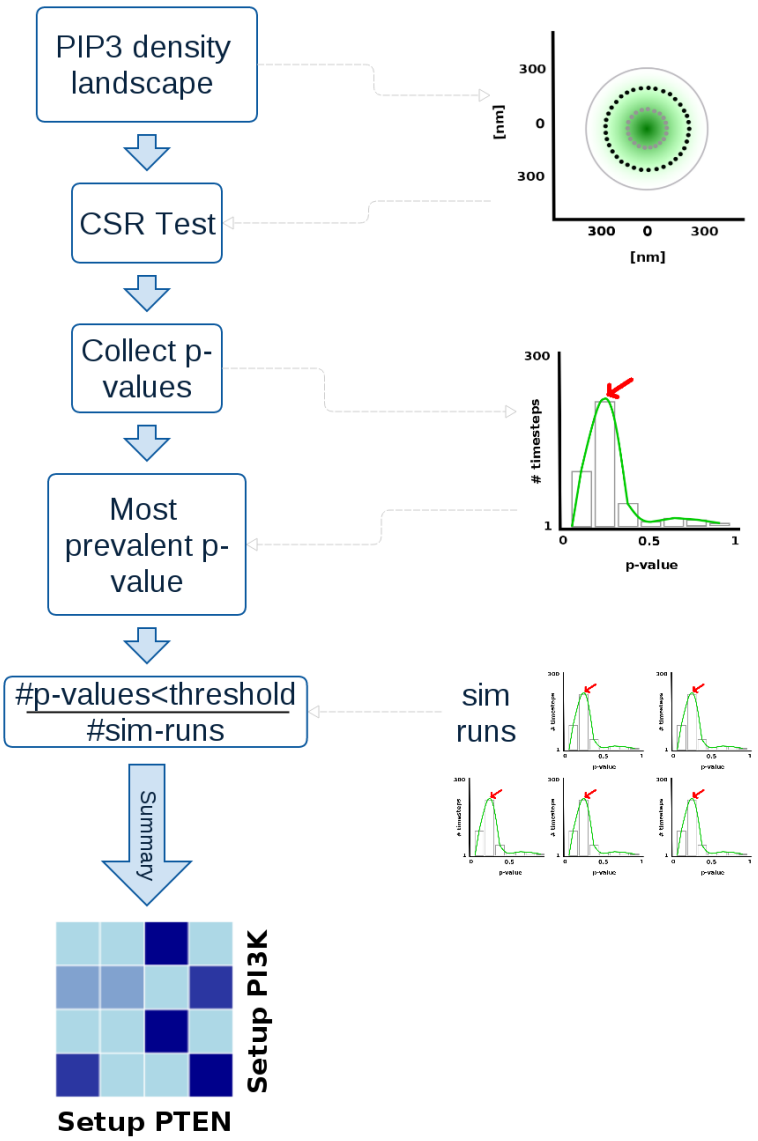

Figure 20: Illustration of CSR Testing procedure
The CSR test itself is carried out on the PIP3 distribution pattern of a single time step. The resulting p-values are collected. Two slightly different procedures yield a summary fraction by which the time course is judged. The first summary fraction is simply the fraction of time frames that yield a p-value below the significance threshold of 0.05 (which indicates clustering). The second procedure determines the most prevalent p-value over the whole set of time frames. The fraction of simulation runs that show a prevalent p-value below the significance threshold is reported.

The results of applying this testing procedure to test the different spatial configurations for CSR are shown in figure 21. While figure (a) depicts the results based on time frame fractions only, figure (b) gives the results for evaluating the prevalent p-value and taking fractions over simulation runs afterwards.

(a) Entirely fraction-based

(b) Fractions of p-values

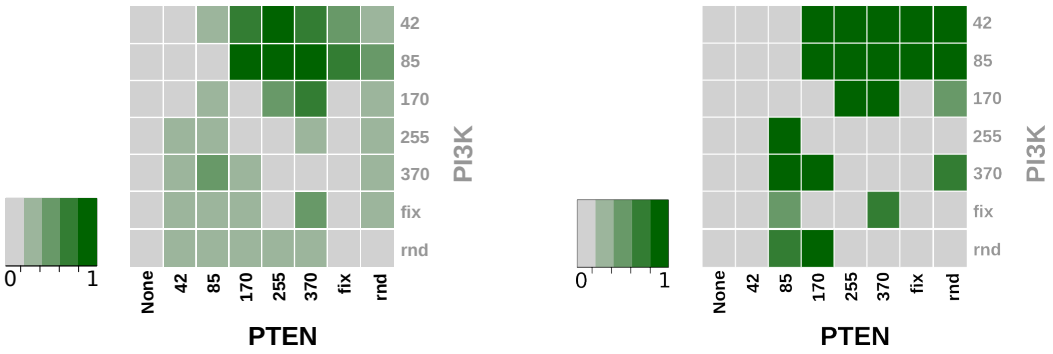

Figure 21: CSR testing indicates non-random PIP3 distributions on the PSD
(a) The heat map gives the fraction of time frames with a p-value below the significance threshold 0.05 over all time frames of 5 simulation runs per spatial setting.
(b) The heat map gives the fraction of the 5 simulation runs with a prevalent p-value below the significance threshold of 0.05.

Spatial settings without PTEN and those with r(PI3K) = r(PTEN) do not show any indication of spatial structuring as expected. The latter is due to the very low number of PIP3 molecules produced. Most of the spatial settings with r(PI3K) $\leq$ r(PTEN) have a high fraction of overall time frames (>50%) classified as clustered. The fraction of simulation runs with a prevalent p-value below 0.05 is accordingly high. Simulations with r(PI3K) $\geq$ r(PTEN) show fractions of around 20-40% time frames being clustered, while the corresponding fraction of prevalent p-values indicates a stronger tendency towards clustering in some cases and no clustering in others in contrast to the solely fraction based approach.
Spatial settings containing either phosphatase or kinase in a randomly diffusing

setup indicate clustering to a certain degree (20-40%). Those settings having a random but fixed component have a more heterogeneous appearance. Only r(PI3K)={42,85} with r(PTEN)=fix indicate clustering, while most of the r(PI3K)=fix show some degree of spatial structure.

3.4.7 Analysis of the pair correlation function verifies previous CSR results

The pair correlation function (PCF) is a second order characteristic of a point pattern that provides further insights into possible structural features. Here, the PCF is used in an analysis similar to the previous CSR tests. The PCF for each steady state time frame is determined. Since g(r)>1 indicates clustering, the (discrete) PCF is evaluated with regards to it's percentage being above one. The mean of this fraction over all time frames and simulation runs of a spatial setting are taken as a measure of non-randomness. The results shown in figure 22 are in good agreement with the previously shown CSR results highlighting the r(PI3K)<r(PTEN) spatial settings. Those spatial settings that indicated predominantly clustering (>60%) were analyzed further to describe the formed signaling peak in more detail. Inspection of the PCF itself can yield information about internal structure of the pattern. However, determining the maximum of each time frame's PCF and evaluating the most prevalent radius over all time frames of a simulation did not indicate a relation between this radius and the spatial setting (figure 45, Appendix). The standard deviation associated with the radii determined in this analysis is quite high, indicating that the fluctuation is too high to be a useful characteristic of the signaling peak.

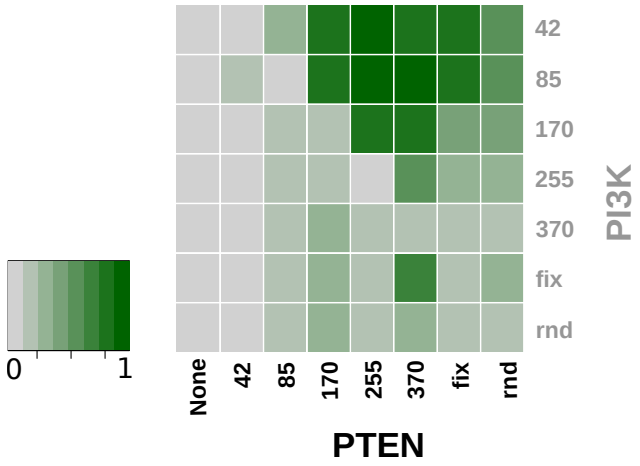

Figure 22: PCF analysis confirms PIP3 aggregates at the PSD
Given are the overall fractions for which the PCF g(r) > 1 over all time frames. Shown is the mean of this fraction over 5 simulation runs (mean values and standard deviation are given in table 9, Appendix).

3.4.8 The diameter of the signaling peak increases with r(PTEN) and r(PI3K)

From the visual inspection of pattern densities shown before it can be concluded that the clustered spatial settings are forming a central signaling peak. The extent of the signaling peak was quantified by averaging the pairwise longest distances per point (per time frame) of clustered patterns:

$$D = \frac{1}{n} \sum_{i=1}^{n} max(d(ij_{1 \leq j \leq n}))$$

The result is shown in figure 23 (means and standard deviations are given in table 9, Appendix).

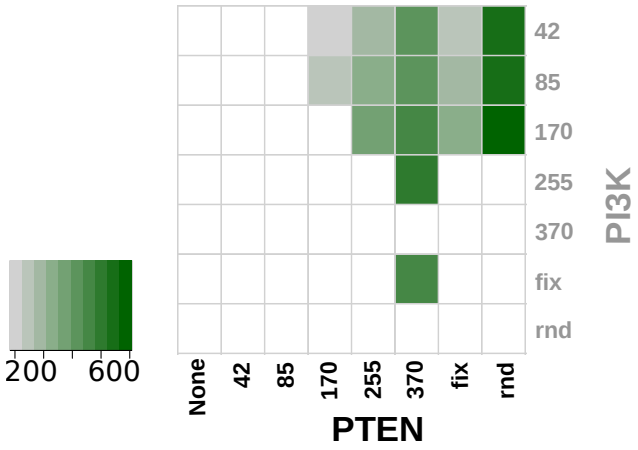

Figure 23: Diameter of PIP3 PSD aggregates depends on the spatial setup
The average diameter of the PIP3 PSD aggregates was calculated for those spatial setups that show a non- random distribution of PIP3 on the PSD surface in CSR testing and evaluation of the PCF. Shown is the mean diameter over 5 simulation runs for each setup (mean values and standard deviation are given in table 9, Appendix).

This quantification shows the expected relationship between increasing r(PTEN) and increasing peak diameter. Keeping r(PTEN) constant and increasing r(PI3K) results in an increase of peak diameter as well but the main determining factor is r(PTEN).
To automate this procedure in case of unknown or variable numbers of signaling clusters, a clustering algorithm can be used to determine the clusters themselves. The calculation of cluster diameters can then be done in the same way as before.

3.4.9 Summary

The simulation results suggest that the circular spatial setups with PI3K on the inner circle and PTEN on the outer are most efficient in focusing the signal to the PSD. To maintain a constant, stationary signaling peak, both - production and degradation - are necessary. Without this steady state, diffusion quickly dilutes any structural spatial characteristic. It seems favorable to keep the signal producer (PI3K) focused at the PSD. In general, focusing the signal works well as long as PTEN is spatially more spread than PI3K. While circular PTEN settings focus PIP3 better to the PSD than randomly fixing it to the PSD (see figure 15), randomly diffusing PTEN restores the focus. However, this goes along with an overall increase in signal at the PSD but also in the surrounding membrane area.
Spatial scenarios where r(PTEN)> r(PI3K) are the most efficient ones by means of signal at the PSD to overall signal. The amplitude of the produced signal depends on the spacing of kinase and phosphatases and seems to be more sensitive to changes in r(PTEN) than r(PI3K).
While the absolute steady state PIP3 levels depend on the spatial scenario, the speed at which the system approaches this steady state shows no dependency on the scenario.
CSR testing and the PCF also highlight these most efficient settings by indicating the non-random distribution of molecules on the PSD surface. In cases where both methods indicate clustering, the diameter of the central peak was determined and shows its dependence on phosphatase and kinase distance as well. Clustering algorithms can be combined with this analysis to determine clusters if more complex surface patterns are expected to form.
To finish with a general observation: systems with random distributed elements appear more noisy: Variation in between simulations is bigger especially for those settings that include a random fixed component. Settings containing randomly diffusing elements, especially circular PI3K and random PTEN settings are leaking more PIP3 molecules into the surrounding. This can be considered as noise if the purpose of the signaling system is to focus the signal to a certain location in space and time.
The sequence of analysis established in this chapter provides a tool set to analyze spatial properties of larger spatial signaling models with regards to

the spatial properties they are developing over time. These methods allow to quickly scan a large results data set for interesting spatial properties occurring over the time course of a simulation and to focus possible further analysis on them.

4 Discussion

The spatial properties of signaling systems have often been neglected in computational modeling of signaling systems in the past although different aspects of spatial organization and diffusion are discussed in the literature. The effects of phospho-protein signals forming a gradient are discussed by Brown and Kholodenko (1999) and Kholodenko et al. (2000). These gradients form due to the comparatively slow diffusion of the phospho-protein signal created by a membrane-bound kinase and the fast dephosphorylation by a cytoplasmic phosphatase. They potentially attenuate signal propagation in signaling cascades such as the MAPK cascade between the membrane and the nucleus if they are not overcome by scaffolds and active transport mechanisms (Kholodenko, 2002).

The study presented here shows another spatial property by illustrating how to focus and sustain the signal of a small, quickly diffusing lipid signaling molecule by production and degradation to a specific area of the membrane with the development and analysis of a simple "proof of concept" model for spatial signaling. The control of signaling pathways is usually seen as activation and deactivation of the signal producing and destructing components (short-term) and changes in production and/or degradation of them (long-term). On the spatial level it is recruiting of molecules to appropriate area. This example shows that merely the spatial arrangement of components could contribute to the fine tuning of a signals amplitude or adjusting it to the spatial extent of the area in question. This level of control takes effect after activation and recruitment of the signal producers/destructors.

A spatial configuration of signaling components like the ones identified as the most efficient ones above could be created in the environment of the spine in the vicinity of the PSD. PI3K class I kinases are heterodimers consisting of a catalytic p110 subunit and a regulatory subunit. The regulatory subunit

mediates binding of the kinase to tails of activated tyrosine kinase receptors such as TrkB via its SH2 domains. The location of PI3K is hence determined by the location of activated receptor. There are indications that TrkB is mainly lining up along the PSD (Drake et al., 1999; Petralia et al., 2005). It is possible that it forms a ring like structure inside the PSD. PTEN on the other hand is recruited by binding to PIP2 in the membrane via its C2 domain (Lee et al., 1999). PIP2 is present in the membrane surface regardless of receptor activation. PTEN might not be able to reach the membrane in the area of the PSD as the dense mesh of proteins should hinder free diffusion of larger molecules. PTEN, binding to PIP2 in the area around the PSD, could get caught by diffusive trapping when it reaches the PSD. This could create an outer ring to constrain the PIP3 signal to the PSD boundaries in proximity to PI3K. This tight control of signaling lipids is in line with observations that implicate enhancing effects on PTENs phosphatase activity by the PI3K p85 subunit (Chagpar et al., 2010). With regard to the size of the spine and the amount of molecules involved it is likely that such a spatial signaling pattern at the spine resembles the situation forming one single PIP3 patch or microdomains in other systems. Peripheral neuronal growth cones have a diameter of 100-400 nm (Martin et al., 2013) and the average size of lipid rafts is below 700 nm in diameter (Simons and Vaz, 2004). Visual inspection of single time step PIP3 densities suggest as well that one patch forms in case of ring-like spatial conformations but a random distribution of PIP3 in cases of random molecular conformations, even if one of the molecules or both are fixed as indicated by the CSR test. It seems unlikely that several PIP3 clusters form on the surface of a single PSD due to the spatial constrains and the low amount of molecules involved. However, large spines can exhibit more than one PSD and the surface of whole cells could have similar configurations of signaling molecules guided by special membrane environments and signaling complexes such as lipid rafts.

This analysis highlights, how important it is to consider the spatial properties of signaling systems. The "well-mixed" assumption often applied in systems biology models does not hold true and results vary based on the concrete spatial setup found in a system where all other parameters are kept constant (Enzymatic rate constants, diffusion coefficients and molecular numbers).

The battle of Helm's Deep is over;
the battle for Middle Earth is about to begin.
- Gandalf -

3 TrkB signaling in long-term potentiation

1 Introduction

Brain-derived neurotrophic factor (BDNF) and its receptor tropomyosin-related kinase B (TrkB) are known to play an important role in the processes of long-term potentation (LTP) at the postsynaptic sides of synapses (Minichiello, 2009). The diversity of the triggered pathways provide many different possibilities for cross-talk with the signaling pathways triggered by NMDAR-dependent LTP processes (see chapter 1). Studying the TrkB initiated signaling pathways will provide further insights into the finetuning of LTP and the signaling responses involved.

TrkB binds BDNF via two distinct binding sites (Haniu, 1997). BDNF itself is a short peptide, a dimer of two identical 100 amino acids (Ernfors and Bramham, 2003). TrkB dimerizes and autophosphorylates itself upon binding of BDNF providing binding sites for other kinases and signaling complexes such as the PLCγ and PI3K.

Phospholipase Cγ (PLCγ) is directly phosphorylated by the receptor when it binds to phosphorylated tyrosine residues in the tail for actived TrkB with its SH2 domain (Middlemas et al., 1994). Rapid activation of PLCγ was found as a response to BDNF stimulation in cell cultures from all major brain regions (Widmer et al., 1993) and LTP and learning were shown to be impaired in mice where the PLCγ binding site was mutated (Gruart et al., 2006).

The PI3K pathway was found to be required for the expression of LTP but not necessarily its induction (Sanna et al., 2002). PIP3 however, the main product

of PI3K activity, is required to maintain the distribution of AMPAR at the PSD and typical inhibitors of PI3K have a negative influence on this process (Arendt et al., 2010). PI3K does not bind to TrkB directly. Instead, a cascade of adapter proteins (Shc, Grb2 and Gab1) are recruited by the activated TrkB receptor (Minichiello, 2009). The adapter Grb2 was shown to interfere with one of the three activating PLCγ tyrosine residues suggesting a negative regulatory role of the PI3K activating scaffold on the PLCγ induced pathway (Choi et al., 2005). The modulation of phospholipid pools by PI3K and PLC and especially the production of phosphatidylinositol-3,4,5-trisphosphate (PIP3) by PI3K in the membrane deliver a precise spatial signal.
Khodakhah and Ogden (1995) were the first to show IP3 dependent release of Calcium from intracellular stores in neurons. At least 50% of the neuronal spine population seems to contain endoplasmic reticulum (ER) (Spacek and Harris, 1997). The ER itself seems to have a high frequency of turnover. Spines frequently lose and gain SER (Toresson and Grant, 2005) with larger mushroom shaped spines being more likely to contain ER (Spacek and Harris, 1997; Holbro et al., 2009). The importance of ER presence in hippocampal spines was demonstrated by deficits in learning and LTP in mice that do not have it in their spines (Deller et al., 2003). In addition, BDNF induced Calcium transients via IP3 receptors from intracellular stores were shown to induce the translocation of AMPA receptor GluR1 subunits to the postsynaptic membrane underlining its possible role in the studied signaling pathway (Nakata and Nakamura, 2007). In contrast to intracellular Calcium that is dominated by immediate binding of Calcium to buffering proteins, Calcium within the ER appears to be more mobile.Amongst the plethora of kinases that can be activated by Calcium is the family of protein kinase C (PKC). There are at least 11 isoforms of PKC present in humans (UniProt (The UniProt Consortium, 2012)). Their main catalytic characteristic is the phosphorylation of serine and threonine residues. PKCs are grouped into conventional PKC (cPKC), novel and atypical ones depending on their activation mechanism (Sossin, 2007). PKCα is the most common cPKC while PKCγ is the neuron specific cPKC. cPKCs are located in the cytoplasm in their inactive form with a pseudo substrate blocking its catalytic side. cPKC bind Calcium in the cytoplasm to become activated. This enhances the electrostatic interactions

of the enzyme with the plasma membrane. To become fully active, a pseudo substrate has to be released by DAG binding. Since DAG is located in the membrane, the enhanced electrostatic interactions increase the probability for PKC activation. This integrates Calcium and DAG signals and links TrkB activation to the phosphorylation of AMPARs via PKC. Novel PKCs differ from cPKCs in that they do not require Calcium for activation. DAG is sufficient.
In the hippocampus PKCλ/ι and PKMζ represent the atypical type. These kinases are not sensitive to Calcium and DAG. They get activated by PIP3 instead and the activation mechanisms are considered to be very similar (Selbie et al., 1993; Suzuki et al., 2003). Increasing evidence shows the activation of atypical kinases in the PI3K kinase signaling cascades downstream of tyrosine kinase receptors such as epidermal growth factor (EGF) and nerve growth factor (NGF) receptors (Akimoto et al., 1996; Wooten et al., 2000). The Trk family is one of the major NGF receptor families.

AMPAR are modified in various ways during LTP signaling to increase their conductance and change their trafficking behavior. The most abundant AMPAR forms present in the hippocampus are of the GluR1/GluR2 type. It appears to be their trafficking behavior that is changed predominantly during LTP (Adesnik and Nicoll, 2007; Gray et al., 2007). The GluR1 subunit has a cytoplasmic tail that contains several residues that are modified during LTP signaling and were associated with the changes in AMPAR numbers at the synapse and their conductance observed.

- Phosphorylation of Serine 818 by PKC facilitates AMPAR insertion into the postsynaptic site (Boehm et al., 2006). This interaction is most likely mediated by enhancing the binding of GluR1 to the PSD scaffolding protein 4.1N (Lin et al., 2009). Recent studies suggest, that serine 818 is phosphorylated by the atypical PKCλ/ι via PI3K induction (Ren et al., 2013).

- Serine 831 is phosphorylated by PKC and CaMKII (Barria et al., 1997). The main consequence of S831 phosphorylation are increases in the

conductance of AMPAR (Derkach et al., 1999; Jenkins and Traynelis, 2012).

- Serine 845 is the target of protein kinase A (PKA) mediated signaling (Roche et al., 1996). This residue seems to have a major role in promoting AMPAR insertion into the membrane and stabilizing it at perisynaptic sides (Oh et al., 2006). PKA mediated GluR1 phosphorylation was shown to be triggered in response to β_1 adrenergic (Amanda M Vanhoose, 2003) and D1 dompamine receptors (Price et al., 1999).

- Threonine 840 shows high basal phosphorylation in vivo and is rapidly turned over Lee et al. (2007). The phosphorylation itself is likely mediated by p70S6 kinase and counterbalanced by protein phosphatase 1 or 2A in response to NMDAR activity. Decreases in T840 phosphorylation during long-term depression (LTD) and no increase in LTP stimulating protocols suggest a regulatory role of this residue in LTD rather than LTP (Delgado et al., 2007).

Objectives

TrkB Signaling encompasses many interesting possibilities for signal integration and crosstalk. The activity flow diagram in figure 24 gives an overview of the signaling events described above that are further considered in this chapter.

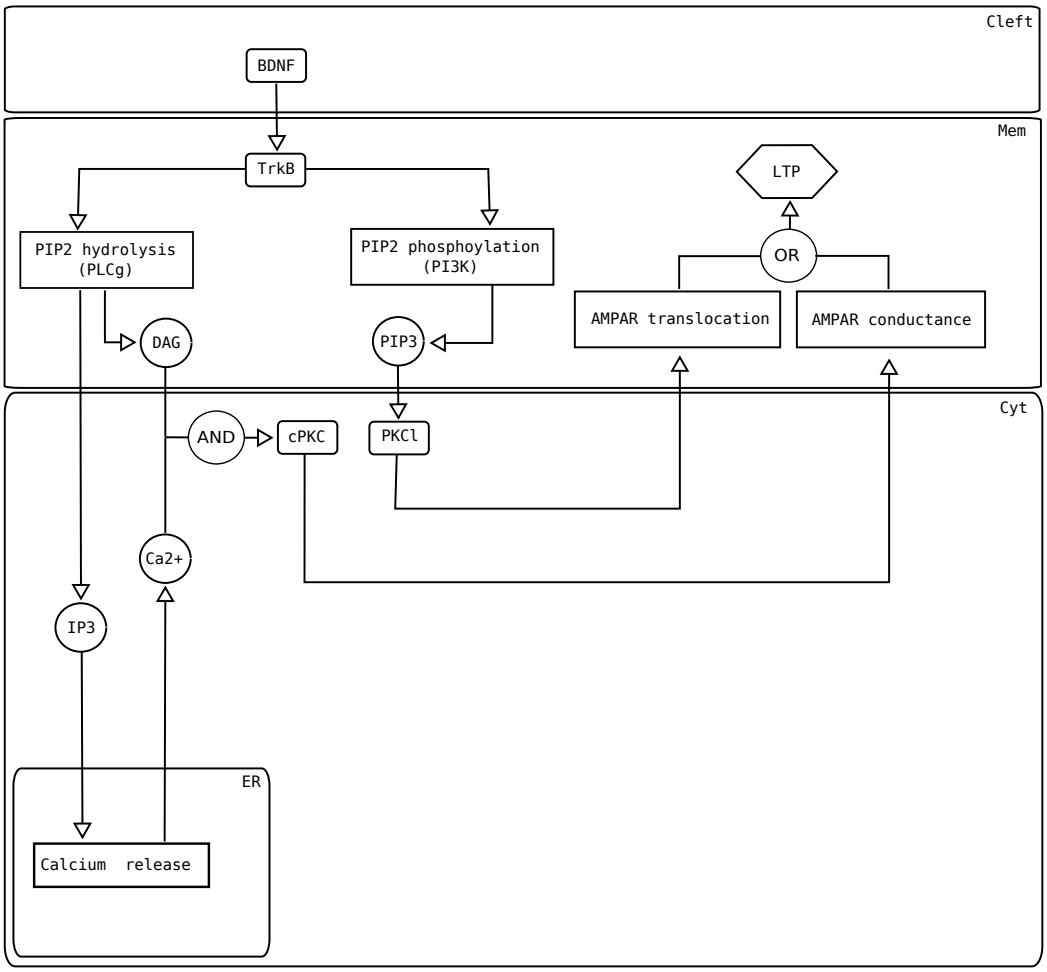

Figure 24: SBGN activity flow diagram (Le Novère et al., 2009) of the implemented spatial TrkB signaling model in the neuronal spine

When TrkB Signaling is initiated, the two enzymes PI3K kinase and PLCγ1 compete for the same substrate: PIP2. Their products IP3 (and the release of Calcium from intracellular stores), DAG and PIP3 in turn can activate different isoforms of the PKC family that were shown to phosphorylate AMPA subunits and modulate their behavior during the course of LTP. The spatial environment of these signaling events is highly compartmentalized and structured and it is important to notice that the second messengers produced and utilized in these pathways are acting in different spatial locations and dimensions. Phosphatidylinositol lipids and DAG contain fatty acids that confine them to membranes. Their signaling range is the membrane system of a cell which is two-dimensional. On the contrary, IP3 and Calcium are water-soluble and can diffuse through the cytoplasm. Their spatial signaling range is less restricted than that of lipids.
This chapter presents a computational model to aid the understanding of TrkB signaling events in space and time with regards to their effects of AMPAR phosphorylation. This biochemical model is explicitly integrated into an accurate three-dimensional representation of the neuronal spine. The small size of the system and the low molecule numbers require a stochastic model to allow for stochastic effects that might influence signaling outcomes.

2 Methods

The simulations in this chapter were run using the single particle stochastic simulator Smoldyn on the computing farm at the European Bioinformatics Institute as described in chapter 2. All reactions are modeled using mass action law (MAL) and catalytic reactions are split accordingly (see figure 2.2, chapter 2). The reaction parameters were found in the public model repository BioModels Database (Le Novère et al., 2006) if the corresponding reaction has been part of a deposited model before. If not, other database sources such as the Braunschweig Enzyme Database BRENDA (Schomburg et al., 2002) were used.Parameters were estimated from literature resources. Diffusion coefficients for the spatial three dimensional model were gathered from the literature or estimated as described in chapter 2 section 2.3.

The Smoldyn implementation of the model[1] was developed alongside an implementation for simulation with Copasi (Hoops et al., 2006) for the purpose of parameter estimation and general quick overview of the modeled system. This model implementation is a non-spatial single compartment model based on continuous molecule concentrations. The reaction structure and parameters are exactly the same as in the Smoldyn implementation. Molecular concentrations are adjusted to reflect the concentrations present in the various compartments of the Smoldyn model.
The analysis of the simulation results was performed using the statistical programming language R.

3 Results

The biochemical components of the model presented in this chapter are the PI3K and the PLCγ signaling pathways emanating from the TrkB receptor. They are two of the three main TrkB signaling pathways involved in long term potentiation. The third, the MAPK pathway is induced by PI3K as well, but it is mostly important for the late phase of long term potentiation and the induction of gene transcription which is not considered in this work. The PLCγ pathway triggers the release of Calcium from internal stores and produces the lipid messenger DAG while PI3K syntheses PIP3. The pathways converge in the activation of PKC and ultimately AMPAR phosphorylation changing its trafficking behavior.

3.1 Model setup

The diagram in figure 25 gives a detailed description of the modeled processes (see figure 24 above for an overview). The figure uses the Systems Biology Graphical Notation (SBGN) (Le Novère et al., 2009) to give a detailed graphical representation of the involved processes. All biochemical reactions corresponding to the diagram are listed with their corresponding parameters in table 5. The parameters were either reused from already published models or extracted from the literature. The references are given accordingly.

[1] The Smoldyn configuration files are availabe at https://github.com/yetime/SmoldynConfigs.git

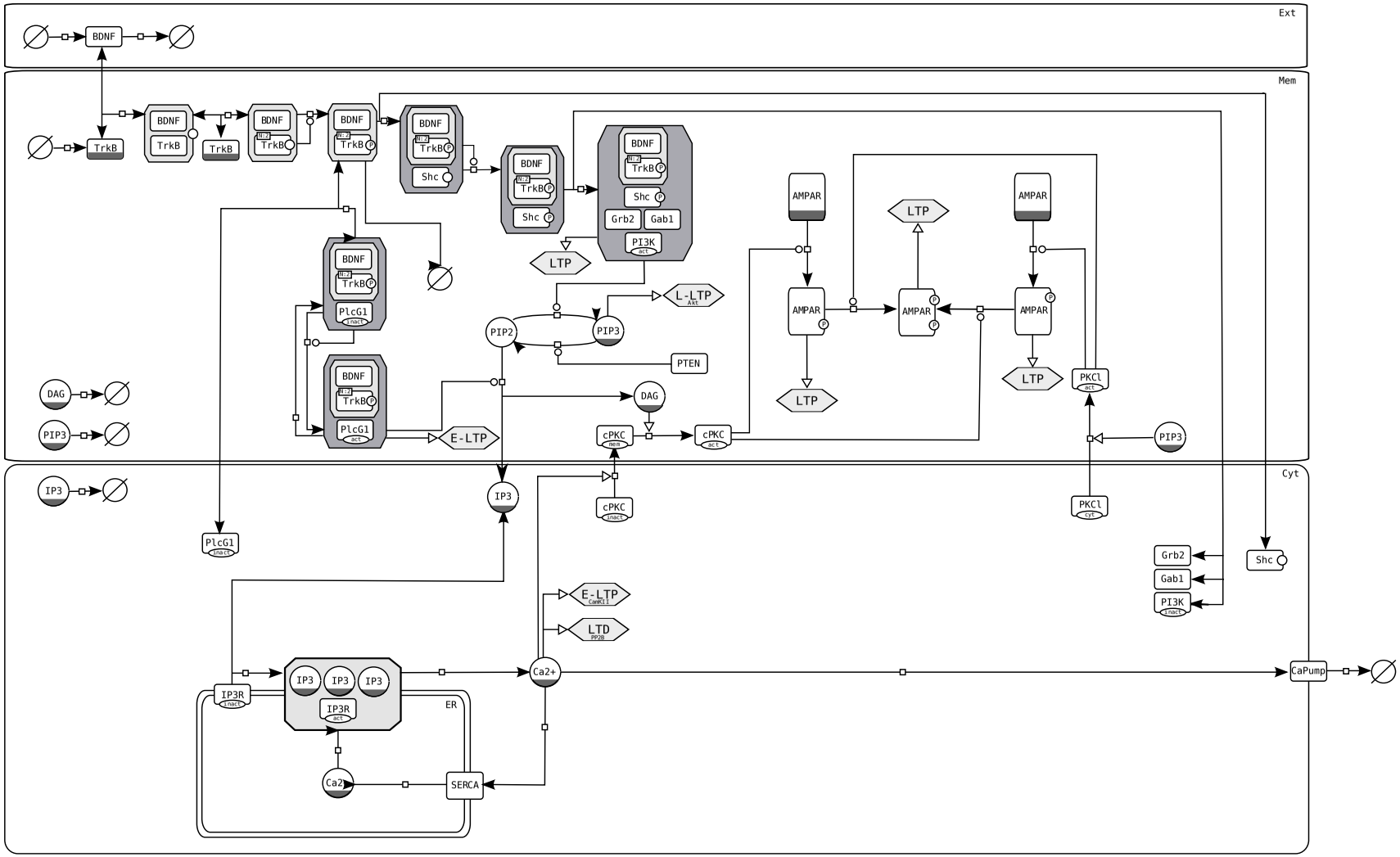

Figure 25: SBGN process description (Le Novère et al., 2009) of the implemented spatial TrkB signaling model in the neuronal spine

TrkB activation and dimerization			
R1:TrkB + BDNF ↔ BDNFTrkB			Jain and Bhalla, 2009
R1 kf	1660000	molecules $nm^{-3}\,s^{-1}$	
R1 kb	0.05 s^{-1}		
R2: BDNFTrkB + TrkB ↔ BDNF2TkB			Jain and Bhalla, 2009
R2 kf	1660000	molecules $nm^{-3}\,s^{-1}$	
R3: BDNF2TrkB → BDNF2TrkBP			Jain and Bhalla, 2009
R3 kf	0.02 s^{-1}		
TrkB receptor cycling and inactivation			
R4: BDNF2TrkB → 0			Jain and Bhalla, 2009
R4 kf	0.01 s^{-1}		
R5: 0 ↔ TrkB			Jain and Bhalla, 2009
R5 kf	0.0005 s^{-1}		
R5 kb	0.001 s^{-1}		
PLCγ1 Pathway			
R6: BDNF2TrkBP + PLCG1 ↔ PLCG1M → PLCG1MP			Jain and Bhalla, 2009
R6 kf	13800000	molecules $nm^{-3}\,s^{-1}$	
R6 kb	2 s^{-1}		
R6 kcat	0.5 s^{-1}		
R7: PLCG1MP → PLCG1			Jain and Bhalla, 2009
R7 kf	0.07 s^{-1}		
R8:PLCG1MP + PIP2 ↔ PlcG1MPPIP2 → IP3 + DAG + PLCG1MP			Bhalla and Iyengar, 1999
R8 kf	1200000	molecules $nm^{-3}\,s^{-1}$	
R8 kb	56 s^{-1}		
R8_kcat	14 s^{-1}		
PI3K Pathway			

R9: BDNF2TrkBP + Shc ↔ ShcM → ShcMP			Jain and Bhalla, 2009
R9 kf	2990236	molecules	
	$nm^{-3}\,s^{-1}$		
R9 kb	1.2 s^{-1}		
R9 kcat	0.3 s^{-1}		
R10: ShcMP → ShcM			Jain and Bhalla, 2009
R9 kf	0.2 s^{-1}		
R11: ShcMP + Grb2 ↔ ShcGrb2			Jain and Bhalla, 2009
R11 kf	1660578	molecules	
	$nm^{-3}\,s^{-1}$		
R11 kb	$1s^{-1}$		
R12:ShcGrb2 + Gab1 ↔ ShcGrb2Gab1			Jain and Bhalla, 2009
R12 kf	498173.4	molecules	
	$nm^{-3}\,s^{-1}$		
R12 kb	$1s^{-1}$		
R13: ShcGrb2Gab1 + PI3K ↔ PI3KM			Jain and Bhalla, 2009
R13 kf	8302889	molecules	
	$nm^{-3}\,s^{-1}$		
R13 kb	$0.08s^{-1}$		
R14:PI3KM + PIP2 ↔ PI3KMPIP2			Jain and Bhalla, 2009
→ PI3KM + PIP3			
R14 kf	8302889	molecules	
	$nm^{-3}\,s^{-1}$		
R14 kb	16 s^{-1}		
R14 kcat	4 s^{-1}		
R15: PTEN + PIP3 ↔ PTEN_PIP3			Yong et al., 2008
→ PTEN + PIP2			
R15 kf	8302889	molecules	
	$nm^{-3}\,s^{-1}$		
R15 kb	0.5 s^{-1}		
R15 kcat	5 s^{-1}		
IP3 Receptor			
R16a:IP3R + IP3 ↔ IP3RIP3			Maeda et al., 2006

R16a kf	265692461	molecules $nm^{-3}\,s^{-1}$	
R16a kb	3	s^{-1}	
R16b:IP3RIP3 + IP3 ↔ IP3R2IP3			Maeda et al., 2006
R16b kf	265692461	molecules $nm^{-3}\,s^{-1}$	
R16b kb	2	s^{-1}	
R16c: IP3R2IP3 + IP3 ↔ IP3R3IP3			Maeda et al., 2006
R16c kf	265692461	molecules $nm^{-3}\,s^{-1}$	
R16c kb	1	s^{-1}	
R17: IP3R3IP3 + CaER → IP3R3IP3 + CaCyt			Maeda et al., 2006
R17 kf	24909	molecules $nm^{-3}\,s^{-1}$	
Calcium pumps			
R20: Serca + CaCyt → SercaCa + CaCyt → Serca2Ca			Maeda et al., 2006
R20 kf1	9133178	molecules $nm^{-3}\,s^{-1}$	
R20 kf2	8302889	molecules $nm^{-3}\,s^{-1}$	
R20 kb	3	s^{-1}	
R21: Serca2Ca → Serca + CaER + CaER			Maeda et al., 2006
R21 kf	1	s^{-1}	
R22: ExtCaPump + CaCyt → CaExtPumpCa →CaExtPump			Maeda et al., 2006
R22 kf	1017103952	molecules $nm^{-3}\,s^{-1}$	
R22 kb	19.6	molecules s^{-1}	
R22 kcat	4.9	molecules s^{-1}	
cPKC and AMPAR			
R23a: cPKC + CaCyt ↔ PKC_Ca			Maurer et al., 1992
R23a kf	21587512	molecules $nm^{-3}\,s^{-1}$	

R23a kb	0.1 molecules s^{-1}	
R23b: cPKC_Ca + CaCyt ↔ PKC_2Ca		Maurer et al., 1992
R23b kf	21587512 molecules $nm^{-3}\,s^{-1}$	
R23b kb	0.1 molecules s^{-1}	
R23c: cPKC_2Ca + CaCyt ↔ PKC_3Ca		Maurer et al., 1992
R23c kf	21587512 molecules $nm^{-3}\,s^{-1}$	
R23c kb	0.1 molecules s^{-1}	
R24: cPKC_3Ca + DAG ↔ PKC_3CaDAG		Ananthanarayanan et al., 2003
R24kf	16605779 molecules $nm^{-3}\,s^{-1}$	
R24kb	0.1 molecules s^{-1}	
R25: cPKC_3CaDAG + AMPAR ↔ PKC_AMPAR → cPKC_3CaDAG + AMPAR_P		Invitrogen[2]
R25 kf	183000 molecules $nm^{-3}\,s^{-1}$	
R25 kb	13.2 molecules s^{-1}	
R25 kcat	146 molecules s^{-1}	
PKCλ and AMPAR		
R26: PKCλ + PIP3 ↔ PKCλM		Invitrogen[3]
R26 kf	8302889 molecules $nm^{-3}\,s^{-1}$	adjusted according to Nakanishi et al., 1993
R26 kb	0.5 molecules s^{-1}	
R27: PKCλM + AMPAR ← AMPAR_P2		see R26
R27 kf	183000 molecules $nm^{-3}\,s^{-1}$	
R27 kb	13.2 molecules s^{-1}	
R27 kcat	146 molecules s^{-1}	

[2]Invitrogen Corporation, 1600 Faraday Avenue Carlsbad, CA92008, PRKCG (PKC gamma) Recombinant Human Protein, P2233, 39126l

[3]Invitrogen Corporation, 1600 Faraday Avenue Carlsbad, CA92008, Recombinant Human Protein Kinase C Iota, PV3183, 29127C

cPKC/PKCλ and AMPAR_P1/P2		
See reaction R25 and R27, respectively		
Substrate in R25/R27: AMPAR_P2/AMPAR_P1		
Product in both cases: double phosphorylated AMPAR_P1P2		
AMPAR scaffold binding		
R28: AMPAR_P2/P1P2 ↔ AMPAR_Stat		adjusted Czöndör et al., 2012
R28 kf	0.001 s^{-1}	and Nakata and Nakamura, 2007
R28 kb	0.00001 s^{-1}	
Signal shutdown		
R21a: IP3 → 0		Maeda et al., 2006
R21a kf	2.5 s^{-1}	
R21b: DAG → 0		Maeda et al., 2006
R21b kf	0.15 s^{-1}	
R21c:BDNF → 0		Jain and Bhalla, 2009
R21c kf	0.1s^{-1}	
R21d: PIP3 → 0		Jain and Bhalla, 2009
R21d kf	0.01s^{-1}	

Table 5: Parameters of biochemical reactions
This table lists all of the implemented biochemical reactions with the chosen parameters and their references. Molecular species in the cytosol, ER or the cleft that diffuse in three dimensions are colored in blue to distinguish them from those located at the membrane and indicate those reactions that are transitions of molecules from the cytoplasm to the membrane.

Diffusion coefficients were extracted from the literature. In cases where none were found, they were estimated based on the molecular weight according to Young et al. (1980) as described in chapter 2.3. The same estimate was used to calculate the diffusion coefficients of complexes based on the sum of their molecular weights. The estimated diffusion coefficients for molecules located at the membrane were reduced by a factor 1000 since diffusion is approximately 100 to 1000 times slower in the membrane compared to the cytoplasm (McCloskey and Poo, 1986). Table 7 lists the modeled diffusion

Table 6: Diffusion coefficients of the monomeric model components and their sources
This table lists the diffusion coefficients used to model the molecular movement of monomeric components in the cytosol (cyt) and on the membrane (mem). Estimates for complexes are based on the sum of their molecular weights.

	D cyt [$\mu m^2 s^{-1}$]	**D mem** [$\mu m^2 s^{-1}$]	**Reference**
BDNF	45	-	Stroh et al., 2004
TrkB	-	0.023	est. Young et al., 1980
PLCγ1	19	0.019	est. Young et al., 1980
Shc	26	0.026	est. Young et al., 1980
Gab1	24	0.024	est. Young et al., 1980
Grb2	35	0.035	est. Young et al., 1980
IP3R	-	0.017	Pantazaka and Taylor, 2011
Serca	-	0.029	est. Young et al., 1980
PKCγ	5.45	0.00545	Craske et al., 2005
PKCλ	24	0.024	est. Young et al., 1980
AMPAR	-	0.045	Tolle and Novère, 2010
AMPAR Scaffold	-	0	fixed
Calcium	400	-	Holcman et al., 2004
PI3K	17	0.017	est. Young et al., 1980
PTEN	28	0.028	est. Young et al., 1980
PIP2	-	0.08	Xu et al., 2003
PIP3	-	0.08	Xu et al., 2003
DAG	-	0.4	Prieto et al., 1994 Vaz and Almeida, 1991
IP3	283	-	Allbritton et al., 1992

coefficients.

Molecular numbers are based on concentrations used in published models or were found in the literature. Molecular densities are hardly found for proteins. In those cases, concentration based values were transformed into molecular densities taking the cellular volume and surface area into account. The spine surface is modeled as described previously in chapter 2 section 3 with the dimensions given in chapter 2 table 3. The geometry of the model was extended as illustrated in figure 26. This extension involves an explicit

Table 7: Initial molecule numbers
This table lists the initial molecule numbers at the start of a simulation and their location.

	Initial molecule numbers	Location	Reference
TrkB	20	PSD	Jain and Bhalla, 2009
PIP2	2107	membrane	Xu et al., 2003
PTEN	81	membrane	Maeda et al., 2006
IP3R	64	SER memrane	Maeda et al., 2006
Serca	64	SER membrane	Maeda et al., 2006
CaExtPump	30	membrane	Maeda et al., 2006
AMPAR	66	Spine	Tolle and Novère, 2010
AMPAR	100	PSD	Chen et al., 2011; Nicholson et al., 2006
PLCG1	30	cytoplasm	Jain and Bhalla, 2009
Shc	150	cytoplasm	Jain and Bhalla, 2009
Grb2	301	cytoplasm	Jain and Bhalla, 2009
Gab1	210	cytoplasm	Jain and Bhalla, 2009
PI3K	30	cytoplasm	Jain and Bhalla, 2009
CaER	750	SER	Maeda et al., 2006
cPKC	30	cytoplasm	estimate, similar to other kinases in the system
PKCλ	30	cytoplasm	estimate, similar to other kinases in the system

representation of the smooth endoplasmic reticulum (SER) as Calcium store (figure 26, red) and the synaptic cleft as compartment for the release of BDNF (figure 26, blue). The volume of the SER is set up to be 1.5 % of the spines volume (Harris and Stevens, 1988). The size of the cleft spans the area of the PSD and has a width of 20 nm (Zuber et al., 2005).

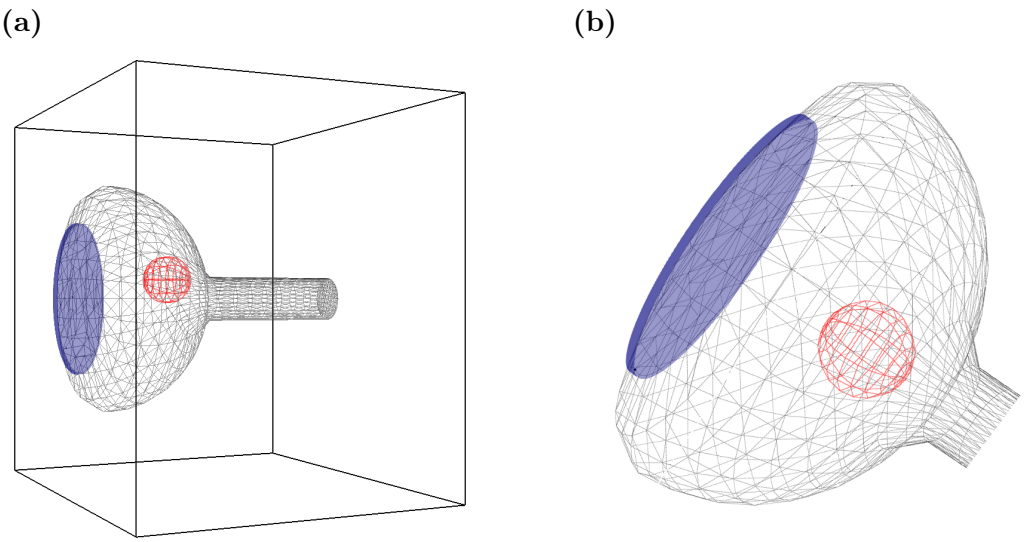

Figure 26: Illustration of the models geometry
(a) Illustration of the implemented geometry of the model.
(b) Magnification of the spine head.
The red sphere represents the SER and the thin blue cylinder the synaptic cleft on top of the postsynaptic density.

The number of AMPAR at the PSD is used as a measure for the strength of LTP assuming that this is proportional to the excitatory postsynaptic current (EPSC) because the single channel currents sum up. AMPAR phosphorylated at S831 have a higher conductivity and contribute more to the current. Therefore, their number is weighted by 1.8 to account for the increased conductance based on Jenkins and Traynelis (2012).

3.2 The onset of TrkB signaling is characterized by the competition of PI3K and PLCγ for their common substrate PIP2

The first upstream layer of signaling events is characterized by the competition of the two enzymes PI3K and PLCγ that utilize the same substrate (see figure 24 and 25). The previously described model was truncated downstream of PI3K and PLCγ to analyze the onset of signaling events as illustrated in figure 27.

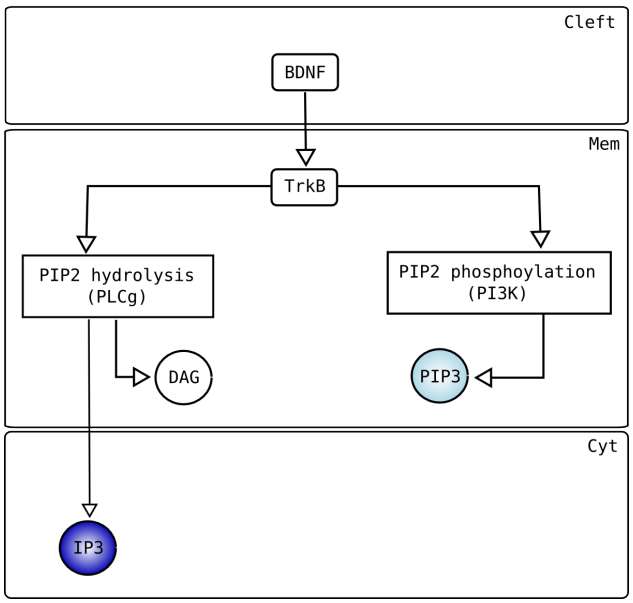

Figure 27: Activity flow of the truncated TrkB signaling model
The readouts that are used in this analysis are colored according to later usage: IP3 as readout for PLCγ activity in darkblue and PIP3 as readout for PI3K activity in lightblue

The model was simulated with varying levels of BDNF as stimulus corresponding to BDNF stimulation protocols found in the literature between 10 and 500 $\mathrm{ng\,ml^{-1}}$. Molecule numbers were calculated based on the volume of the synaptic cleft and BDNF molecules were released into the synaptic cleft. Each simulation was repeated 10 times with the same amount of BDNF The timecourses of PIP3 and IP3 development in the model were monitored over 300s.

The simulation results appear to fall into four major categories based on the onset of IP3 and PIP3 production and the overall dominant signaling molecule produced by the end of the simulation. The different categories are illustrated with examples in figure 28. Category II represents timecourses with IP3 being the first molecular species produced and remaining the dominant species (figure 28a). The same initial conditions can also give rise to simulations that are characterized by an earlier onset of PIP3 production and PIP3 remaining the dominant species (Category PP, figure 28b). Between those are the intermediate categories IP (early onset of IP3 signal production but PIP3 being the dominant species in the end, figure 28c) and PI, the opposite of IP (figure 28d).

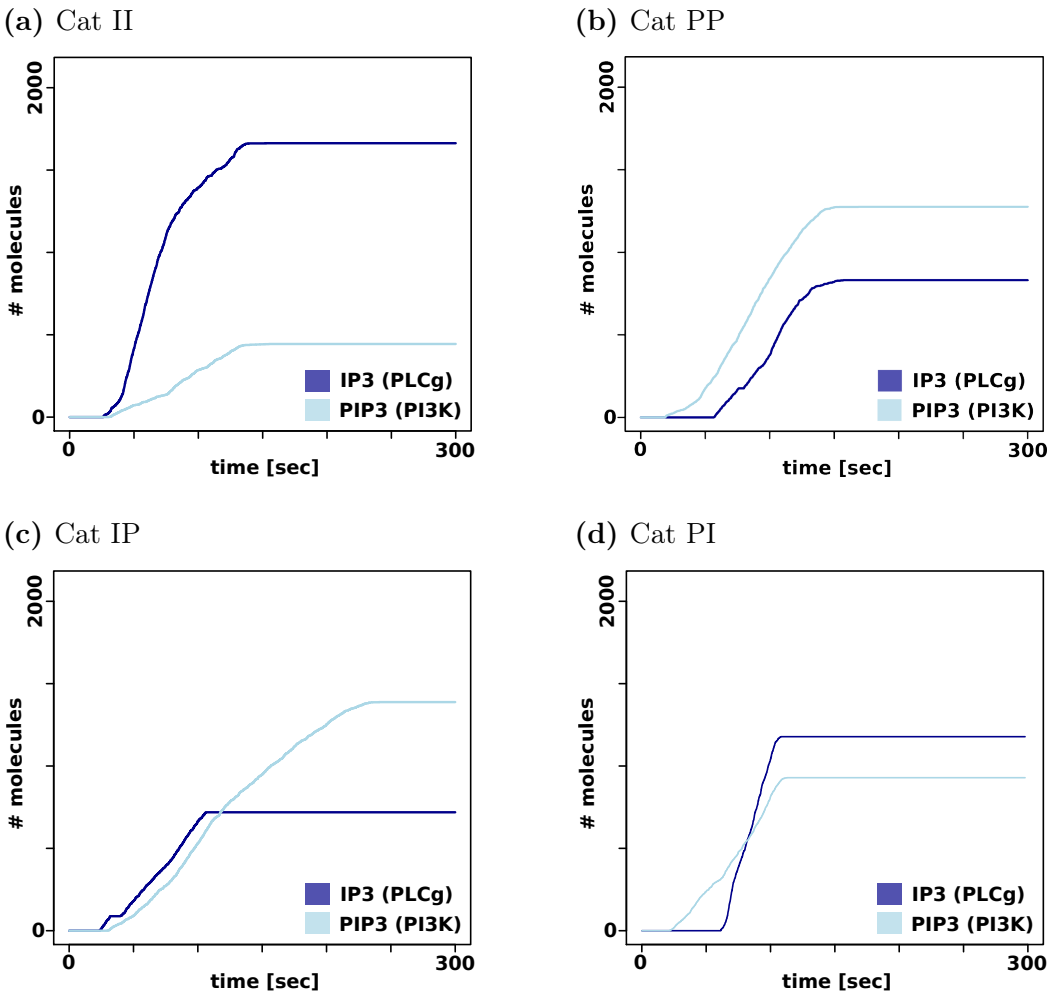

Figure 28: Different signaling outcomes of the PI3K and PLCγ signaling pathways

The figures show timecourses of single simulation runs showing IP3 (darkblue) as readout for PLCγ activity and PIP3 (lightblue) for PI3K. These timecourses illustrate the four different principal results of PLCγ and PI3K competition for PIP2.

(a) IP3 is the first product to rise and shows the higher overall signal levels.

(b) PIP3 is the first product to rise and shows the higher overall signal levels.

(c) IP3 rises first but PIP3 reaches the overall higher signal level.

(d) PIP3 rises first but IP3 reaches the overall higher signal level.

The ten different simulation runs for each BDNF stimulus are composed of these categories with varying contributions of each of them. Figure 29 depicts the different percentage with which each category is observed depending on the BDNF stimulus. Interestingly, most simulations fell into the PP category at low concentrations of BDNF indicating a dominance of PI3K signaling while high concentrations of BDNF evoke PLCγ dominance. The intermediate categories PI and IP follow a similar pattern as the II and PP categories respectively as shown in figure 29a. This indicates that the common characteristic is rather the dominance of one signaling pathway at the end than the onset of it. Combining PI with II and IP with PP yields an even clearer result. Low concentrations of BDNF are followed by dominance of the PI3K pathway while high concentrations of BDNF are characterized by PLCγ dominance (see figure 29b).

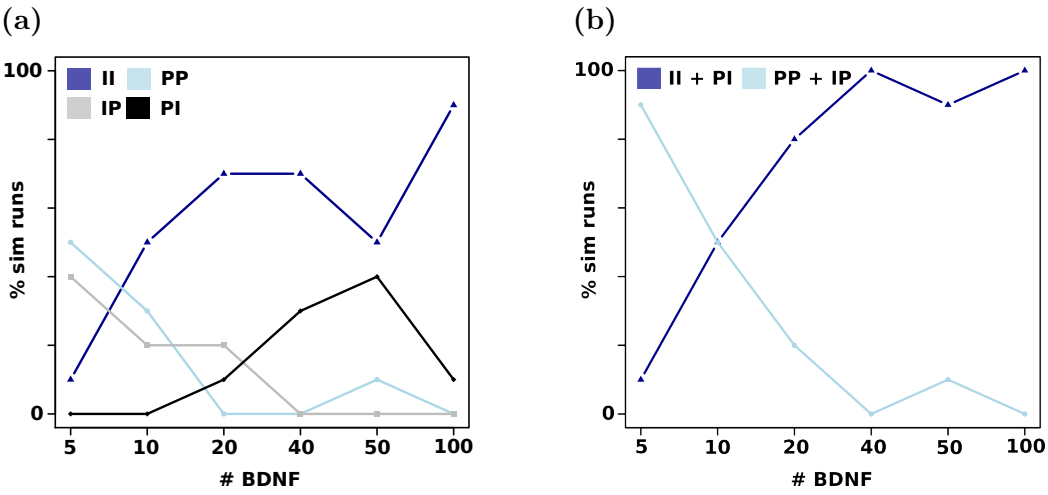

Figure 29: IP3 and PIP3 levels depend on the BDNF stimulus
The figures show the dependency of BDNF/TrkB signaling output on the applied BDNF stimulus. The percentage of signaling results categorized according to figure 28 are shown.
(a) Low BDNF stimulus concentrations result in PIP3 being the main signal produced by PI3K from PIP2 while high BDNF concentrations result in a shift towards IP3 and PLCγ. Category IP follows a similar relation as PP and category PI is similar to II.
(b) Grouping IP with PP and PI with II indicates that the concentration dependence mainly manifests in the final signaling outcome but not the onset of the reactions.

3.3 AMPAR potentiation depends on the upstream signaling outcome

The influence of the concentration dependent signaling outcome at the level of PI3K and PLCγ was analyzed further downstream in the signaling pathway. Specifically, signal integration at the level of AMPAR behavior is of interest. To be able to compare the outcome of the full model simulation to those of the truncated model, the same set of random seeds was used to initialize the simulations. Four typical examples of AMPAR behavior are shown in figure 30. The figures give the total number of AMPAR located at the PSD in red. The purple timecourse profile represents AMPAR numbers as well, but those receptors that are phosphorylated at S831 by cPKC have the previously stated weight of 1.8 to account for their increased conductance, while the red profile is only counting the unweighted numbers of all present forms of AMPAR. With this in mind, figure 30a shows the time course of synaptic potentiation due to conductance change (cPKC phosphorylation) indicated by the increased spacing between the red and purple lines. Figure 30b shows the opposite, potentiation due to trapping of more AMPAR at the PSD (PKCλ phosphorylation) with no conductance change at all. The lower row of figures illustrates combined outcomes with most of the conductance changes happening before more AMPARs get trapped (30c) and increases due to trapping and then conductance changes (30d).
Overall, low concentrations of BDNF stimulus result in most simulations showing either one or the other mode of potentiation but rarely both while increasing concentrations assure that both pathways are activated as depicted in figure 31.

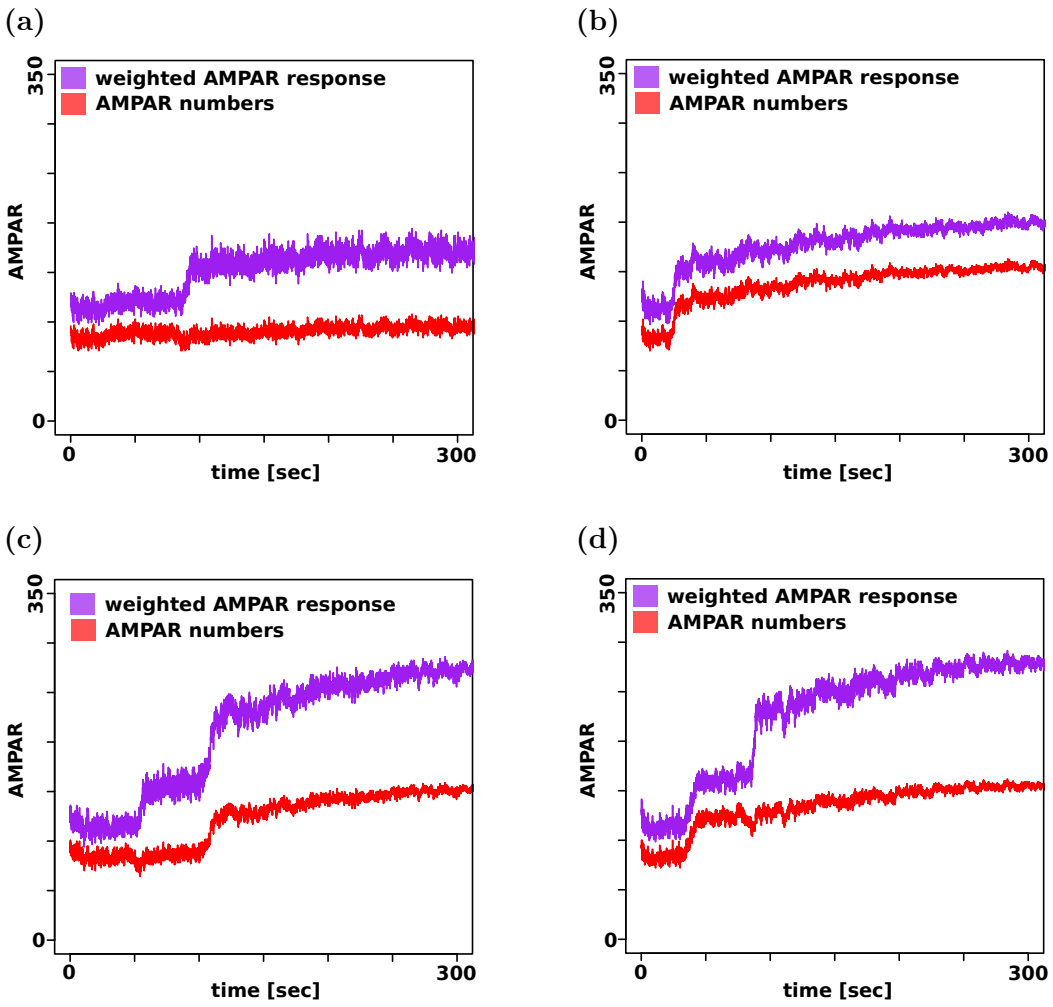

Figure 30: The four AMPAR phosphorylation responses to TrkB activation

The figures illustrate the four principal responses of AMPAR at the PSD to the BDNF stimulus. The red line gives the total number of AMPAR present at the PSD while the purple line gives the weighted number of AMPAR at the PSD indicating the strength of the potentiation as a result of S831 phosphorylation by cPKC increasing AMPAR conductance.

a) Potentiation of the synapse as result of changes in AMPAR conductance only.

b) Potentiation of the synapse as result of changes in AMPAR trapping only.

c) Potentiation of the synapse due to both effects, onset of changes in AMPAR conductance happens before changes in trapping behavior.

d) Potentiation of the synapse due to both effects, onset of changes in AMPAR trapping behavior happens before changes in conductance.

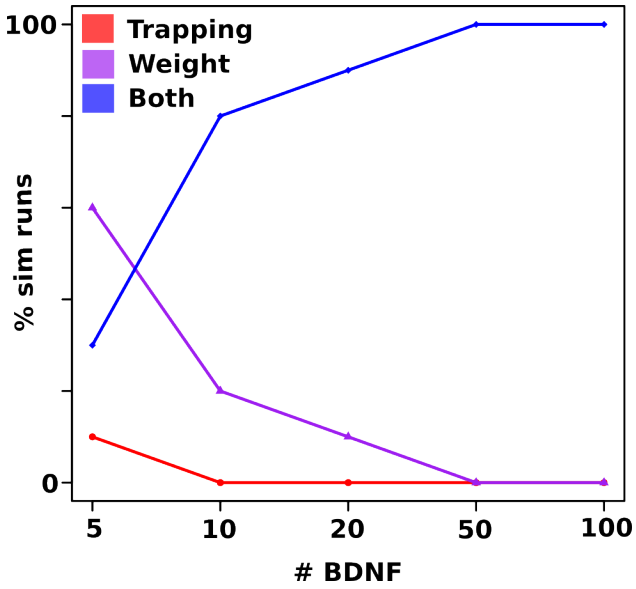

Figure 31: Increases in BDNF concentration ensures both potentiation pathways to be effective
The dependency of AMPAR potentiation on the strength of the BDNF stimulus is illustrated by giving the percentage of simulation runs that show either the weighted (purple), the trapped (red) or a combined (blue) response (compare figure 30). Increasing the amplitude of the BDNF stimulus increases the overall percentage of both pathways being active while low concentrations mostly trigger the cPKC pathway resulting in conductance changes of already PSD resident AMPAR.

Interestingly, these results do not immediately follow from the analysis of upstream events at the level of PI3K and PLCγ. However, the level of PKC activation is located between upstream events and those happening at the level of AMPAR representing another level of signal integration. Looking at the levels of PKCλ activation, the kinase that is activated by PIP3 and phosphorylates S818 that traps AMPAR, one notices that low concentrations of BDNF stimulus fail to activate it in contrast to cPKC. If PKCλ gets activated, the activation is higher at low concentrations than observed at higher stimuli, see figure 31. The values shown in this figure are computed by integrating the amounts of active PKC isoforms over time for each simulation run and BDNF concentration and then averaged (time courses without activation of the respective kinases are not included in the calculation of the mean). cPKC does not show a dependence of activation levels on the BDNF stimulus in contrast to PKCλ. Significance in the difference between active PKCλ at the PSD at very low and very high concentrations are significant between 0 and 50 BDNF and 0 and 100 BDNF as indicated by the grey bars in figure 32 (Student's T-Test, significance level 5%).

Of further interest is the ratio of kinase activity at the PSD compared to the rest of the membrane. The BDNF stimulus is highly localized within the synaptic cleft while the small molecules and kinases diffuse across the whole membrane. Figure 32b gives the ratio of active kinases at the PSD over active PKC kinases across the rest of the membrane. Assuming an even distribution of active kinases over the membrane solely based on the diffusion properties of them, the expected ratio would be around 8% of kinases located at the PSD (based on the ratio of the PSD to extrasynaptic membrane area). Figure 32b indicates that the levels of kinases are between 20-30%, which is higher than the expected value. This ratio does not show stimuli dependency but it illustrates that the overall activation of signaling tends to happen closer to or within the PSD area where the entire signaling pathway is triggered.

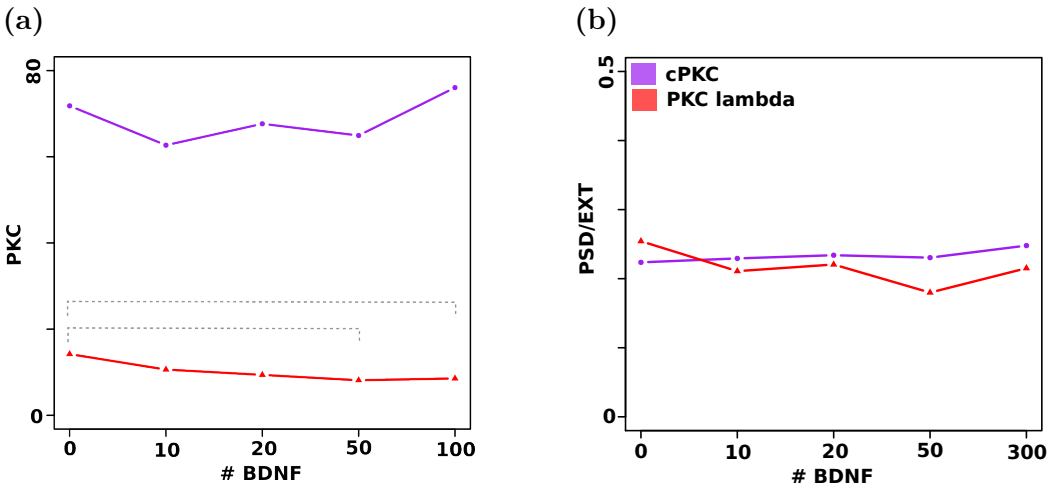

Figure 32: The PSD ratio of active PKC isoforms is similar across all stimuli concentrations

The figures illustrates the overall amount of active PKC kinases in dependency of the BDNF stimulus. Results for cPKC are given in purple, PKCλ is shown in red. The compared values are active kinases over time as calculated as integral of single PKC timecourses. Each value is the average over 10 simulation runs.

a) Total of active kinase for the PSD. Each datapoint represents the mean over 10 simulation runs (σ: +- 20-30 for cPKC and 2.2 - 4.6 for PKCλ) The grey lines denote two pairs that are significantly different)

b) Ratio of active kinases between PSD and spine. The dotted line gives the expected ratio of 0.08 based on the ratio of PSD to total membrane area. Each datapoint represents the mean over 10 simulation runs (σ: +- 0.06 - 0.2)

3.4 The special diffusion environment of the PSD could increase signaling efficiency

In the previous model, diffusion coefficients (except for AMPAR) were treated as being the same over the entire membrane surface. However, the high density of the PSD creates a specific environment for diffusion where not only AMPAR get trapped but also the diffusion of other molecules might be influenced. Another set of simulation runs of the full model were performed to analyze, if the diffusive properties of the PSD have an additional positive effect and focus the signal more efficiently to the PSD. This time, a ten times slower diffusion coefficient was assigned to every involved protein component when it is located at the PSD. The results are shown in figure 33.

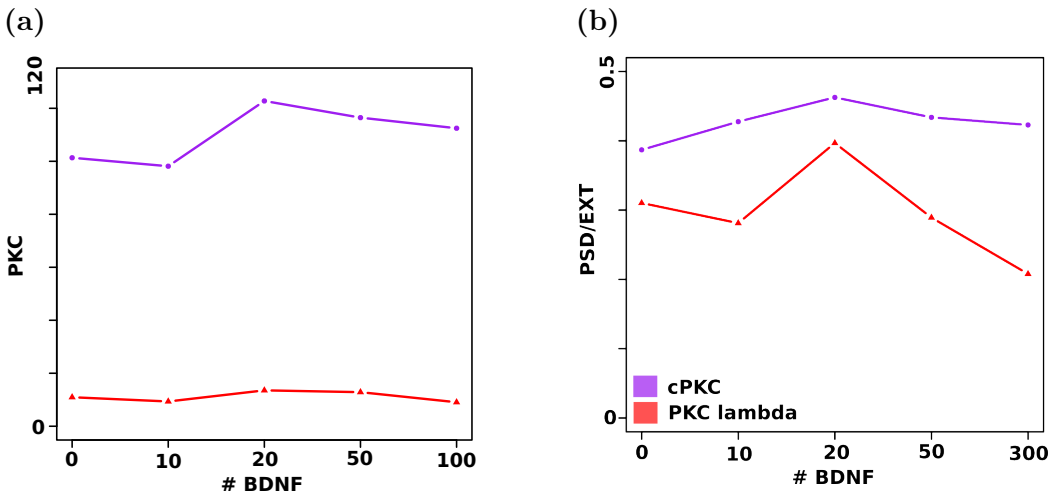

Figure 33: Slower diffusion of proteins at the PSD focuses the signal towards the PSD membrane
a) Total of active kinase for the PSD. Each datapoint represents the mean over 10 simulation runs (σ: $\pm$ 20 to $\pm$ 35 for cPKC and $\pm$ 3.1 to $\pm$ 5.6 for PKCλ)
b) Ratio of active kinases between PSD and spine membrane. Each data point represents the mean over 10 simulation runs (σ: $\pm$ 0.05 to $\pm$0.08)

Comparing PKC activation in this scenario with that of the previous section indicates an increase of overall active PKC kinases at the PSD as manifested in total number of active kinases at the PSD and the ratio of kinases between the PSD and the rest of the membrane.
The increase is significant compared to the results in the previous section (Student's T-Test, significance level 5%). The downstream effect at the level of AMPAR phosphorylation appears to be a shift of the previously shown behavior towards lower concentrations of BDNF (see figure 34). The signaling pathways are more efficient in phosphorylating both S831 and S818. This creates a more reliable potentiation effect at lower concentrations of BDNF. It illustrates the positive effect of increased local concentration of signaling molecules due to diffusion trapping at the PSD on the downstream signaling events.

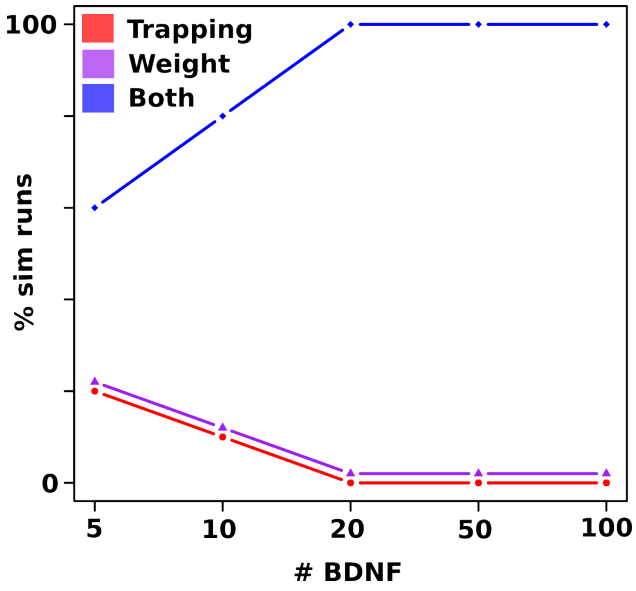

Figure 34: The special diffusion environment of the PSD allows more reliable AMPAR potentiation
The dependency of AMPAR potentiation on the strength of the BDNF stimulus is illustrated by giving the the percentage of simulation runs that show either the weighted(purple), the trapped(red) or a combined (blue) response (compare figure 30). Full potentiation caused by both PKC pathways is already achieved at lower BDNF concentrations compared to the results shown before (figure 31)

3.5 Partial inhibition of PLCγ results in a more reliable activation of both AMPAR potentiation pathways

Choi et al. (2005) reported an inhibitory effect of Grb2 on PLCγ activation in case of epidermal growth factor (EGF) receptor signaling. EGF is another tyrosine kinase receptor with very similar signaling properties to TrkB. The model studied in the previous paragraphs was expanded by an additional reaction inactivating PLCγ to address the potential influence of this inhibition on the signaling pathways. The inactivation was set up to achieve the reported 40-50% reduction in IP3 production. The results in dependency of the BDNF stimulus are shown in figure 35. They indicate a shift towards PIP3 dominated signaling of the IP type (compare categories in figure 28). The influence of BDNF concentration itself is much less pronounced.

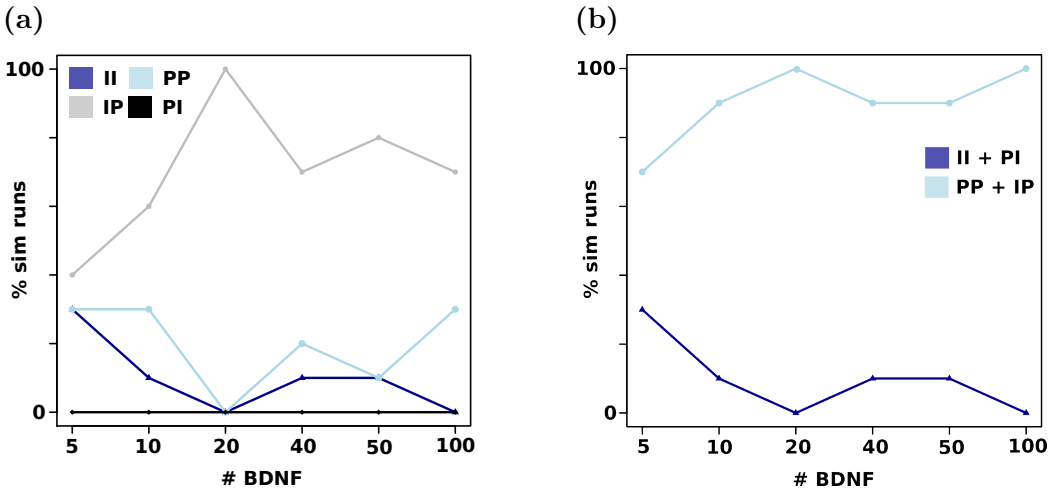

Figure 35: Partial inhibition of PLCγ stabilizes TrkB signaling events
The figures show the dependency of BDNF/TrkB signaling output on the applied BDNF stimulus categorized as in figure 29. The implemented partial inhibition of PLCγ results in a more efficient phosphorylation of both residues with regard to the applied BDNF stimulus. The most abundant signaling outcome is of the IP type (compare figure 28c). (a) and (b) as in figure 29

The downstream signaling effects of Grb2 inhibition on AMPAR potentiation are given in figures 36 and 37. The main observable effect at the PKC integration level is a decrease in total active cPKC at the PSD (see figure 36b with a tendency to increase with higher BDNF stimuli. The ratio of PKC distribution is similar to the observed one for the non-inhibited model (figure 32b).

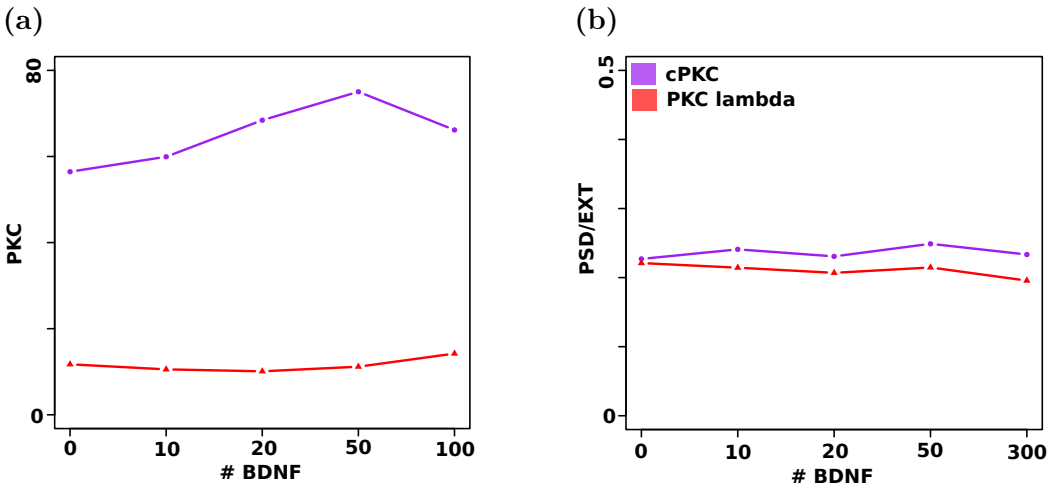

Figure 36: Inhibition of PLCγ changes the activation of cPKC
Partial inhibition of PLCγ reduces the amount of activated cPKC especially for low concentrations ofthe BDNF stimulus. The overall ratio of signaling molecules at the PSD is similar to the previously observed ones (see figure 32. a) Total activity of the kinases at the PSD. Each data point represents the mean over 10 simulation runs (σ: $\pm$ 13 to $\pm$ 20 for cPKC and 3.3 - 9 for PKCλ)
b) Ratio of active kinases between PSD and spine. Each data point represents the mean over 10 simulation runs (σ: $\pm$ 0.03 to $\pm$ 0.04)

The effect of partial PLCγ inhibition at the level of AMPAR potentiation is again an increase in the reliability to activate both pathways (the cPKC and the PKCλ pathway) ensuring maximal potentiation. Especially for higher concentrations, potentiation due to trapping occurs shortly before conductance increases (see figure 30d). This shows, together with the shift in the dynamics of IP3 and PIP3 production shown before towards and early IP3 and late PIP3 dominated timecourse, that higher levels of PIP3 later on ensure the activation of PKCλ although cPKC signaling starts earlier. The PKCλ pathway appears to be the faster one.

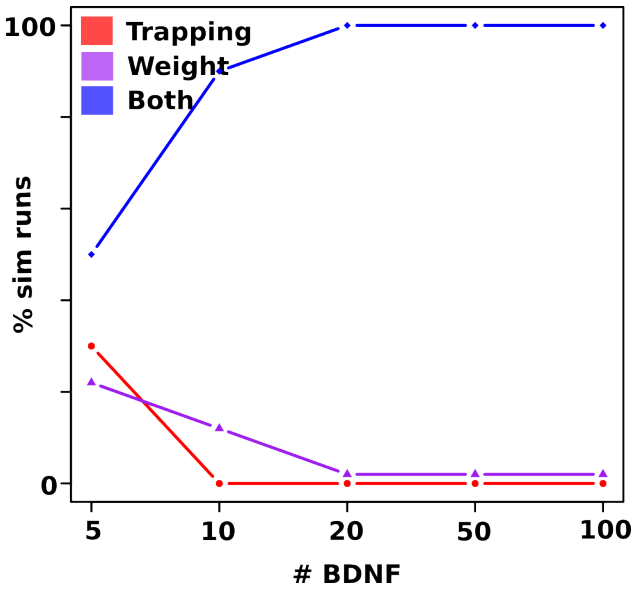

Figure 37: Inhibition of PLCγ influences AMPAR potentiation
Partial PLCγ inhibition could create more reliable AMPAR potentiation already at lower BDNF stimulus concentrations since both pathways (cPKC and PKCλ) are active in parallel).

4 Summary

This chapter introduced a spatial and stochastic model to study BDNF/TrkB triggered signaling pathways in the spine. The model contains a spatially detailed geometry representing the dendritic spine in three dimensions. The extension of the simulator Smoldyn described in chapter 4 enables the simulation of the PSD as a distinct diffusion environment within the membrane. The models biochemical parameters are entirely based on literature resources. The results demonstrate the dependence of the signaling output at different depth of the modeled pathways based on the concentration of the BDNF stimulus. Low stimulus concentrations frequently fail to activate the PIP3 dependent PKCλ isoform in the context of the entire model. In these cases, potentiation happens solely due to conductance changes of already PSD resident AMPAR mediated by cPKC. The frequency of signaling outputs with both pathways activated (AMPAR conductance changes and recruiting more receptors to the PSD) rises with increasing concentrations of the stimulator BDNF.
Modeling the PSD as an entirely different diffusion environment by slowing down diffusion of protein components in contrast to the surrounding virtually increases the amount of active signaling molecules at the PSD due to diffusive trapping. This increased local concentration results in more reliable activation of both potentiation pathways.
The model was also used to test the potential effect of a reported inhibitory effect of Grb2 on PLCγ showing again that the resulting signaling output activates both pathways more reliably at lower concentrations. In contrast to the increased local concentration effect the reason in this case seems to be to assure that PIP3 levels are getting high enough to activate PKCλ and to reduce the cPKC dominance.

5 Discussion

The choice to implement this model for simulation within a stochastic framework was based on the huge influence of stochastic effects that are likely to influence signaling outcomes especially in the range of very low molecule

abundances. Deterministic simulations with Copasi show a change in the activity of the different pathways with varying stimuli as well. The stochastic simulations however, clearly show that the signaling output is more a matter of changing the abundances of certain signaling outcomes than a change in the average activity. While the deterministic regime proposes the same outcome for each stimulated spine, the stochastic simulation shows that occasionally rare deviations from the average behavior appear. This could be interpreted as a measure to keep the system more responsive at lower concentrations, while high concentrations always yield the full response.

This chapter also indicates different qualitative signaling properties of the two different PKC isoforms. cPKC with its dependence on Calcium appears to be less sensitive to changes in signal induction than PKCλ. The main difference causing this effect could be the additional step in cPKC activation that releases Calcium from internal stores in this model providing an additional adjustable signaling step. Considering glutamate signaling at the spine in addition, the necessary Calcium could come from other sources as well such as ion influx through the glutamate receptor while the produced DAG determines the time frame of the signal and the signal location as described in Gallegos and Newton (2008). Phosphorylation of already PSD resident receptors increasing their conductance could be the overall quicker and less long lasting effect over recruitment of new receptors from the extra synaptic space. Considering this, it is a plausible behavior that low stimulus concentrations trigger potentiation via conductance changes preferentially while higher BDNF stimuli increase the contribution of receptor trapping creating a longer lasting change by adapting the molecule composition at the PSD.

Both modifications of the signaling pathways addressed in this chapter yield a similar result. Partial inhibition of PLCγ and modeling the PSD as an entirely different diffusive compartment within the membrane increase the efficiency with which both potentiation pathways are activated at lower stimulus concentrations. The results demonstrate how spatial properties and signal interaction might be utilized for the fine tuning of signaling responses. Especially the importance of signal localization and the influence of heterogeneous membrane environments on the outcome of entire signaling pathways are clearly visible. The involvement of a PIP3 activated isoform of PKC implies that the necessity

of PIP3 for the maintenance of LTP as reported by Arendt et al. (2010) might not only be important for maintaining PSD scaffolding properties but also for the phosphorylation of S818 via PKCλ thus changing the trapping behavior of AMPAR.
The model provides further interesting extension possibilities. Possible interesting cross-talks could be the integration of PKA phosphorylation of GluR1 S845 as well as the integration of CaMKII S831 phosphorylation. CaMKII and cPKC compete for the same binding site on AMPA GluR1 changing the conductance. Given that CaMKII activation solely depends on Calcium (bound to calmodulin), the time course and contributions of both kinases to the overall phosphorylation would be of great interest. CaMKII might be the faster acting one upon Calcium influx while cPKC might be responsible to maintain the signal due to its dependence on DAG for sustained signaling. In addition, CaMKII phosphorylates SAP97 which disrupts the interactions of PKC with AKAP79. However, this is important for PKC mediated phosphorylation of S831 (Brooks and Tavalin, 2011; Jenkins and Traynelis, 2012). This supports a hypothesis of CaMKII dependent induction and a possible later phase with stronger PKC dependence.
Last but not least, it would be interesting to implement the presented model in the context of an glutamate signaling model to analyze the overall contributions of TrkB signaling to NMDAR mediated LTP.

The Road goes ever on and on
Down from the door where it began.
Now far ahead the Road has gone,
And I must follow, if I can,
Pursuing it with eager feet,
Until it joins some larger way
Where many paths and errands meet.
And whither then? I cannot say.
- Bilbo -

4 Extending Smoldyn to allow surface dependent diffusion

1 Introduction

The post-synaptic density (PSD) is a highly organized structure, visible in electron microscopy micrographs as an electron dense area in spine heads (Sosinsky et al., 2008) (see also chapter 1). Research techniques such as single-particle tracking, showed that molecules including α-amino-3-hydroxy-5-methyl-4-isoxazolepropionic acid receptor (AMPAR) exhibit different macroscopic diffusive behavior when they are moving within the PSD or the extrasynaptic membrane (Triller and Choquet, 2003; Jaskolski and Henley, 2009; Choquet and Triller, 2013). The environment of the PSD acts as a trap for receptor molecules depending on synaptic activity, hence regulating synaptic strength (Borgdorff and Choquet, 2002; Tolle and Novère, 2010). The subdiffusive behavior of molecules depending on their membrane environment is frequently observed in biology (Nicolau et al., 2007; Espinoza et al., 2012). To study these sub-diffusive effects in the context of signaling pathways, these areas have to be explicitly represented in the geometry of the models, and exhibit different properties from the surrounding areas. This integration should help to better understand the importance of spatially organized and regulated signaling pathways.

Currently available simulators, including the new versions of Smoldyn ($\geq$ V2.21) usually require the introduction of an artificial boundary surface sur-

rounding the desired surface area. Upon crossing this boundary, a molecule changes its type. A new type of behavior can be specified. However, this comes at the costs of explicitly defining the interactions with the boundary surface. Smoldyn for example requires the explicit definition of transition rates for molecules crossing the surface which is an artificial concept. In addition, reactions that take place on all types of surfaces have to be defined for all variants of molecules for each surface type. This results in an explosion of molecule and reaction definitions in the model. This practical issue becomes more important as numbers of molecule and surface types increase.
This chapter introduces a Smoldyn extension to model surface dependent diffusion that I started to develop based on Smoldyn V2.16. This version did not provide any means of changing a molecule's behavior located on a surface. Boundary surfaces as described above became available in later versions of Smoldyn ($\geq$ 2.21) and I ported my implementation to Smoldyn V2.21. This modified version - Smoldyn V2.21_M - allows the macroscopic modeling of different diffusive areas of a biological membrane. Artificially introduced boundary surfaces intersecting the diffusive surface as described above are not necessary. Diffusive trapping of receptors such as AMPAR in the PSD can easily be simulated. The modified version Smoldyn V2.21_M is described in the following and tested against the original Smoldyn V2.21. An example based on AMPAR diffusion in the dendritic spine illustrates its use.

2 Smoldyn supporting surface dependent diffusion: Smoldyn V2.21_M

The modifications implemented in the context of this work change the control flow of the Smoldyn simulator. The new version Smoldyn V2.21_M implements surfaces that hold the information for specific diffusion coefficients for the respective surface in addition to the global list of diffusion coefficients implemented in the original version of Smoldyn. These specific diffusion coefficients are accessible for each surface via molecule id and state. Whenever a diffusion coefficient is needed to calculate diffusion step lengths or binding parameters, Smoldyn V2.21_M checks whether a molecule is located on a

surface that specifies a specific diffusion coefficient for that surface. Based on this, reaction parameters such as diffusion step lengths, binding and unbinding radii are now calculated in a surface dependent manner using the original methods provided by Smoldyn.
The main modifications to the Smoldyn source code affect the structures that hold the surface and reaction data and the functions operating on them. The modified files (`smolmolec.c`, `smolreact.c`, `smolsurface.c`) as well as the complete source code are available online and can be downloaded from GitHub[1]. Surface specific diffusion coefficients are assigned in the configuration file. A new statement was added to the configuration file syntax to define different surface dependent diffusion coefficients. This new statement has the form:

```
surface [surface] sdifc [species] [state] [diffusionconstant]
```

It is meant to be used in addition to the standard Smoldyn `difc` statement and can be interpreted as adding exemptions to the general diffusive behavior of a molecule species for a specific surface.

2.1 Testing

Surface diffusion, unimolecular and bimolecular reactions were simulated using Smoldyn V2.21 and compared to equivalent simulations performed using the modified Smoldyn V2.21_M. These tests show that the core simulation functions of Smoldyn are still functioning in the expected way despite the new functionality of surface specific diffusion that was added [2].

2.1.1 Diffusion

The spatial geometry used to test diffusion is illustrated in figure 38a. A rectangular plane was created inside a 3-dimensional box. The plane is separated in two triangular panels, each defined as a surface in its own right. A specific diffusion coefficient can be defined for each triangle in Smoldyn V2.21_M, a slow and a fast one. Figure 38b gives an example

[1] https://github.com/yetime/SmoldynV2.22M
[2] The Smoldyn configuration files are availabe at https://github.com/yetime/SmoldynConfigs.git

path of a molecule diffusing on this plane. The assigned diffusion coefficient is hundredfold faster on the "fast" triangle compared to the "slow" one. The figure clearly shows the different behavior depending on the surface the molecule is currently on.

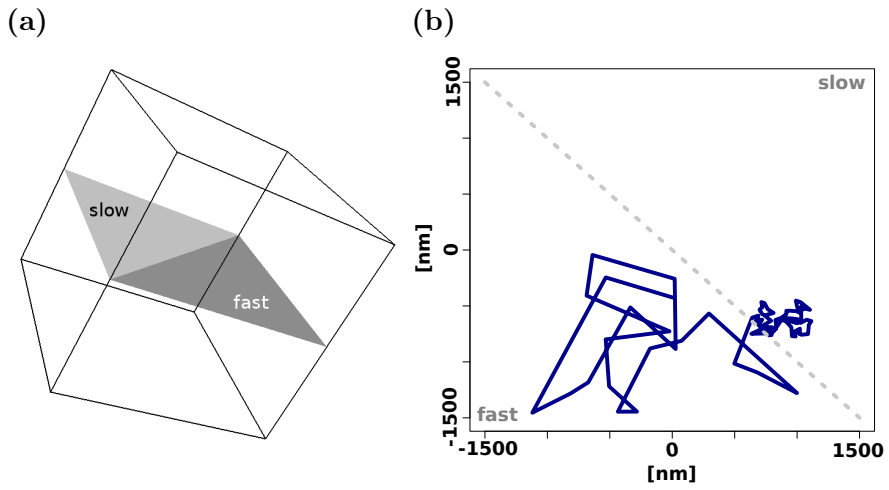

Figure 38: Random diffusion of single molecules was tested on a rectangular plane
(a) Geometry of the testing environment. The plane the molecules are diffusing on is separated into two parts. A molecules diffusion coefficient can be set depending on the surface it is diffusing on.
(b) Example of a single molecule random walk crossing from a fast diffusion environment to the slow diffusion environment. The blue line indicates the path of the molecule, the grey line indicates the separation between the fast and the slow diffusing environment.

Random walks of molecules simulated using a fixed random seed to initialize the simulator show identical paths for the simulated molecules in case of either "slow" or "fast" diffusion.
In addition, the mean square displacement (MSD) (Berg, 1993) of the diffusion processes was calculated and compared between Smoldyn V2.21 and Smoldyn V2.21_M. The MSD can be interpreted as the space explored by particles over time. The MSD of random diffusion is expected to be linear over time. The diffusion of single molecules was simulated to be able to track the particles. The "fast" triangle had a hundredfold faster diffusion coefficient than the "slow" one. The default diffusion definition in Smoldyn does not allow for different surface dependent diffusion coefficients. Therefore, the amount of simulations performed was doubled in V2.21 compared to V2.21_M to simulate the slow and the fast diffusion. In addition, molecules were not allowed to cross between the two surfaces in this case, in contrast to the example shown before in figure 38b. Figure 39a and 39b show the MSD over time for the slow (a) and the fast (b) process. The MSD results are equivalent for Smoldyn V2.21 (red) or V2.21_M (blue). The linear dependency indicates the expected random movement in all cases.
If the molecules are allowed to cross between the triangles, the MSD shows the anomalous behavior expected from such a system as shown in figure 39c (Smoldyn V2.21_M only) indicating sub-diffusion, a behavior that is observed for example in systems that exhibit molecular crowding (Banks and Fradin, 2005).

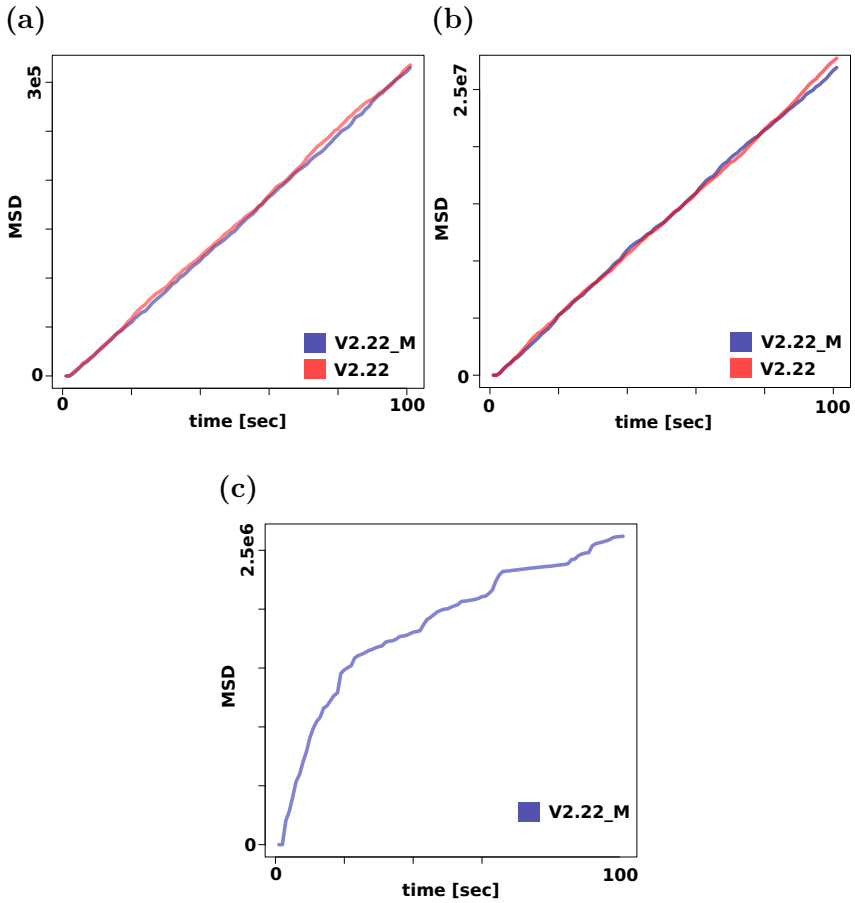

Figure 39: The mean square displacement (MSD)
(a)-(b) The MSD of particles in the same diffusion environment shows the same diffusive behavior using the modified and the original version of Smoldyn (blue: modified Smoldyn, red: Smoldyn V2.21). Figure (a) shows the MSD for the slow diffusion environment while (b) shows it for the fast surface environment.
(c) The MSD of particles diffusing in different diffusion environments shows anomalous Diffusion

2.1.2 Reactions

The same geometry as described before in section 2.1.1 was used to run a set of simulations to compare Smoldyn 2.21 and 2.21_M. The modeled reaction is based on the phosphorylation of the phosphoinositide PIP2 by phosphatidyl-inositol-3-kinase (PI3K) using the kinetic parameters given earlier (see section 3). Again, diffusion on the "fast" surface is 100x faster compared to the slow one. Simulations are initiated with 3 kinases and 500 molecules of PIP2 on each surface. PIP2 is not allowed to move between surfaces. As before, simulations using the two different diffusion coefficients were run using Smoldyn V2.21_M, while the amount of simulations had to be doubled to simulate fast and slow diffusion in Smoldyn V2.21. Figure 40 shows the time courses of PIP3 production indicating equivalent simulation results for Smoldyn V2.21_M and V2.21. Smoldyn V2.21_M results are given in blue while red shows Smoldyn V2.21 results. Darker colors represent reactions on the "fast" surface, light colors those on the "slow" surface.

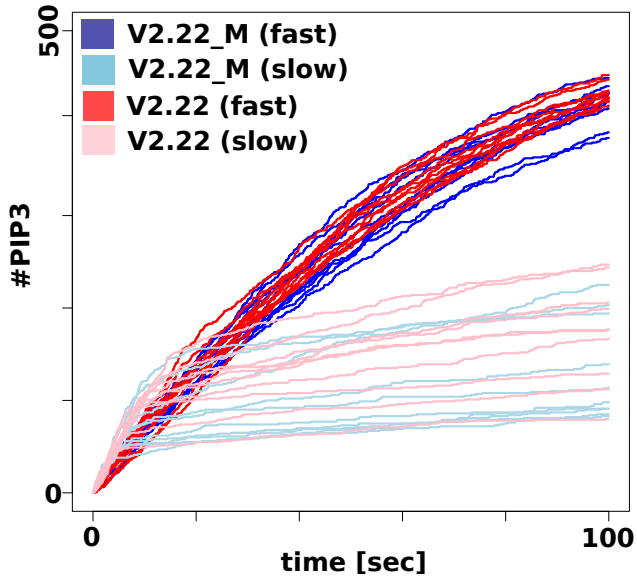

Figure 40: Reaction simulations comparing Smoldyn V2.21 and Smoldyn V2.21_M
The same realistic spine geometry shown in chapter 2 figure 38a was used as spatial environment for these simulations.
The modeled production of PIP3 by PI3K was simulated using Smoldyn V2.21 (red) and Smoldyn V2.21_M (blue) using a fast (dark) and a slow diffusion coefficient. Smoldyn V2.21_M simulations use the surface specific `sdifc` to set the diffusion coefficient for PIP2 and PIP3, while the default `difc` statement is used for simulations performed with Smoldyn V2.21. Ten different simulations of each, using the slow and the fast diffusion constant, were performed with each simulator.
Red: Smoldyn V2.21, Blue: Smoldyn V2.21_M, dark colours: fast diffusion coefficient, light colours: slow DC

Smoldyn provides the possibility to set the seed for the random number generator explicitly, allowing to test whether both versions produce identical results if they are based on the same sequence of random numbers. In this case however, simulations run with Smoldyn V2.21_M had to be split in two as well to ensure that the same amount of random numbers are used. Comparing a Smoldyn V2.21_M simulation with two different diffusion coefficients is not possible because the diffusion coefficient changes the probability of reactions and hence the amount of random numbers used. The results cannot be expected to be identical.
Splitting the Smoldyn V2.21_M simulation in two as well but using the surface dependent diffusion coefficient to define diffusion in V2.21_M produces identical results for a fixed random seed as shown in figure 41. The results of Smoldyn V2.21_M and V2.21 are identical. The overlap of the results is indicated by the purple color.
In addition, a simulation was run in Smoldyn V2.21_M connecting the two surfaces, setting the two different diffusion coefficients and allowing PIP2 to cross between surfaces. The same random seed was used as before. The development of PIP3 is shown for both surfaces in figure 41 in blue. The trapping of PIP2 molecules on the "slow" diffusion surface causes an increase in the local concentration compared to the "fast" surface. Therefore, more PIP3 is produced on the slow than on the fast surface in this case compared to the other cases where crossing of molecules between surfaces was not possible.

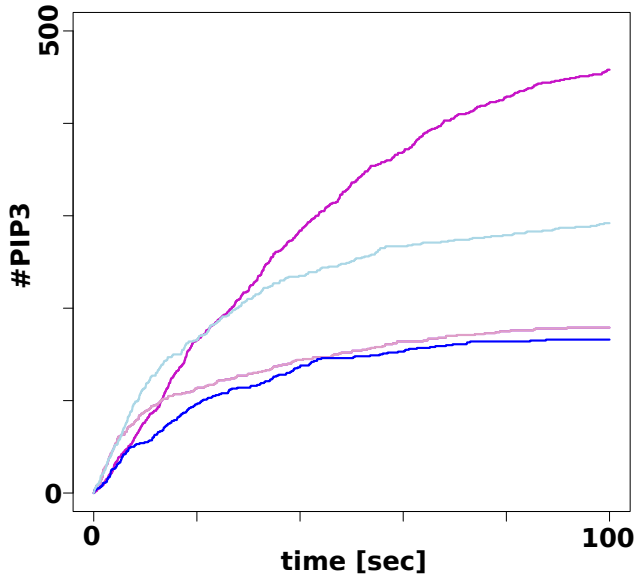

Figure 41: Reaction simulations comparing Smoldyn V2.21 and Smoldyn V2.21_M

The same realistic spine geometry shown in chapter 2 figure 38a was used as spatial environment for these simulations.

Ten simulations of identical reaction systems were performed using a fixed identical random number seed. This ensures that the sequence of random numbers used in the simulations to determine the stochastic effects is the same. Simulations performed using Smoldyn V2.21 and Smoldyn V2.21_M produce identical results (illustrated here by increase of PIP3 over time) for different diffusion coefficients (DC). The purple color indicates the overlay of the corresponding V2.21 and V2.21_M results. In Smoldyn V2.21_M it is possible to run simulations with molecules crossing over from one surface to the other adopting a new diffusion constant in the process. The results by means of PIP3 development on the fast/slow surface are shown in dark/light purple.

Purple: Smoldyn V2.21 and V2.21_M, separate simulations per diffusion constant,
Blue: Smoldyn V2.21_M different diffusion constants in the same simulation.

2.2 Modeling AMPAR trapping

The increase in synaptic AMPAR numbers is one of the major processes of long term potentiation (LTP). Sources for new AMPAR at the synapse are exocytosis and lateral diffusion (Newpher and Ehlers, 2008). This section shows an application for surface dependent diffusion coefficients to study the latter (lateral diffusion) based on a model proposed by Tolle and Novère, 2010.

2.2.1 Different macroscopic diffusion environments can mimic scaffold binding

Frequently, binding partners and mechanisms of detainment of molecules in specific areas of the membrane are unknown, only vaguely defined or very broad. This can render explicit modeling difficult. Molecular behavior could also be solely influenced by crowded environments. Different macroscopic diffusion environments can be used to abstract from this level of detail as shown for example in figure 42.
Based on the model for AMPAR trapping at the PSD in Tolle and Novère, 2010 that models scaffold binding of AMPAR explicitly, simulations were run in Smoldyn V2.21_M using different diffusive environments for AMPAR at the PSD and the extra synaptic membrane (ESM). The parameters for the model were taken from Tolle and Novère, 2010 (D_{ESM} =0.45 $\mu m^2\,s^{-1}$, n(AMPAR): 66, n(Scaffold)= 132). Diffusion coefficients for AMPAR at the PSD were decreased six times by a factor of 10 between simulations based on a diffusion coefficient of D_{ESM} =0.45 $\mu m^2\,s^{-1}$ for AMPAR at the ESM. The enrichment of AMPAR at the PSD is shown for a range of PSD diffusion coefficients of D_{PSD} =0.45 $\mu m^2\,s^{-1}$ to D_{PSD} =0.45 e^{-6} $\mu m^2/s$. Lighter colors indicate slower diffusion at the PSD. The pink time course indicates AMPAR trafficking due to explicit scaffold binding when D_{ESM} = D_{PSD} =0.45 $\mu m^2\,s^{-1}$, see also section 2.2.2 below. The figure indicates that the time course of actual scaffold binding resembles trapping due to slower diffusion with D_{PSD} =0.45 10^{-5} $\mu m^2/s$.

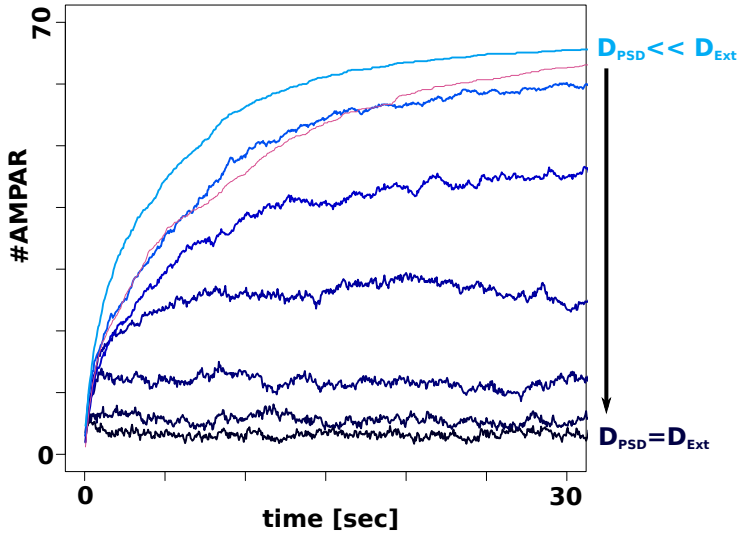

Figure 42: Trapping of AMPAR at the PSD
Time courses of AMPAR numbers at the PSD are shown. Diffusion coefficients (D) on the extra synaptic membrane (ESM) are kept constant, while they are changed for AMPAR diffusion on the PSD. The coloring indicates the ratio of D_{PSD} to D_{ESM}. The differences changed in 10-folds starting from $D_{PSD} = D_{ESM}$ (darkblue) to $D_{PSD} \cdot 1.000.000 = D_{ESM}$ (lightblue). The amount of AMPAR present at the PSD in case of $D_{PSD} = D_{ESM}$ (darkblue) reflects the area ratios of PSD to ESM. The bigger the difference between D_{PSD} and D_{EMS} becomes (indicated by lighter shades of blue), the more AMPAR get trapped at the PSD.
The pink time course indicates trapping of AMPAR due to binding of AMPAR to scaffolding elements instead of changes in diffusive behavior.
All time courses are averages of 10 simulation runs. The geometry used for these simulation is the same as shown in figure 7b.

2.2.2 Different diffusive environments enhance receptor trapping at the synapse

Tolle and Novère, 2010 used explicit modeling of the PSD boundaries to show the effects of AMPAR receptor confinement to the PSD on receptor trapping. They vary the probability that AMPAR are reflected back into the PSD upon encounter of this boundary instead of diffusing into the extra synaptic space. Increased confinement of AMPAR to the PSD decreases the time needed to bind most receptors to the scaffold due to increased probabilities of AMPAR encountering binding scaffold elements.
As shown before, a different macroscopic diffusion environment is enough to enrich receptors at the PSD without the need of explicitly modeling a reflective boundary around it. Simulations were run using Smoldyn V2.21_M modeling two different diffusive environments for AMPAR. Results are shown in shown in figure 43. The parameters for the model are taken from Tolle and Novère, 2010 (D_{ESM} =0.45 $\mu m^2\,s^{-1}$, n(AMPAR): 66, n(Scaffold)= 132). The extra synaptic diffusion coefficient is the same for all simulations (D_{ESM} =0.45 $\mu m^2\,s^{-1}$). The diffusion coefficient for the PSD is changed five times by a factor of ten from D_{PSD} =0.45 $\mu m^2\,s^{-1}$ to D_{PSD} =0.45 10^{-5} $\mu m^2/s$. Scaffolding elements and AMPAR binding to them is modeled explicitly. The results clearly indicate the positive effect of slower AMPAR diffusion at the PSD on the overall time that is needed to trap AMPAR by scaffold binding at the PSD. This improvement however has its limitations once diffusion at the PSD gets too slow to enable AMPAR to encounter the scaffold elements.

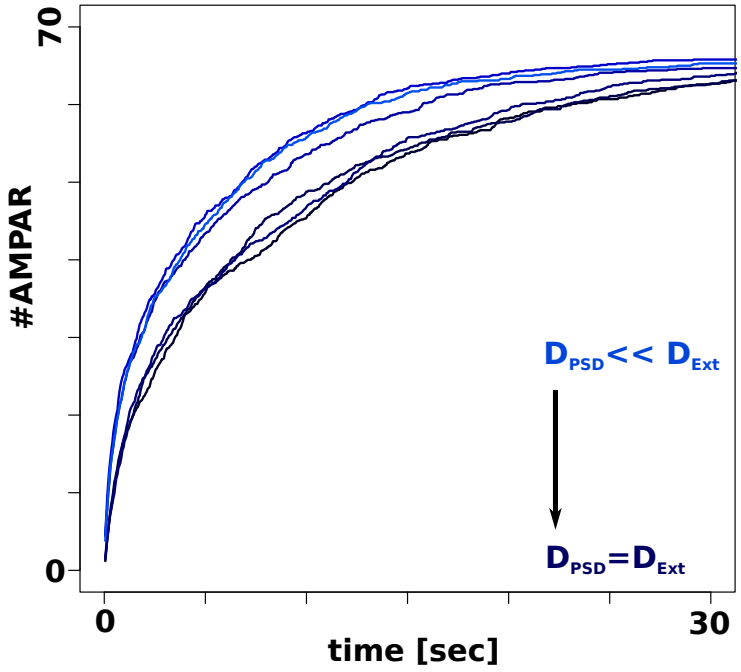

Figure 43: Trapping of AMPAR at the PSD via scaffolds
Time courses of AMPAR binding to scaffolding elements at the PSD are shown. The number of scaffold-bound AMPAR is depicted over time. Diffusion coefficients are changed in the same way as in (a) from $D_{PSD} = D_{ESM}$ (darkblue) to $D_{PSD} \cdot 100.000 = D_{ESM}$ (lightblue).
All time courses are averages of 10 simulation runs. The geometry used for these simulation is the same as shown in figure 7b.

3 Discussion

This section demonstrated the idea of defining molecular properties based on the current environment of a molecule. The implementation of surface dependent diffusion coefficients was described, validated and illustrated as an extension to the simulator Smoldyn V2.21.
The shown examples demonstrate, that Smoldyn V2.21_M behaves as expected compared to Smoldyn V2.21 when such a comparison is directly possible. The new extension enables simulations showing interesting aspects such as anomalous diffusion due to different diffusive areas or the enhancement of reaction speed by enriching substrate molecules.
Simulations of AMPAR trafficking at the PSD show that a change in diffusion coefficient can substitute for explicit modeling of binding reactions, especially in cases where binding partners are unknown, not well defined or an abundance of unspecific associations slows the movement of molecules down. Especially in case of the latter, modeling the behavior based on macroscopic diffusive behavior might be the easier and also biologically more realistic abstraction. It has to be kept in mind though that the results are not the same with regards to the spatial distribution of the trapped molecules. Modeling molecular trapping by unspecified scaffolds defines the position of receptors via the positioning of the scaffold. Trapping them via a change in diffusivity concentrates them on the boundaries of the subarea in the beginning. Achieving a random or uniform distribution of molecules via macroscopic diffusion in that subarea might take longer since the molecules have to distribute within this subarea via the slower diffusion coefficient.
In general, being able to easily model membranes as surfaces composed of subareas that exhibit different properties is a great feature to study the influence of special sub diffusive membrane environments like the PSD.

We cannot achieve victory by arms, but by arms we can give the Ring-bearer his only chance, frail though it be.

- Gandalf -

5 Conclusions

The general background of this thesis was the postsynaptic signal integration of brain derived neurotrophic growth factor signaling pathways and their influence on long term potentiation, the processes that strengthens the connections between neurons as basis of memory and learning as outlined in Chapter 1. These complex interactions are difficult to understand by pen and paper and computational modeling appears to be the method of choice to gain further insights into the complex behavior of the system itself rather than each of its parts on their own.
Due to the extremely small size of the postsynaptic signaling environment (the dendritic spine) and the low amounts of molecules, stochastic processes are likely to play an important role and influence signaling outcomes. In addition, the extremely heterogeneous and versatile spatial environment of the spine determined the decision to develop a model within a stochastic single particle modeling framework. The simulation environment Smoldyn together with an extension developed and described in chapter 4 enabled the development of a detailed spatial representation of the dendritic spine, with explicit representation of the postsynaptic density (PSD) as distinct diffusion compartment within the spines membrane. The single particle nature of the simulation allows full control over the positioning and movement of all molecules together with the possibility to track them in space and time.

Firstly, chapter 2 takes a step back from the complicated interaction network of BDNF signaling and focuses on the small subnetwork compris-

ing phosphoinositide-3-kinase (PI3K), the phosphatase and tensin homolog (PTEN) and the two phosphoinositides PIP2 and PIP3.
One of the goals of the initial study was to develop a set of methods to facilitate the automated statistical analysis of spatial molecular distributions at the PSD membrane over time and in space. Spatial geostatistics was found to be a closely related field providing a comprehensive toolbox for the analysis of point patterns distributed in space. A software package implemented for the use in geostatistics (Spatstat) within the context of the statistical scripting language R was utilized to develop analysis pipelines that deal with the generated spatial output format of the simulator Smoldyn.
The study demonstrated key aspects of the important role of space in signaling pathways, regardless of the identity of the actual chosen phosphatase and kinase interaction. The relative positioning of positive and negative regulators in space creates a focused and localized signal of an otherwise small and quickly diffusing signaling substance. Space as a potential signaling parameter itself is able to adjust and fine-tune the signaling outcome of otherwise identical systems. Studies found in the experimental literature outlined in chapter 4 illustrate that the studied ring-like spatial layout could indeed be a realistic representation of biological reality.

Secondly, chapter 3 returns to the larger system of BDNF signaling in long term potentiation and presents a model that integrates possible signaling events downstream of the receptor. The implementation of the model relies on the Smoldyn extension described in chapter 4.
Three different layers of signal interaction and integration were considered:

- The competition of PI3K and phospholipase C (PLC) for the same substrate PIP2.

- Two different isoforms of protein kinase C (PKC) that were shown to modify AMPAR conductance and trapping behavior as described in chapter 1.

- The integration of conductance changes and trafficking behavior at the level of AMPARs as a measure for the extend of synapse potentiation.

Simulations varying the amount of the stimulus BDNF show that the competition of the kinase PI3K and PLCγ for the same substrate is dominated by PI3K at lower and PLCγ at higher levels of BDNF. Further downstream, the model predicts that lower concentrations of BDNF potentiate the synapse mainly by changing the conductance of already PSD resident AMPAR while the AMPAR trapping modification due to the PI3K dependent pathway operate more within an all or nothing regime. Higher concentrations of BDNF reliably trigger both, AMPAR trapping and conductance changes.
The addition of an inhibitory effect on PLCγ shifts the response towards full potentiation of the synapse due to the activation of both pathways at lower concentrations of BDNF. Defining the PSD as a different diffusion environment for all protein components which simulates diffusion trapping has a similar effect. The reasons for this effect however are different. Molecular trapping results in an increase of local concentration of the important signaling components, thus lower concentrations have a similar effect to higher ones in the unmodified model. Inactivation of PLCγ on the other hand provides the necessary advantage for the PI3K pathway to reach the necessary signaling levels to trigger downstream signaling. It seems reasonable from a biological point of view to increase synapse strength by changing the conductance of AMPAR first and at lower concentrations because this process involves receptors already present at the PSD. Later and at higher concentration the recruitment of more receptors to the PSD by trapping mechanisms creates a potentially longer lasting potentiation because it changes the molecular composition of the PSD.
Chapter 3 relied on the implementation of the Smoldyn extension introduced in chapter 4. This extension allowed an accurate representation of the PSD as diffusion microdomain. Showing the influence of an increase in local concentration due to different diffusion properties at the PSD would have been impossible otherwise.

The spine itself is still extremely close to the resolution limit of light microscopy techniques that allow the real time tracking of molecular movements and events. Typical fluorescent microscopy studies allow the distinction of two cases : (a) A protein is in the spine and (b) it is not (see the publications

on AMPAR movement done by Arendt et al. (2010) and Tardin et al. (2003) for examples). Colocalization studies rely on detecting the spatial overlap of the fluorescent signal with typical synaptic marker proteins (Tardin et al., 2003). The advent of new high resolution techniques such as STED microscopy for example are capable of resolving structures in the 50 nm range such as vesicles (Kempf et al., 2013). These dimensions are still huge compared to the diameter of the PSD of around 600 nm given in chapter 2. With this resolution, it is impossible to see details of single molecular movements within the PSD.
Ultrastructure studies such as immunogold electron microscopy (Tao-Cheng et al., 2011) on the other hand miss the dynamic component. Computational models, like the one proposed, allow to combine the static view of high resolution imaging giving accurate positions of molecules with the dynamic perspectives gained from fluorescence microscopy. They allow further to extrapolate from observations done within a larger context to the conditions and events happening on the small spatial scale of the spine and test hypothesis on the dynamic distribution of molecules over time within the PSD.

The TrkB signaling model as described in this thesis provides interesting possibilities to address further questions. Some of them require smaller some larger extensions to the model.
Release of BDNF studied here resembles more bath application experiments of BDNF although BDNF is released into the context of the synaptic cleft. The current model does not make any assumptions whether BDNF release is postsynaptic (Hartmann et al., 2001), presynaptic (Dieni et al., 2012) or both (Kojima et al., 2001; Matsuda et al., 2009). However, experiments indicate the BDNF release is activity dependent as is glutamate release and an interesting question to answer using modeling is the integration of the glutamate signal with the BDNF signal addressing both, temporal and spatial coordination. Further downstream, addressing the spatial and temporal integration of TrkB mediated calcium release from internal stores with calcium that enters through glutamate receptors on the downstream targets is an interesting topic as well and could allow the relative quantification of contributions of both, the glutamate and BDNF pathways, to LTP processes. These questions however,

require the extension of the presented model by an appropriate glutamate dependent signaling model.
Furthermore, a realistic representation of the electric properties arising from the involvement of ionic currents would be interesting and help to compare simulation results with experiments measuring postsynaptic potentials as result of signaling events. This is however beyond the capabilities of Smoldyn. Attempts have been made of integrating biochemical simulations with electrical ones such as the VirtualNeuron (Brown et al., 2011) or TimeScales (Mattioni and Le Novère, 2013). Especially the methodology developed in TimeScales is of interest. The author is running two different simulators in parallel, synchronizing them in an event driven manner. The purpose of TimeScales is the integration of these two simulators and the conversions of events happening between them. A similar integration might be possible for Smoldyn to not only address the influence of spatial events on the electrical signal of a single spine but also over several spines on a dendrite. The electrical summation of spines showing the stochastic behavior as described in chapter 3 depending on BDNF concentration would be an interesting prospect.

The simulator Smoldyn has been used throughout this work as simulation environment of choice. The current available version V2.31 of Smoldyn provides interesting new features such as moveable surface panels, excluded volume reactions and rule-based modeling allowing the easier implementation of complex models. The implemented extension presented in chapter 4 is based on version V2.19 and V2.21. Due to major redesign of the Smoldyn source code in the recent past, these versions are currently not compatible. It might be interesting to re-enter the conversion about environment specific features of molecules like diffusion as introduced here as it was mentioned in the Smoldyn programmers manual of version V2.23 (Andrews, 2011).
In general, there are certain aspects of Smoldyn usability that could be addressed in the future to make Smoldyn accessible to a wider range of audience. The lack of model development and analysis tools results in a steep learning curve. Once the initial steps are mastered, Smoldyn becomes a powerful tool for simulation.
A model editing environment as seen in other simulators would facilitate the

implementation of Smoldyn models. In addition, instant feedback on syntax and possibly semantic components could be included to increase the efficiency of model implementation.
The development of a toolbox potentially in R and based on scripts that were implemented for this thesis would benefit the user community. This toolbox could range from global time course output and analysis functions as seen in many other simulation environments such as Copasi or VCell to the generation of spatial statistics to compare molecular distributions across time and space.
Input and output filters to enable easier sharing of Smoldyn models with the systems biology community would be desirable. Already import and export of the biochemical components into standard markup languages of systems biology such as SBML (Hucka et al., 2003) would be of great benefit. In addition, SBML Version 3 is on its way to support spatial features (Hucka et al., 2010; Schaff et al., 2013).

Overall, the increase in available data and the improvement and development of new technologies enables more and more parameters of models to be determined accurately. The prospect of creating more realistic and detailed models is tempting. However, one has to keep in mind when developing more and more realistic and therefore complex models, that simplification and abstraction of a problem can be an important step in modeling. It helps to identify and understand the important components and aspects of the underlying questions. Extending a model solely for the purpose of increased realism could cause the loss of focus on the original question.

Despite this conclusion, the benefit of including space as a variable parameter was shown in this thesis with regards to the signaling events at the single spine level. The possibility to build computational models and modifying them to address the influence of parameters and aspects that are very difficult to alter in experimental settings such as diffusion properties is one of the huge benefits of modeling and systems biology. A system is more than its parts and although we have to understand the single components first, bringing them back into their context is characterized by the emergence of new and

exciting properties that none of the single components is able to show alone.

After all, no living cell is a simple container of isolated biochemical components mixed together but a highly organized machinery of complex interactions and components in time and space. This observation is true throughout all different layers of complexity from single cells to tissues, organisms and ecosystems. Life is organization of interaction and communication in time and space and stochasticity has its share.

Home is behind, the world ahead,and there are many paths to tread through shadows to the edge of night,until the stars are all alight.
- Pippin's song -

List of Publications

- Baldi B. F., Hoyer C., Le Novère N. "Schizophrenic: forever young?" Genome Med. 2010; 2(5): 32.

- Contributions to Biomodels.NET [1] - Model of the Month

  Model No. 223 Review of Borisov et al. (2009), Systems-level interactions between insulin-EGF networks amplify mitogenic signaling, published online March 2010

  Model No. 215 Review of Schulz et al., (2009), Sequential polarization and imprinting of type 1 T helper lymphocytes by interferon-gamma and interleukin-12, published online January 2011

  Model No. 328 Review of Bucher et al. 2011. A systems biology approach to dynamic modeling and inter-subject variability of statin pharmacokinetics in human hepatocytes, published online February 2012

  Model No. 415 Review of December 2012 on Mellor et al. (2010). Reduction of off-flavor generation in soybean homogenates: a mathematical model, published online December 2012

  Hoyer C., Le Novère N. "Significance of the Kinase and Phosphatase Localisation on the Formation of Lipid Signaling Domains in Dendritic Spines." 13th International Conference On Systems Biology, Toronto, Canada, 2012, Poster presentation. Genome Med. 2010; 2(5): 32.

[1] http://www.ebi.ac.uk/biomodels-main/modelmonth

Appendix

r(PI3K)	r(PTEN)	**Total**	**PSD**	$\frac{PSD}{Total}$	d[nm]
42	none	2103.145± 1.32	216.33± 2.01	0.10	-
42	42	140.54± 5.30	7.83±0.13	0.06	54
42	85	7.86± 1.16	1.12±0.10	0.14	87
42	170	11.94± 2.67	4.37± 0.28	0.39	173
42	255	13.89± 1.72	8.97± 0.28	0.65	257
42	370	17.62± 0.60	16.79±0.49	0.95	317
42	fix	5.60± 1.07	4.38± 0.34	0.80	253
42	rnd	48.98± 3.19	36.31 ± 1.90	0.74	735
85	none	1937.41± 4.65	104.65± 2.07	0.05	-
85	42	1020.45± 20.53	55.77 ± 0.89	0.05	90
85	85	76.55± 5.17	3.95± 0.17	0.05	106
85	170	18.88± 2.86	5.86± 0.15	0.32	181
85	255	22.24± 2.95	12.61± 0.17	0.58	262
85	370	25.03± 0.57	23.86± 0.54	0.95	375
85	fix	8.89 ± 3.03	6.37± 0.50	0.77	255
85	rnd	66.37± 1.06	49.73± 0.41	0.75	738
170	none	2007.69 ± 3.82	108.50± 1.72	0.05	-
170	42	1549.91± 13.65	80.40± 1.42	0.05	173
170	85	1081.34 ±19.23	53.71 ±0.70	0.050	180
170	170	38.09 ±8.98	1.96± 0.15	0.05	216
170	255	25.75± 3.08	10.58 ± 0.35	0.41	284
170	370	29.78 ± 1.10	27.19± 0.59	0.91	390

170	fix	14.50 ± 7.17	4.78 ± 0.70	0.41	277
170	rnd	88.57 ±4.33	64.02 ± 2.55	0.72	743
255	none	2039.29± 5.94	110.08± 2.07	0.05	-
255	42	1712.90± 15.72	83.72 ± 0.83	0.05	257
255	85	1444.57± 31.15	66.39± 0.86	0.05	261
255	170	693.66± 7.36	27.78± 0.50	0.04	284
255	255	36.46± 5.80	1.96±0.12	0.06	325
255	370	25.09± 0.99	21.75 ± 0.32	0.87	415
255	fix	43.99± 22.48	5.13± 0.45	0.15	330
255	rnd	100.28± 3.52	68.67 ± 2.69	0.684	752
370	none	2103.73 ±1.03	107.37± 1.34	0.05	-
370	42	1992.44± 8.67	85.54±2.09	0.04	3710
370	85	1888.32 ± 10.784	74.00 ± 1.01	0.04	384
370	170	1367.79±14.34	43.53± 0.66	0.03	398
370	255	707.93± 15.62	16.682± 0.40	0.02	424
370	370	9.84±2.69	2.89± 0.11	0.31	484
370	fix	273.35 ± 65.20	9.30 ± 1.010	0.04	428
370	rnd	231.90± 6.38	136.40± 2.10	0.59	769
fix	none	2057.67± 23.64	90.16± 37.02	0.04	-
fix	42	1751.96± 91.36	82.14± 2.24	0.05	255
fix	85	1324.07± 58.24	61.20± 2.45	0.05	247
fix	170	712.60± 56.23	27.18± 1.71	0.04	272
fix	255	254.23± 72.94	10.89± 0.52	0.05	325
fix	370	27.09± 2.39	21.79 ±2.11	0.81	416
fix	fix	86.89± 29.46	5.81 ± 1.18	0.07	326
fix	rnd	116.29± 11.86	77.57 ± 5.84	0.67	756
rnd	none	2107± 0	108.94 ±1.60	0.05	
rnd	42	1986.41± 6.80	53.10 ±1.66	0.03	733
rnd	85	1943.96± 11.20	38.75 ± 1.40	0.02	739
rnd	170	1894.90± 6.00	22.42± 0.47	0.01	741
rnd	255	1842.10± 9.05	13.74± 0.23	0.02	755
rnd	370	1427.69± 3.89	2.04± 0.44	0.00	769
rnd	fix	1757.63± 48.11	9.59± 1.55	0.01	761
rnd	rnd	39.80 ±3.26	3.86± 1.27	0.10	1003

Table 8: Steady State Maximum PIP3 levels in # molecules at the PSD and over the whole surface

r(PI3K)	r(PTEN)	**f(CSR)**	**f (mCSR)**	**f(pcf)**	**r(PCF) [nm]**	**r(dia) [nm]**
42	none	0.139± 0.011	0	0.279± 0.006	-	-
42	42	0.047± 0.010	0	0.298± 0.011	-	-
42	85	0.375± 0.028	0	0.450± 0.129	-	-
42	170	0.767± 0.030	1	0.887± 0.009	84± 53	184±6
42	255	0.835± 0.011	1	0.909± 0.005	74± 9	283 ±4
42	370	0.713± 0.039	1	0.853± 0.009	67± 26	426 ± 4
42	fix	0.559± 0.058	1	0.867± 0.015	49± 5	212 ± 24
42	rnd	0.382±0.029	1	0.614± 0.014	23± 2	574 ± 4
85	none	0.148± 0.022	0	0.270 ± 0.003	-	-
85	42	0.094± 0.010	0	0.305 ± 0.002	-	-
85	85	0.049± 0.012	0	0.282 ± 0.029	-	-
85	170	0.856± 0.016	1	0.898 ± 0.014	55± 14	239±9
85	255	0.927± 0.024	1	0.943 ± 0.005	71± 6	323 ± 2
85	370	0.834± 0.021	1	0.905 ± 0.010	39± 15	446 ±5
85	fix	0.693± 0.036	1	0.859 ± 0.018	61± 25	280±19

85	rnd	0.452± 0.049	1	0.621 ± 0.017	22± 1	588 ±1
170	none	0.157± 0.028	0	0.259 ± 0.006	-	-
170	42	0.199± 0.007	0	0.279 ±0.008	-	-
170	85	0.2337± 0.012	0	0.324 ± 0.009 -	-	
170	170	0.159± 0.022	0	0.327 ± 0.058 -	-	
170	255	0.587± 0.027	1	0.841 ± 0.012	58± 24	363±4
170	370	0.630± 0.039	1	0.868 ± 0.005	31± 6	477±4
170	fix	0.117± 0.036	0.4	0.561 ±0.040	118± 31	317±30
170	rnd	0.322± 0.021	0.6	0.563 ±0.011	20± 1	607±2
255	none	0.162± 0.021	0	0.252± 0.004	-	-
255	42	0.213± 0.011	0	0.270± 0.006	-	-
255	85	0.333± 0.013	1	0.329± 0.007	-	-
255	170	0.156± 0.008	0	0.387± 0.010	-	-
255	255	0.175± 0.013	0	0.296± 0.056	-	-
255	370	0.259± 0.016	0	0.693± 0.009	43± 12	502±1
255	fix	0.069± 0.012	0	0.404± 0.017	-	-
255	rnd	0.217± 0.018	0	0.468± 0.010	-	-

370	none	0.148± 0.023	0	0.234± 0.008	-	-
370	42	0.261± 0.020	0	0.270± 0.006	-	-
370	85	0.445± 0.029	1	0.310± 0.003	-	-
370	170	0.320± 0.019	1	0.400± 0.009	-	-
370	255	0.145± 0.027	0	0.371± 0.005	-	-
370	370	0.096± 0.008	0	0.337± 0.033	-	-
370	fix	0.134± 0.041	0	0.383± 0.030	-	-
370	rnd	0.331± 0.012	0.8	0.368± 0.011	-	-
fix	none	0.157± 0.018	0	0.249± 0.011	-	-
fix	42	0.233± 0.037	0	0.266± 0.016	-	-
fix	85	0.313± 0.070	0.6	0.337± 0.016	-	-
fix	170	0.217± 0.124	0.2	0.406± 0.067	-	-
fix	255	0.109± 0.048	0	0.344± 0.042	-	-
fix	370	0.402± 0.073	0.8	0.741± 0.033	50± 28	496±2
fix	fix	0.105± 0.026	0	0.391± 0.042	-	-
fix	rnd	0.27± 0.040	0	0.484± 0.025	-	-

rnd	none	0.133± 0.024	0	0.234± 0.003	-	-
rnd	42	0.251± 0.011	0	0.281± 0.009	-	-
rnd	85	0.351± 0.057	0.8	0.348± 0.012	-	-
rnd	170	0.345± 0.048	1	0.410± 0.005	-	-
rnd	255	0.211± 0.022	0	0.351± 0.007	-	-
rnd	370	0.243± 0.041	0	0.481± 0.033	100± 42	224 ±54
rnd	fix	0.173± 0.030	0	0.352± 0.018	-	-
rnd	rnd	0.171± 0.041	0	0.388± 0.015	-	-

Table 9: Means and standart deviation by spatial simulation setup of the CSR test and the PCFs
CSR Fractions: The fraction of overall timeframes with a p-value below the significance threshold of .05
CSR Mode Fractions: The fraction simulation runs where the most-prevalent p-value is below .05
r(PCF): The most prevalent maximum of each time frames PCF function

	Estimate	Std. Error	t value	Pr(>|t|)	Sig.
a	0.0005362	0.0001014	5.286	5.02e-05	***
k	1.7501096	0.0326114	53.666	< 2e-16	***

Table 10: Parameters of power law fit for settings with r(PI3K)=42 X r(PTEN)={85,170,255,370}
Fitted function: $a \cdot x^k = y$
Significance Codes: 0: ***; 0.001: **; 0.01: *; 0.05: .

	Estimate	Std. Error	t value	Pr(>|t|)	
r(PI3K)=rnd X r(PTEN)={42,85,170,255,370}					
d	7.165e+01	1.201e+00	59.663	< 2e-16	.
x=r(PTEN), c	-5.091e-01	2.698e-02	-18.871	1.19e-14	***
x=r(PTEN), b	1.639e-03	1.539e-04	10.653	6.33e-10	***
x=r(PTEN), a	-2.086e-06	2.459e-07	-8.483	3.18e-08	***
r(PTEN)=rnd X r(PI3K)={42,85,170,255,370}					
d	6.152e+00	3.133e+00	1.964	0.0629	***
x=r(PTEN), c	8.792e-01	7.036e-02	12.495	3.44e-11	***
x=r(PTEN), b	-4.784e-03	4.013e-04	-11.920	8.23e-11	***
x=r(PTEN), a	9.075e-06	6.414e-07	14.148	3.30e-12	***

Table 11: Parameters of cubic fit for spatial setups r(PI3K)=rnd X r(PTEN)={42,85,170,255,370} and r(PTEN)=rnd X r(PI3K)={42,85,170,255,370}
Fitted function: $a \cdot x^3 + b \cdot x^2 + c \cdot x + d = y$
Significance Codes: 0: ***; 0.001: **; 0.01: *; 0.05: .

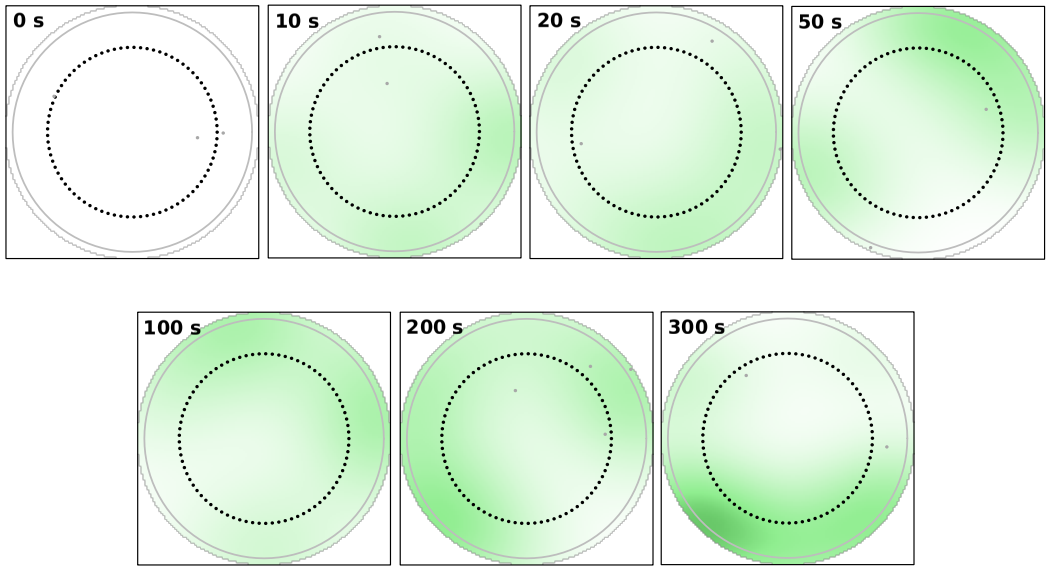

Figure 44: Example 2D time frame series of one PI3K diff PTEN 255 simulation run
The figure shows density plots of time frames at t=0, 10, 20, 50, 100, 200, 300 s. The spatial configuration is freely diffusing PI3K with PTEN fixed in a circular formation with r(PTEN)=255 nm. This more detailed 2D density time frame series corresponds to panel d) in figure 15

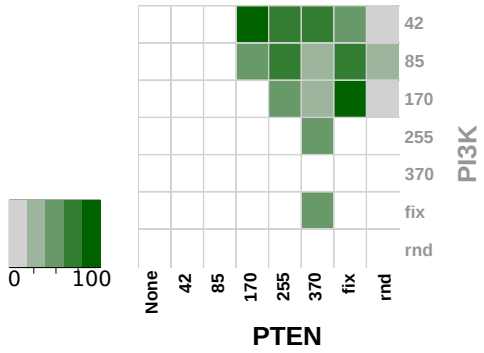

Figure 45: PCF based estimation of signalling peak radii

.

(a) $t_{1/2}$ PSD

(b) t/MaxPIP3 PSD

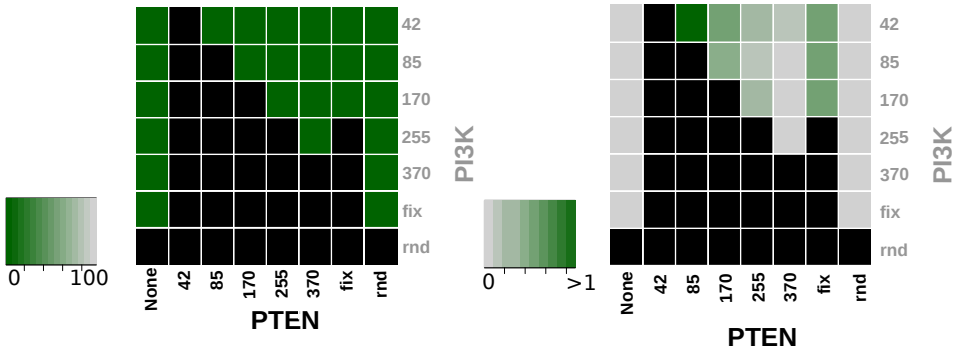

Figure 46: $t_{1/2}$ for reaching the steady state depends on the spatial setup.

References

Adesnik, Hillel and Roger A Nicoll (2007). "Conservation of glutamate receptor 2-containing AMPA receptors during long-term potentiation." *The Journal of neuroscience : the official journal of the Society for Neuroscience* 27.17 (Apr. 2007), pp. 4598–602.

Adra, Salem, Tao Sun, Sheila MacNeil, Mike Holcombe, and Rod Smallwood (2010). "Development of a three dimensional multiscale computational model of the human epidermis." *PloS one* 5.1 (Jan. 2010), e8511.

Adrian Baddeley, Rolf Turner (2005). "Spatstat: An R package for analyzing spatial point patterns". *Journal of Statistical Software* 12.6 (2005).

Ajay, Sriram M and Upinder S Bhalla (2007). "A propagating ERKII switch forms zones of elevated dendritic activation correlated with plasticity." *HFSP journal* 1.1 (May 2007), pp. 49–66.

Akimoto, K, R Takahashi, S Moriya, N Nishioka, J Takayanagi, K Kimura, Y Fukui, S i Osada, K Mizuno, S i Hirai, A Kazlauskas, and S Ohno (1996). "EGF or PDGF receptors activate atypical PKClambda through phosphatidylinositol 3-kinase." *The EMBO journal* 15.4 (Mar. 1996), pp. 788–98.

Allbritton, N L, T Meyer, and L Stryer (1992). "Range of messenger action of calcium ion and inositol 1,4,5-trisphosphate." *Science (New York, N.Y.)* 258.5089 (Dec. 1992), pp. 1812–5.

Allen, Shelley J, Judy J Watson, and David Dawbarn (2011). "The neurotrophins and their role in Alzheimer's disease." *Current neuropharmacology* 9.4 (Dec. 2011), pp. 559–73.

Amanda M Vanhoose, Danny G Winder (2003). "NMDA and beta1-adrenergic receptors differentially signal phosphorylation of gluta-

mate receptor type 1 in area CA1 of hippocampus." *The Journal of neuroscience : the official journal of the Society for Neuroscience* 23.13 (2003), pp. 5827 –34.

Amaral, Michelle D and Lucas Pozzo-Miller (2007a). "BDNF induces calcium elevations associated with IBDNF, a nonselective cationic current mediated by TRPC channels." *J Neurophysiol* 98.4 (Oct. 2007), pp. 2476–2482.

Amaral, Michelle D and Lucas Pozzo-Miller (2007b). "TRPC3 channels are necessary for brain-derived neurotrophic factor to activate a nonselective cationic current and to induce dendritic spine formation." *The Journal of neuroscience : the official journal of the Society for Neuroscience* 27.19 (May 2007), pp. 5179–89.

Amaral, Michelle D and Lucas Pozzo-Miller (2012). "Intracellular Ca2+ stores and Ca2+ influx are both required for BDNF to rapidly increase quantal vesicular transmitter release." *Neural plasticity* 2012 (Jan. 2012), p. 203536.

Ananthanarayanan, Bharath, Robert V Stahelin, Michelle A Digman, and Wonhwa Cho (2003). "Activation mechanisms of conventional protein kinase C isoforms are determined by the ligand affinity and conformational flexibility of their C1 domains." *J Biol Chem* 278.47 (Nov. 2003), pp. 46886–46894.

Andrews, Steve (2011). *Smoldyn Programmer's Manual V2.23*. 2011.

Andrews, Steven S (2009). "Accurate particle-based simulation of adsorption, desorption and partial transmission." *Physical biology* 6.4 (Jan. 2009), p. 046015.

Andrews, Steven S and Dennis Bray (2004). "Stochastic simulation of chemical reactions with spatial resolution and single molecule detail." *Phys Biol* 1.3-4 (Dec. 2004), pp. 137–151.

Andrews, Steven S, Nathan J Addy, Roger Brent, and Adam P Arkin (2010). "Detailed simulations of cell biology with Smoldyn 2.1." *PLoS Comput Biol* 6.3 (2010), e1000705.

Araya, Roberto, Jiang Jiang, Kenneth B Eisenthal, and Rafael Yuste (2006). "The spine neck filters membrane potentials." *Proceedings of the National Academy of Sciences of the United States of America* 103.47 (Nov. 2006), pp. 17961–6.

Arellano, Jon I, Ruth Benavides-Piccione, Javier Defelipe, and Rafael Yuste (2007). "Ultrastructure of dendritic spines: correlation between synaptic and spine morphologies." *Frontiers in neuroscience* 1.1 (Nov. 2007), pp. 131–43.

Arendt, Kristin L, María Royo, Mónica Fernández-Monreal, Shira Knafo, Cortney N Petrok, Jeffrey R Martens, and José A Esteban (2010). "PIP3 controls synaptic function by maintaining AMPA receptor

clustering at the postsynaptic membrane." *Nature neuroscience* 13.1 (Jan. 2010), pp. 36–44.

Arkin, A, J Ross, and H H McAdams (1998). "Stochastic kinetic analysis of developmental pathway bifurcation in phage lambda-infected Escherichia coli cells." *Genetics* 149.4 (Aug. 1998), pp. 1633–48.

Aslam, Naveed, Yoshi Kubota, David Wells, and Harel Z Shouval (2009). "Translational switch for long-term maintenance of synaptic plasticity." *Molecular systems biology* 5 (Jan. 2009), p. 284.

Bakker, Barbara M, Karen van Eunen, Jeroen A L Jeneson, Natal A W van Riel, Frank J Bruggeman, and Bas Teusink (2010). "Systems biology from micro-organisms to human metabolic diseases: the role of detailed kinetic models." *Biochemical Society transactions* 38.5 (Oct. 2010), pp. 1294–301.

Balkowiec, A and D M Katz (2000). "Activity-dependent release of endogenous brain-derived neurotrophic factor from primary sensory neurons detected by ELISA in situ." *The Journal of neuroscience : the official journal of the Society for Neuroscience* 20.19 (Oct. 2000), pp. 7417–23.

Balkowiec, Agnieszka and David M Katz (2002). "Cellular mechanisms regulating activity-dependent release of native brain-derived neurotrophic factor from hippocampal neurons." *The Journal of neuroscience : the official journal of the Society for Neuroscience* 22.23 (Dec. 2002), pp. 10399–407.

Banks, Daniel S and Cécile Fradin (2005). "Anomalous diffusion of proteins due to molecular crowding." *Biophysical journal* 89.5 (Nov. 2005), pp. 2960–71.

Barde, Y A, D Edgar, and H Thoenen (1982). "Purification of a new neurotrophic factor from mammalian brain." *The EMBO journal* 1.5 (Jan. 1982), pp. 549–53.

Bariohay, Bruno, Julien Roux, Catherine Tardivel, Jérôme Trouslard, Andre Jean, and Bruno Lebrun (2009). "Brain-derived neurotrophic factor/tropomyosin-related kinase receptor type B signaling is a downstream effector of the brainstem melanocortin system in food intake control." *Endocrinology* 150.6 (June 2009), pp. 2646–53.

Barria, A, V Derkach, and T Soderling (1997). "Identification of the Ca2+/calmodulin-dependent protein kinase II regulatory phosphorylation site in the alpha-amino-3-hydroxyl-5-methyl-4-isoxazolepropionate-type glutamate receptor." *The Journal of biological chemistry* 272.52 (Dec. 1997), pp. 32727–30.

Bayés, Alex, Louie N van de Lagemaat, Mark O Collins, Mike D R Croning, Ian R Whittle, Jyoti S Choudhary, and Seth G N Grant (2011). "Characterization of the proteome, diseases and evolution

of the human postsynaptic density." *Nature neuroscience* 14.1 (Jan. 2011), pp. 19–21.

Beck, Martin, Alexander Schmidt, Johan Malmstroem, Manfred Claassen, Alessandro Ori, Anna Szymborska, Franz Herzog, Oliver Rinner, Jan Ellenberg, and Ruedi Aebersold (2011). "The quantitative proteome of a human cell line." *Molecular systems biology* 7 (Jan. 2011), p. 549.

Berg, Howard C. (1993). *Random Walks in Biology*. Princeton University Press, 1993, p. 164.

Berman, M, M F Weiss, and E Shahn (1962a). "Some formal approaches to the analysis of kinetic data in terms of linear compartmental systems." *Biophysical journal* 2 (May 1962), pp. 289–316.

Berman, M, E Shahn, and M F Weiss (1962b). "The routine fitting of kinetic data to models: a mathematical formalism for digital computers." *Biophysical journal* 2 (May 1962), pp. 275–87.

Bernard, V, P Somogyi, and J P Bolam (1997). "Cellular, subcellular, and subsynaptic distribution of AMPA-type glutamate receptor subunits in the neostriatum of the rat." *The Journal of neuroscience : the official journal of the Society for Neuroscience* 17.2 (Jan. 1997), pp. 819–33.

Bhalla, U S and R Iyengar (1999). "Emergent properties of networks of biological signaling pathways." *Science (New York, N.Y.)* 283.5400 (Jan. 1999), pp. 381–7.

Bhalla, Upinder S. (2000). *Modeling Networks of Signaling Pathways*. Ed. by Erik De Schutter. CRC Press; Har/Cdr edition (22 Nov 2000), 2000.

Bhalla, Upinder S (2002). "Mechanisms for temporal tuning and filtering by postsynaptic signaling pathways." *Biophysical journal* 83.2 (Aug. 2002), pp. 740–52.

Bhalla, Upinder S (2004). "Signaling in small subcellular volumes. II. Stochastic and diffusion effects on synaptic network properties." *Biophysical journal* 87.2 (Aug. 2004), pp. 745–53.

Birtwistle, Marc R, Mariko Hatakeyama, Noriko Yumoto, Babatunde A Ogunnaike, Jan B Hoek, and Boris N Kholodenko (2007). "Ligand-dependent responses of the ErbB signaling network: experimental and modeling analyses." en. *Molecular systems biology* 3 (Jan. 2007), p. 144.

Bliss, T V and G L Collingridge (1993). "A synaptic model of memory: long-term potentiation in the hippocampus." *Nature* 361.6407 (Jan. 1993), pp. 31–9.

Bliss, T. V. P. and T. Lomo (1973). "Long-lasting potentiation of synaptic transmission in the dentate area of the anaesthetized rabbit

following stimulation of the perforant path". *J. Physiol.* 232.2 (July 1973), pp. 331–356.

Blum, Robert, Karl W Kafitz, and Arthur Konnerth (2002). "Neurotrophin-evoked depolarization requires the sodium channel Na(V)1.9." *Nature* 419.6908 (Oct. 2002), pp. 687–693.

Boehm, Jannic, Myoung-Goo Kang, Richard C Johnson, Jose Esteban, Richard L Huganir, and Roberto Malinow (2006). "Synaptic incorporation of AMPA receptors during LTP is controlled by a PKC phosphorylation site on GluR1." *Neuron* 51.2 (July 2006), pp. 213–225.

Borgdorff, Aren J and Daniel Choquet (2002). "Regulation of AMPA receptor lateral movements." *Nature* 417.6889 (June 2002), pp. 649–53.

Borisov, Nikolay, Edita Aksamitiene, Anatoly Kiyatkin, Stefan Legewie, Jan Berkhout, Thomas Maiwald, Nikolai P Kaimachnikov, Jens Timmer, Jan B Hoek, and Boris N Kholodenko (2009). "Systems-level interactions between insulin-EGF networks amplify mitogenic signaling." *Molecular systems biology* 5.256 (Jan. 2009), p. 256.

Brooks, Ian M and Steven J Tavalin (2011). "Ca2+/calmodulin-dependent protein kinase II inhibitors disrupt AKAP79-dependent PKC signaling to GluA1 AMPA receptors." *The Journal of biological chemistry* 286.8 (Feb. 2011), pp. 6697–706.

Brown, Guy C. and Boris N. Kholodenko (1999). "Spatial gradients of cellular phospho-proteins". *FEBS Letters* 457.3 (Sept. 1999), pp. 452–454.

Brown, Sherry-Ann, Ion I Moraru, James C Schaff, and Leslie M Loew (2011). "Virtual NEURON: a strategy for merged biochemical and electrophysiological modeling." *Journal of computational neuroscience* 31.2 (Oct. 2011), pp. 385–400.

Byrne, Michael J, M Neal Waxham, and Yoshihisa Kubota (2010). "Cellular dynamic simulator: an event driven molecular simulation environment for cellular physiology." *Neuroinformatics* 8.2 (June 2010), pp. 63–82.

Catania, M V, T R Tölle, and H Monyer (1995). "Differential expression of AMPA receptor subunits in NOS-positive neurons of cortex, striatum, and hippocampus." *The Journal of neuroscience : the official journal of the Society for Neuroscience* 15.11 (Nov. 1995), pp. 7046–61.

Chagpar, Ryaz B, Philip H Links, M Chris Pastor, Levi A Furber, Andrea D Hawrysh, M Dean Chamberlain, and Deborah H Anderson (2010). "Direct positive regulation of PTEN by the p85 subunit of phosphatidylinositol 3-kinase." *Proceedings of the National Academy*

of Sciences of the United States of America 107.12 (Mar. 2010), pp. 5471–6.

Chance, B, D Garfinkel, J Higgins, and B Hess (1960). "Metabolic control mechanisms. 5. A solution for the equations representing interaction between glycolysis and respiration in ascites tumor cells." en. *The Journal of biological chemistry* 235 (Aug. 1960), pp. 2426–39.

Chen, H X, N Otmakhov, S Strack, R J Colbran, and J E Lisman (2001). "Is persistent activity of calcium/calmodulin-dependent kinase required for the maintenance of LTP?": *Journal of neurophysiology* 85.4 (Apr. 2001), pp. 1368–76.

Chen, Xiaobing, Christopher D Nelson, Xiang Li, Christine A Winters, Rita Azzam, Alioscka A Sousa, Richard D Leapman, Harold Gainer, Morgan Sheng, and Thomas S Reese (2011). "PSD-95 is required to sustain the molecular organization of the postsynaptic density." *The Journal of neuroscience : the official journal of the Society for Neuroscience* 31.17 (Apr. 2011), pp. 6329–38.

Cheng, Dongmei, Casper C Hoogenraad, John Rush, Elizabeth Ramm, Max A Schlager, Duc M Duong, Ping Xu, Sameera R Wijayawardana, John Hanfelt, Terunaga Nakagawa, Morgan Sheng, and Junmin Peng (2006). "Relative and absolute quantification of postsynaptic density proteome isolated from rat forebrain and cerebellum." *Molecular & cellular proteomics : MCP* 5.6 (June 2006), pp. 1158–70.

Choi, Jang Hyun, Won-Pyo Hong, Sanguk Yun, Hyeon Soo Kim, Jong-Ryul Lee, Jong Bae Park, Yun Soo Bae, Sung Ho Ryu, and Pann-Ghill Suh (2005). "Grb2 negatively regulates epidermal growth factor-induced phospholipase C-γ1 activity through the direct interaction with tyrosine-phosphorylated phospholipase C-γ1". *Cellular Signalling* 17.10 (Oct. 2005), pp. 1289–1299.

Choquet, Daniel and Antoine Triller (2013). "The dynamic synapse." *Neuron* 80.3 (Oct. 2013), pp. 691–703.

Citri, Ami and Robert C Malenka (2008). "Synaptic plasticity: multiple forms, functions, and mechanisms." *Neuropsychopharmacology : official publication of the American College of Neuropsychopharmacology* 33.1 (Jan. 2008), pp. 18–41.

Collingridge, G L, S J Kehl, and H McLennan (1983). "Excitatory amino acids in synaptic transmission in the Schaffer collateral-commissural pathway of the rat hippocampus." *The Journal of physiology* 334 (Jan. 1983), pp. 33–46.

Craske, Madeleine L, Marc Fivaz, Nizar N Batada, and Tobias Meyer (2005). "Spines and neurite branches function as geometric attractors that enhance protein kinase C action." *The Journal of cell biology* 170.7 (Sept. 2005), pp. 1147–58.

Czöndör, Katalin, Magali Mondin, Mikael Garcia, Martin Heine, Renato Frischknecht, Daniel Choquet, Jean-Baptiste Sibarita, and Olivier R Thoumine (2012). "Unified quantitative model of AMPA receptor trafficking at synapses." *Proceedings of the National Academy of Sciences of the United States of America* 109.9 (Feb. 2012), pp. 3522–7.

Delgado, Jary Y, Marcelo Coba, Christopher N G Anderson, Kimberly R Thompson, Erin E Gray, Carrie L Heusner, Kelsey C Martin, Seth G N Grant, and Thomas J O'Dell (2007). "NMDA receptor activation dephosphorylates AMPA receptor glutamate receptor 1 subunits at threonine 840." *The Journal of neuroscience : the official journal of the Society for Neuroscience* 27.48 (Nov. 2007), pp. 13210–21.

Deller, Thomas, Martin Korte, Sophie Chabanis, Alexander Drakew, Herbert Schwegler, Giulia Good Stefani, Aimee Zuniga, Karin Schwarz, Tobias Bonhoeffer, Rolf Zeller, Michael Frotscher, and Peter Mundel (2003). "Synaptopodin-deficient mice lack a spine apparatus and show deficits in synaptic plasticity." *Proceedings of the National Academy of Sciences of the United States of America* 100.18 (Sept. 2003), pp. 10494–9.

Derkach, V, A Barria, and T R Soderling (1999). "Ca2+/calmodulin-kinase II enhances channel conductance of alpha-amino-3-hydroxy-5-methyl-4-isoxazolepropionate type glutamate receptors." *Proceedings of the National Academy of Sciences of the United States of America* 96.6 (Mar. 1999), pp. 3269–74.

Derkach, Victor A, Michael C Oh, Eric S Guire, and Thomas R Soderling (2007). "Regulatory mechanisms of AMPA receptors in synaptic plasticity." *Nature reviews. Neuroscience* 8.2 (Feb. 2007), pp. 101–13.

Dieni, Sandra, Tomoya Matsumoto, Martijn Dekkers, Stefanie Rauskolb, Mihai S Ionescu, Ruben Deogracias, Eckart D Gundelfinger, Masami Kojima, Sigrun Nestel, Michael Frotscher, and Yves-Alain Barde (2012). "BDNF and its pro-peptide are stored in presynaptic dense core vesicles in brain neurons." *The Journal of cell biology* 196.6 (Mar. 2012), pp. 775–88.

Diggle, Peter (1985). *A Kernel Method for Smoothing Point Process Data*. 1985.

Drake, C. T., T. A. Milner, and S. L. Patterson (1999). "Ultrastructural Localization of Full-Length trkB Immunoreactivity in Rat Hippocampus Suggests Multiple Roles in Modulating Activity-Dependent Synaptic Plasticity". *J. Neurosci.* 19.18 (Sept. 1999), pp. 8009–8026.

Edelstein, Arieh L. and Noam Agmon (1993). "Brownian dynamics simulations of reversible reactions in one dimension". *Journal of Chemical Physics* 99.7 (1993), p. 9.

Elf, J. and M. Ehrenberg (2004). "Spontaneous separation of bi-stable biochemical systems into spatial domains of opposite phases". English. *Systems Biology* 1.2 (Dec. 2004), pp. 230–236.

Ernfors, Patrik and Clive R Bramham (2003). "The coupling of a trkB tyrosine residue to LTP." *Trends Neurosci* 26.4 (Apr. 2003), pp. 171–173.

Espinoza, Flor A, Michael J Wester, Janet M Oliver, Bridget S Wilson, Nicholas L Andrews, Diane S Lidke, and Stanly L Steinberg (2012). "Insights into cell membrane microdomain organization from live cell single particle tracking of the IgE high affinity receptor FcĬţRI of mast cells." *Bulletin of mathematical biology* 74.8 (Aug. 2012), pp. 1857–911.

F. Baras, M. Mansour (1997). *Microscopic Simulations of Chemical Instabilities*. Ed. by I. Prigogine and Stuart A. Rice. Vol. 100. Advances in Chemical Physics. Hoboken, NJ, USA: John Wiley & Sons, Inc., Jan. 1997.

Faas, Guido C, Sridhar Raghavachari, John E Lisman, and Istvan Mody (2011). "Calmodulin as a direct detector of Ca2+ signals." *Nature neuroscience* 14.3 (Mar. 2011), pp. 301–4.

Fange, David, Otto G Berg, Paul Sjöberg, and Johan Elf (2010). "Stochastic reaction-diffusion kinetics in the microscopic limit." *Proceedings of the National Academy of Sciences of the United States of America* 107.46 (Nov. 2010), pp. 19820–5.

Fernandez, Eric, Renaud Schiappa, Jean-Antoine Girault, and Nicolas Le Novère (2006). "DARPP-32 is a robust integrator of dopamine and glutamate signals." *PLoS computational biology* 2.12 (Dec. 2006), e176.

Field, Richard J. (1974). "Oscillations in chemical systems. IV. Limit cycle behavior in a model of a real chemical reaction". *The Journal of Chemical Physics* 60.5 (Aug. 1974), p. 1877.

Fonnum, F (1984). "Glutamate: a neurotransmitter in mammalian brain." *Journal of neurochemistry* 42.1 (Jan. 1984), pp. 1–11.

Franks, Kevin M., Thomas M. Bartol, and Terrence J. Sejnowski (2001). "An MCell model of calcium dynamics and frequency-dependence of calmodulin activation in dendritic spines". *Neurocomputing* 38 (2001), pp. 9–16.

Fraser, Dawn and Mads Kaern (2009). "A chance at survival: gene expression noise and phenotypic diversification strategies." *Molecular microbiology* 71.6 (Mar. 2009), pp. 1333–40.

Fukunaga, K, L Stoppini, E Miyamoto, and D Muller (1993). "Long-term potentiation is associated with an increased activity of Ca2+/calmodulin-dependent protein kinase II." *The Journal of biological chemistry* 268.11 (Apr. 1993), pp. 7863–7.

Fukunaga, K, D Muller, and E Miyamoto (1995). "Increased phosphorylation of Ca2+/calmodulin-dependent protein kinase II and its endogenous substrates in the induction of long-term potentiation." *The Journal of biological chemistry* 270.11 (Mar. 1995), pp. 6119–24.

Fuxe, Kjell, Luigi Agnati, Francisco Mora, Juan A. De Carlos, and José Borrell (2007). "A historical reflection of the contributions of Cajal and Golgi to the foundations of neuroscience". *Brain Research Reviews* 55.1 (2007), pp. 8–16.

Gallegos, Lisa L and Alexandra C Newton (2008). "Spatiotemporal dynamics of lipid signaling: protein kinase C as a paradigm." *IUBMB Life* 60.12 (Dec. 2008), pp. 782–789.

Garfinkel, D, L Garfinkel, M Pring, S B Green, and B Chance (1970). "Computer applications to biochemical kinetics." *Annual review of biochemistry* 39 (Jan. 1970), pp. 473–98.

Garfinkel, David (1968). "A machine-independent language for the simulation of complex chemical and biochemical systems". *Computers and Biomedical Research* 2.1 (1968), pp. 31–44.

Gerisch, Günther, Britta Schroth-Diez, Annette Müller-Taubenberger, and Mary Ecke (2012). "PIP3 waves and PTEN dynamics in the emergence of cell polarity." *Biophysical journal* 103.6 (Sept. 2012), pp. 1170–8.

Gillespie, Daniel T. (1977). "Exact stochastic simulation of coupled chemical reactions". *The Journal of Physical Chemistry* 81.25 (Dec. 1977), pp. 2340–2361.

Govern, Christopher C and Arup K Chakraborty (2013). "Stochastic responses may allow genetically diverse cell populations to optimize performance with simpler signaling networks." *PloS one* 8.8 (Jan. 2013), e65086.

Gray, E G (1959). "Axo-somatic and axo-dendritic synapses of the cerebral cortex: an electron microscope study." *Journal of anatomy* 93 (Oct. 1959), pp. 420–33.

Gray, Erin E, Ann E Fink, Joshua Sariñana, Bryce Vissel, and Thomas J O'Dell (2007). "Long-term potentiation in the hippocampal CA1 region does not require insertion and activation of GluR2-lacking AMPA receptors." *Journal of neurophysiology* 98.4 (Oct. 2007), pp. 2488–92.

Gruart, Agnès, Carla Sciarretta, Mauricio Valenzuela-Harrington, José M Delgado-García, and Liliana Minichiello (2006). "Mutation at

the TrkB PLC{gamma}-docking site affects hippocampal LTP and associative learning in conscious mice." *Learning & memory (Cold Spring Harbor, N.Y.)* 14.1 (2006), pp. 54–62.

Halling, P J (1989). "Do the laws of chemistry apply to living cells?": *Trends in biochemical sciences* 14.8 (Aug. 1989), pp. 317–8.

Haniu, M. (1997). "Interactions between Brain-derived Neurotrophic Factor and the TRKB Receptor. IDENTIFICATION OF TWO LIG-AND BINDING DOMAINS IN SOLUBLE TRKB BY AFFINITY SEPARATION AND CHEMICAL CROSS-LINKING". *Journal of Biological Chemistry* 272.40 (Oct. 1997), pp. 25296–25303.

Harlan, J E, P J Hajduk, H S Yoon, and S W Fesik (1994). "Pleckstrin homology domains bind to phosphatidylinositol-4,5-bisphosphate." *Nature* 371.6493 (Sept. 1994), pp. 168–70.

Harris, K M and D M Landis (1986). "Membrane structure at synaptic junctions in area CA1 of the rat hippocampus." *Neuroscience* 19.3 (Nov. 1986), pp. 857–72.

Harris, K M and J K Stevens (1988). "Dendritic spines of rat cerebellar Purkinje cells: serial electron microscopy with reference to their biophysical characteristics." *J Neurosci* 8.12 (Dec. 1988), pp. 4455–4469.

Harris, K M, F E Jensen, and B Tsao (1992). "Three-dimensional structure of dendritic spines and synapses in rat hippocampus (CA1) at postnatal day 15 and adult ages: implications for the maturation of synaptic physiology and long-term potentiation." *The Journal of neuroscience : the official journal of the Society for Neuroscience* 12.7 (July 1992), pp. 2685–705.

Hartmann, M, R Heumann, and V Lessmann (2001). "Synaptic secretion of BDNF after high-frequency stimulation of glutamatergic synapses." *The EMBO journal* 20.21 (Nov. 2001), pp. 5887–97.

Hattne, Johan, David Fange, and Johan Elf (2005a). "Stochastic reaction-diffusion simulation with MesoRD." *Bioinformatics (Oxford, England)* 21.12 (June 2005), pp. 2923–4.

Hattne, Johan, David Fange, and Johan Elf (2005b). "Stochastic reaction-diffusion simulation with MesoRD." *Bioinformatics (Oxford, England)* 21.12 (June 2005), pp. 2923–4.

Hebb, Donald O. (1949). *The Organization of Behavior: A Neuropsychological Theory*. Kindle Edi. Psychology Press; New Ed edition (1 May 2002), 1949, p. 379.

Heck, Nicolas, Sandrine Betuing, Peter Vanhoutte, and Jocelyne Caboche (2012). "A deconvolution method to improve automated 3D-analysis of dendritic spines: application to a mouse model of Huntington's disease." *Brain structure & function* 217.2 (Apr. 2012), pp. 421–34.

Hodgkin, A L and A F Huxley (1952). "Currents carried by sodium and potassium ions through the membrane of the giant axon of Loligo." *The Journal of physiology* 116.4 (Apr. 1952), pp. 449–72.

Hodgkin A L and A F Huxley (1952). "A quantitative description of membrane current and its application to conduction and excitation in nerve." *The Journal of physiology* 117.4 (Aug. 1952), pp. 500–44.

Holbro, Niklaus, Asa Grunditz, and Thomas G Oertner (2009). "Differential distribution of endoplasmic reticulum controls metabotropic signaling and plasticity at hippocampal synapses." *Proceedings of the National Academy of Sciences of the United States of America* 106.35 (Sept. 2009), pp. 15055–60.

Holcman, D, Z Schuss, and E Korkotian (2004). "Calcium dynamics in dendritic spines and spine motility." *Biophysical journal* 87.1 (July 2004), pp. 81–91.

Hoops, Stefan, Sven Sahle, Ralph Gauges, Christine Lee, Jürgen Pahle, Natalia Simus, Mudita Singhal, Liang Xu, Pedro Mendes, and Ursula Kummer (2006). "COPASI–a COmplex PAthway SImulator." *Bioinformatics (Oxford, England)* 22.24 (Dec. 2006), pp. 3067–74.

Horwood, Jennifer M, Franck Dufour, Serge Laroche, and Sabrina Davis (2006). "Signalling mechanisms mediated by the phosphoinositide 3-kinase/Akt cascade in synaptic plasticity and memory in the rat." *The European journal of neuroscience* 23.12 (June 2006), pp. 3375–84.

Hucka, M. et al. (2003). "The systems biology markup language (SBML): a medium for representation and exchange of biochemical network models". *Bioinformatics* 19.4 (Mar. 2003), pp. 524–531.

Hucka, Michael, Frank T. Bergmann, Stefan Hoops, Sarah M. Keating, Sven Sahle, James C. Schaff, Lucian P. Smith, and Daren J. Wilkinson (2010). *The Systems Biology Markup Language (SBML): Language Specification for Level 3 Version 1 Core*. 2010.

Hugel, Sylvain, Mathias Abegg, Vincenzo de Paola, Pico Caroni, Beat H Gähwiler, and R Anne McKinney (2009). "Dendritic spine morphology determines membrane-associated protein exchange between dendritic shafts and spine heads." *Cerebral cortex (New York, N.Y. : 1991)* 19.3 (Mar. 2009), pp. 697–702.

Hyman, C, M Hofer, Y A Barde, M Juhasz, G D Yancopoulos, S P Squinto, and R M Lindsay (1991). "BDNF is a neurotrophic factor for dopaminergic neurons of the substantia nigra." *Nature* 350.6315 (Mar. 1991), pp. 230–2.

Illian, Janine, Antti Penttinen, Helga Stoyan, and Dietrich Stoyan (2008). *Statistical Analysis and Modelling of Spatial Point Patterns*. 1st ed. Chichester: John Wiley & Sons Ltd, 2008.

Insall, Robert H. and Orion D. Weiner (2001). "PIP3, PIP2, and Cell MovementâĂŤSimilar Messages, Different Meanings?": *Developmental Cell* 1.6 (Dec. 2001), pp. 743–747.

Izeddin, Ignacio, Christian G Specht, Mickaël Lelek, Xavier Darzacq, Antoine Triller, Christophe Zimmer, and Maxime Dahan (2011). "Super-resolution dynamic imaging of dendritic spines using a low-affinity photoconvertible actin probe." *PloS one* 6.1 (Jan. 2011), e15611.

Jain, Pragati and Upinder S Bhalla (2009). "Signaling logic of activity-triggered dendritic protein synthesis: an mTOR gate but not a feedback switch." *PLoS Comput Biol* 5.2 (Feb. 2009).

Jaskolski, F and JM Henley (2009). "Synaptic receptor trafficking: the lateral point of view." *Neuroscience* 158.1 (Jan. 2009), pp. 19–24.

Jenkins, Meagan A and Stephen F Traynelis (2012). "PKC phosphorylates GluA1-Ser831 to enhance AMPA receptor conductance." *Channels (Austin, Tex.)* 6.1 (2012), pp. 60–4.

Ji, Yuanyuan, Petti T Pang, Linyin Feng, and Bai Lu (2005). "Cyclic AMP controls BDNF-induced TrkB phosphorylation and dendritic spine formation in mature hippocampal neurons." *Nature neuroscience* 8.2 (Feb. 2005), pp. 164–72.

Jones, G A and G Carpenter (1993). "The regulation of phospholipase C-gamma 1 by phosphatidic acid. Assessment of kinetic parameters." *J Biol Chem* 268.28 (Oct. 1993), pp. 20845–20850.

Kakumoto, Toshiyuki and Takao Nakata (2013). "Optogenetic Control of PIP3: PIP3 Is Sufficient to Induce the Actin-Based Active Part of Growth Cones and Is Regulated via Endocytosis." *PloS one* 8.8 (Jan. 2013), e70861.

Kang, H, A A Welcher, D Shelton, and E M Schuman (1997). "Neurotrophins and time: different roles for TrkB signaling in hippocampal long-term potentiation." *Neuron* 19.3 (Sept. 1997), pp. 653–64.

Karnovsky, M J, A M Kleinfeld, R L Hoover, and R D Klausner (1982). "The concept of lipid domains in membranes." *The Journal of cell biology* 94.1 (July 1982), pp. 1–6.

Kelleher, Raymond J, Arvind Govindarajan, Hae-Yoon Jung, Hyejin Kang, and Susumu Tonegawa (2004). "Translational control by MAPK signaling in long-term synaptic plasticity and memory." *Cell* 116.3 (Feb. 2004), pp. 467–79.

Kempf, Christian, Thorsten Staudt, Pit Bingen, Heinz Horstmann, Johann Engelhardt, Stefan W Hell, and Thomas Kuner (2013). "Tissue multicolor STED nanoscopy of presynaptic proteins in the calyx of held." *PloS one* 8.4 (Jan. 2013), e62893.

Kerr, Rex A, Thomas M Bartol, Boris Kaminsky, Markus Dittrich, Jen-Chien Jack Chang, Scott B Baden, Terrence J Sejnowski, and Joel R Stiles (2008). "FAST MONTE CARLO SIMULATION METHODS FOR BIOLOGICAL REACTION-DIFFUSION SYSTEMS IN SOLUTION AND ON SURFACES." *SIAM journal on scientific computing : a publication of the Society for Industrial and Applied Mathematics* 30.6 (Oct. 2008), p. 3126.

Ketschek, Andrea and Gianluca Gallo (2010). "Nerve growth factor induces axonal filopodia through localized microdomains of phosphoinositide 3-kinase activity that drive the formation of cytoskeletal precursors to filopodia." *The Journal of neuroscience : the official journal of the Society for Neuroscience* 30.36 (Sept. 2010), pp. 12185–97.

Khan, Shahid, Yixiao Zou, Asma Amjad, Ailia Gardezi, Carolyn L Smith, Christine Winters, and Thomas S Reese (2011). "Sequestration of CaMKII in dendritic spines in silico." *Journal of computational neuroscience* 31.3 (Nov. 2011), pp. 581–94.

Khan, Shahid, Thomas S Reese, Nasir Rajpoot, and Ayisha Shabbir (2012). "Spatiotemporal maps of CaMKII in dendritic spines." *Journal of computational neuroscience* 33.1 (Aug. 2012), pp. 123–39.

Khodakhah, K. and D. Ogden (1995). "Fast activation and inactivation of inositol trisphosphate-evoked Ca". *Journal of Physiology* 487.2 (1995), pp. 343–358.

Kholodenko, Boris N. (2002). "MAP kinase cascade signaling and endocytic trafficking: a marriage of convenience?": *Trends in Cell Biology* 12.4 (Apr. 2002), pp. 173–177.

Kholodenko, Borisov, G Brown, and J Hoek (2000). "Diffusion control of protein phosphorylation in signal transduction pathways". en. (Sept. 2000).

Kim, Karam, Jinhee Yang, Xiao-Ping Zhong, Myoung-Hwan Kim, Yun Sook Kim, Hyun Woo Lee, Seungnam Han, Jeonghoon Choi, Kihoon Han, Jinsoo Seo, Stephen M Prescott, Matthew K Topham, Yong Chul Bae, Gary Koretzky, Se-Young Choi, and Eunjoon Kim (2009). "Synaptic removal of diacylglycerol by DGKzeta and PSD-95 regulates dendritic spine maintenance." *EMBO J* 28.8 (Apr. 2009), pp. 1170–1179.

Klein, R, L F Parada, F Coulier, and M Barbacid (1989). "trkB, a novel tyrosine protein kinase receptor expressed during mouse neural development." *The EMBO journal* 8.12 (Dec. 1989), pp. 3701–9.

Klein, R, V Nanduri, S A Jing, F Lamballe, P Tapley, S Bryant, C Cordon-Cardo, K R Jones, L F Reichardt, and M Barbacid (1991). "The trkB tyrosine protein kinase is a receptor for brain-derived

neurotrophic factor and neurotrophin-3." *Cell* 66.2 (July 1991), pp. 395–403.

Kojima, M, N Takei, T Numakawa, Y Ishikawa, S Suzuki, T Matsumoto, R Katoh-Semba, H Nawa, and H Hatanaka (2001). "Biological characterization and optical imaging of brain-derived neurotrophic factor-green fluorescent protein suggest an activity-dependent local release of brain-derived neurotrophic factor in neurites of cultured hippocampal neurons." *Journal of neuroscience research* 64.1 (Apr. 2001), pp. 1–10.

König, Ireen, Juliane P Schwarz, and Kurt I Anderson (2008). "Fluorescence lifetime imaging: association of cortical actin with a PIP3-rich membrane compartment." *European journal of cell biology* 87.8-9 (Sept. 2008), pp. 735–41.

Kötter, R (1994). "Postsynaptic integration of glutamatergic and dopaminergic signals in the striatum." *Progress in neurobiology* 44.2 (Oct. 1994), pp. 163–96.

Kovalchuk, Yury, Knut Holthoff, and Arthur Konnerth (2004). "Neurotrophin action on a rapid timescale." *Curr Opin Neurobiol* 14.5 (Oct. 2004), pp. 558–563.

Kusumi, Akihiro, Takahiro K Fujiwara, Rahul Chadda, Min Xie, Taka A Tsunoyama, Ziya Kalay, Rinshi S Kasai, and Kenichi G N Suzuki (2012). "Dynamic organizing principles of the plasma membrane that regulate signal transduction: commemorating the fortieth anniversary of Singer and Nicolson's fluid-mosaic model." en. *Annual review of cell and developmental biology* 28 (Jan. 2012), pp. 215–50.

Le Novère, Nicolas, Benjamin Bornstein, Alexander Broicher, Mélanie Courtot, Marco Donizelli, Harish Dharuri, Lu Li, Herbert Sauro, Maria Schilstra, Bruce Shapiro, Jacky L Snoep, and Michael Hucka (2006). "BioModels Database: a free, centralized database of curated, published, quantitative kinetic models of biochemical and cellular systems." *Nucleic acids research* 34.Database issue (Jan. 2006), pp. D689–91.

Le Novère, Nicolas et al. (2009). "The Systems Biology Graphical Notation." *Nature biotechnology* 27.8 (Aug. 2009), pp. 735–41.

Lee, Hey-Kyoung, Kogo Takamiya, Kimihiko Kameyama, Kaiwen He, Sandy Yu, Luciano Rossetti, David Wilen, and Richard L Huganir (2007). "Identification and characterization of a novel phosphorylation site on the GluR1 subunit of AMPA receptors." *Molecular and cellular neurosciences* 36.1 (Sept. 2007), pp. 86–94.

Lee, J O, H Yang, M M Georgescu, A Di Cristofano, T Maehama, Y Shi, J E Dixon, P Pandolfi, and N P Pavletich (1999). "Crystal structure of the PTEN tumor suppressor: implications for its phosphoinositide

phosphatase activity and membrane association." *Cell* 99.3 (Oct. 1999), pp. 323–34.

Leibrock, J, F Lottspeich, A Hohn, M Hofer, B Hengerer, P Masiakowski, H Thoenen, and Y A Barde (1989). "Molecular cloning and expression of brain-derived neurotrophic factor." *Nature* 341.6238 (Sept. 1989), pp. 149–52.

Leonard, A. S., I. A. Lim, D. E. Hemsworth, M. C. Horne, and J. W. Hell (1999). "Calcium/calmodulin-dependent protein kinase II is associated with the N-methyl-D-aspartate receptor". *Proceedings of the National Academy of Sciences* 96.6 (Mar. 1999), pp. 3239–3244.

Levine, E S, C F Dreyfus, I B Black, and M R Plummer (1995). "Brain-derived neurotrophic factor rapidly enhances synaptic transmission in hippocampal neurons via postsynaptic tyrosine kinase receptors." *Proceedings of the National Academy of Sciences of the United States of America* 92.17 (Aug. 1995), pp. 8074–7.

Li, Lu, Melanie I Stefan, and Nicolas Le Novère (2012). "Calcium input frequency, duration and amplitude differentially modulate the relative activation of calcineurin and CaMKII." *PloS one* 7.9 (Jan. 2012), e43810.

Li, Y X, Y Zhang, H A Lester, E M Schuman, and N Davidson (1998). "Enhancement of neurotransmitter release induced by brain-derived neurotrophic factor in cultured hippocampal neurons." *The Journal of neuroscience : the official journal of the Society for Neuroscience* 18.24 (Dec. 1998), pp. 10231–40.

Li, Yan, Yi-Chang Jia, Kai Cui, Ning Li, Zai-Yu Zheng, Yi-Zheng Wang, and Xiao-Bing Yuan (2005). "Essential role of TRPC channels in the guidance of nerve growth cones by brain-derived neurotrophic factor." *Nature* 434.7035 (Apr. 2005), pp. 894–8.

Lin, Da-Ting, Yuichi Makino, Kamal Sharma, Takashi Hayashi, Rachael Neve, Kogo Takamiya, and Richard L Huganir (2009). "Regulation of AMPA receptor extrasynaptic insertion by 4.1N, phosphorylation and palmitoylation." *Nat Neurosci* 12.7 (July 2009), pp. 879–887.

Lipkow, Karen (2006). "Changing cellular location of CheZ predicted by molecular simulations." *PLoS computational biology* 2.4 (Apr. 2006). Ed. by Diana Murray, e39.

Lipkow, Karen and David J Odde (2008). "Model for Protein Concentration Gradients in the Cytoplasm." *Cellular and molecular bioengineering* 1.1 (Mar. 2008), pp. 84–92.

Lisman, J E (1985). "A mechanism for memory storage insensitive to molecular turnover: a bistable autophosphorylating kinase." *Proceedings of the National Academy of Sciences of the United States of America* 82.9 (May 1985), pp. 3055–7.

Liu, Siqiong June and R Suzanne Zukin (2007). "Ca2+-permeable AMPA receptors in synaptic plasticity and neuronal death." *Trends in neurosciences* 30.3 (Mar. 2007), pp. 126–34.

Lomo, T (1966). "Frequency potentiation of excitatory synaptic activity in the dentate area of the hippocampal formation". *Acta Physiol. Scand* 68.Suppl 277 (1966).

López-Muñoz, Francisco and Cecilio Alamo (2009). "Historical evolution of the neurotransmission concept". *Journal of Neural Transmission* (2009).

Lotka, A J (1920). "Analytical Note on Certain Rhythmic Relations in Organic Systems." *Proceedings of the National Academy of Sciences of the United States of America* 6.7 (July 1920), pp. 410–5.

Lotka, Alfred J. (1909). "Contribution to the Theory of Periodic Reactions". *The Journal of Physical Chemistry* 14.3 (Jan. 1909), pp. 271–274.

Lotka, Alfred J. (1925). *Elements of Bhysical Biology*. Williams and Wilkins, 1925.

Lu, Wei, Yun Shi, Alexander C. Jackson, Kirsten Bjorgan, Matthew J. During, Rolf Sprengel, Peter H. Seeburg, and Roger A. Nicoll (2009). "Subunit Composition of Synaptic AMPA Receptors Revealed by a Single-Cell Genetic Approach". *Neuron* 62.2 (2009), pp. 254–268.

Lu, Wei, Kaname Isozaki, Katherine W Roche, and Roger A Nicoll (2010). "Synaptic targeting of AMPA receptors is regulated by a CaMKII site in the first intracellular loop of GluA1." *Proceedings of the National Academy of Sciences of the United States of America* 107.51 (Dec. 2010), pp. 22266–71.

Lynch, G, J Larson, S Kelso, G Barrionuevo, and F Schottler (1983). "Intracellular injections of EGTA block induction of hippocampal long-term potentiation." *Nature* 305.5936 (1983), pp. 719–21.

Lynch, M A (2004). "Long-term potentiation and memory." *Physiological reviews* 84.1 (Jan. 2004), pp. 87–136.

Maeda, Akio, Yu-ichi Ozaki, Sudhir Sivakumaran, Tetsuro Akiyama, Hidetoshi Urakubo, Ayako Usami, Miharu Sato, Kozo Kaibuchi, and Shinya Kuroda (2006). "Ca2+ -independent phospholipase A2-dependent sustained Rho-kinase activation exhibits all-or-none response." en. *Genes to cells : devoted to molecular & cellular mechanisms* 11.9 (Sept. 2006), pp. 1071–83.

Maehama, T. (1998). "The Tumor Suppressor, PTEN/MMAC1, Dephosphorylates the Lipid Second Messenger, Phosphatidylinositol 3,4,5-Trisphosphate". *Journal of Biological Chemistry* 273.22 (May 1998), pp. 13375–13378.

Maini, Philip K. (2004). "The Impact of Turing's Work on Pattern Formation in Biology". *Mathematics today* (2004).

Makino, Hiroshi and Roberto Malinow (2009). "AMPA receptor incorporation into synapses during LTP: the role of lateral movement and exocytosis." *Neuron* 64.3 (Nov. 2009), pp. 381–90.

Malenka, R C, J A Kauer, R S Zucker, and R A Nicoll (1988). "Postsynaptic calcium is sufficient for potentiation of hippocampal synaptic transmission." *Science (New York, N.Y.)* 242.4875 (Oct. 1988), pp. 81–4.

Manninen, Tiina, Katri Hituri, Jeanette Hellgren Kotaleski, Kim T Blackwell, and Marja-Leena Linne (2010). "Postsynaptic signal transduction models for long-term potentiation and depression." English. *Frontiers in computational neuroscience* 4 (Jan. 2010), p. 152.

Mansour, Michael, Naveen Nagarajan, Ralf B. Nehring, John D. Clements, and Christian Rosenmund (2001). "Heteromeric AMPA Receptors Assemble with a Preferred Subunit Stoichiometry and Spatial Arrangement". *Neuron* 32.5 (2001), pp. 841–853.

Martin, Marta, Ouafa Benzina, Vivien Szabo, Attila-Gergely Végh, Olivier Lucas, Thierry Cloitre, Frédérique Scamps, and Csilla Gergely (2013). "Morphology and nanomechanics of sensory neurons growth cones following peripheral nerve injury." *PloS one* 8.2 (Jan. 2013), e56286.

Mastro, Andrea M, Michael A Babich, William D Taylor, and Alec D Keith (1984). "Diffusion of a small molecule in the cytoplasm of mammalian cells". 81.June (1984), pp. 3414–3418.

Materi, Wayne and David S Wishart (2007). "Computational systems biology in cancer: modeling methods and applications." *Gene regulation and systems biology* 1 (Jan. 2007), pp. 91–110.

Matsuda, Naoto, Hui Lu, Yuko Fukata, Jun Noritake, Hongfeng Gao, Sujay Mukherjee, Tomomi Nemoto, Masaki Fukata, and Mu-Ming Poo (2009). "Differential activity-dependent secretion of brain-derived neurotrophic factor from axon and dendrite." *The Journal of neuroscience : the official journal of the Society for Neuroscience* 29.45 (Nov. 2009), pp. 14185–98.

Matsuzaki, M, G C Ellis-Davies, T Nemoto, Y Miyashita, M Iino, and H Kasai (2001). "Dendritic spine geometry is critical for AMPA receptor expression in hippocampal CA1 pyramidal neurons." *Nature neuroscience* 4.11 (Nov. 2001), pp. 1086–92.

Matsuzaki, Masanori, Naoki Honkura, Graham C R Ellis-Davies, and Haruo Kasai (2004). "Structural basis of long-term potentiation in single dendritic spines." *Nature* 429.6993 (June 2004), pp. 761–6.

Mattioni, Michele and Nicolas Le Novère (2013). "Integration of biochemical and electrical signaling-multiscale model of the medium spiny neuron of the striatum." *PloS one* 8.7 (Jan. 2013). Ed. by Huibert D. Mansvelder, e66811.

Maurer, Muriel C., Julianne J. Sando, and Charles M. Grisham (1992). "High-affinity calcium and substrate-binding sites on protein kinase C .alpha. as determined by nuclear magnetic resonance spectroscopy". *Biochemistry* 31.33 (Aug. 1992), pp. 7714–7721.

McCloskey, M A and M M Poo (1986). "Rates of membrane-associated reactions: reduction of dimensionality revisited." *J Cell Biol* 102.1 (Jan. 1986), pp. 88–96.

Meier-Schellersheim, Martin, Iain D C Fraser, and Frederick Klauschen (2009). "Multiscale modeling for biologists." *Wiley interdisciplinary reviews. Systems biology and medicine* 1.1 (2009), pp. 4–14.

Melax, S (1998). "A simple, fast, and effective polygon reduction algorithm". *Game Developer Magazine* November (1998), pp. 44 – 49.

Ménager, Céline, Nariko Arimura, Yuko Fukata, and Kozo Kaibuchi (2004). "PIP3 is involved in neuronal polarization and axon formation." *Journal of neurochemistry* 89.1 (Apr. 2004), pp. 109–18.

Middlemas, D S, J Meisenhelder, and T Hunter (1994). "Identification of TrkB autophosphorylation sites and evidence that phospholipase C-gamma 1 is a substrate of the TrkB receptor." *The Journal of biological chemistry* 269.7 (Feb. 1994), pp. 5458–66.

Miller, Paul, Anatol M Zhabotinsky, John E Lisman, and Xiao-Jing Wang (2005). "The stability of a stochastic CaMKII switch: dependence on the number of enzyme molecules and protein turnover." *PLoS biology* 3.4 (Apr. 2005), e107.

Minichiello, L, M Korte, D Wolfer, R Kühn, K Unsicker, V Cestari, C Rossi-Arnaud, H P Lipp, T Bonhoeffer, and R Klein (1999). "Essential role for TrkB receptors in hippocampus-mediated learning." *Neuron* 24.2 (Oct. 1999), pp. 401–14.

Minichiello, Liliana (2009). "TrkB signalling pathways in LTP and learning." *Nature reviews. Neuroscience* 10.12 (Dec. 2009), pp. 850–60.

Moraru, I I, J C Schaff, B M Slepchenko, M L Blinov, F Morgan, A Lakshminarayana, F Gao, Y Li, and L M Loew (2008). "Virtual Cell modelling and simulation software environment." *IET systems biology* 2.5 (Sept. 2008), pp. 352–62.

Morton-Firth, C J and D Bray (1998). "Predicting temporal fluctuations in an intracellular signalling pathway." *Journal of theoretical biology* 192.1 (May 1998), pp. 117–28.

Myers, M. P., I. Pass, I. H. Batty, J. Van der Kaay, J. P. Stolarov, B. A. Hemmings, M. H. Wigler, C. P. Downes, and N. K. Tonks (1998). "The lipid phosphatase activity of PTEN is critical for its tumor supressor function". *Proceedings of the National Academy of Sciences* 95.23 (Nov. 1998), pp. 13513–13518.

Nakanishi, H, K A Brewer, and J H Exton (1993). "Activation of the zeta isozyme of protein kinase C by phosphatidylinositol 3,4,5-trisphosphate." *The Journal of biological chemistry* 268.1 (Jan. 1993), pp. 13–6.

Nakata, Hiroko and Shun Nakamura (2007). "Brain-derived neurotrophic factor regulates AMPA receptor trafficking to post-synaptic densities via IP3R and TRPC calcium signaling." *FEBS Lett* 581.10 (May 2007), pp. 2047–2054.

Newpher, Thomas M and Michael D Ehlers (2008). "Glutamate receptor dynamics in dendritic microdomains." *Neuron* 58.4 (May 2008), pp. 472–97.

Nguyen, P V, T Abel, and E R Kandel (1994). "Requirement of a critical period of transcription for induction of a late phase of LTP." *Science (New York, N.Y.)* 265.5175 (Aug. 1994), pp. 1104–7.

Nicholson, Daniel A., Rachel Trana, Yael Katz, William L. Kath, Nelson Spruston, and Yuri Geinisman (2006). "Distance-Dependent Differences in Synapse Number and AMPA Receptor Expression in Hippocampal CA1 Pyramidal Neurons". *Neuron* 50.3 (2006), pp. 431–442.

Niciu, Mark J, Benjamin Kelmendi, and Gerard Sanacora (2012). "Overview of glutamatergic neurotransmission in the nervous system." *Pharmacology, biochemistry, and behavior* 100.4 (Feb. 2012), pp. 656–64.

Nicolau, Dan V, John F Hancock, and Kevin Burrage (2007). "Sources of anomalous diffusion on cell membranes: a Monte Carlo study." *Biophysical journal* 92.6 (Mar. 2007), pp. 1975–87.

Nusser, Z, R Lujan, G Laube, J D Roberts, E Molnar, and P Somogyi (1998). "Cell type and pathway dependence of synaptic AMPA receptor number and variability in the hippocampus." *Neuron* 21.3 (Sept. 1998), pp. 545–59.

Ochs, Michael F (2010). "Knowledge-based data analysis comes of age." *Briefings in bioinformatics* 11.1 (Jan. 2010), pp. 30–9.

Oh, Michael C, Victor A Derkach, Eric S Guire, and Thomas R Soderling (2006). "Extrasynaptic membrane trafficking regulated by GluR1 serine 845 phosphorylation primes AMPA receptors for long-term potentiation." *The Journal of biological chemistry* 281.2 (Jan. 2006), pp. 752–8.

Otmakhov, N, L C Griffith, and J E Lisman (1997). "Postsynaptic inhibitors of calcium/calmodulin-dependent protein kinase type II block induction but not maintenance of pairing-induced long-term potentiation." *The Journal of neuroscience : the official journal of the Society for Neuroscience* 17.14 (July 1997), pp. 5357–65.

Pantazaka, Evangelia and Colin W Taylor (2011). "Differential distribution, clustering, and lateral diffusion of subtypes of the inositol 1,4,5-trisphosphate receptor." *The Journal of biological chemistry* 286.26 (July 2011), pp. 23378–87.

Park, Mikyoung, Jennifer M Salgado, Linnaea Ostroff, Thomas D Helton, Camenzind G Robinson, Kristen M Harris, and Michael D Ehlers (2006). "Plasticity-induced growth of dendritic spines by exocytic trafficking from recycling endosomes." *Neuron* 52.5 (Dec. 2006), pp. 817–30.

Patterson, Michael A, Erzsebet M Szatmari, and Ryohei Yasuda (2010). "AMPA receptors are exocytosed in stimulated spines and adjacent dendrites in a Ras-ERK-dependent manner during long-term potentiation." *Proceedings of the National Academy of Sciences of the United States of America* 107.36 (Sept. 2010), pp. 15951–6.

Paulsson, J, O G Berg, and M Ehrenberg (2000). "Stochastic focusing: fluctuation-enhanced sensitivity of intracellular regulation." *Proceedings of the National Academy of Sciences of the United States of America* 97.13 (June 2000), pp. 7148–53.

Peters, A and I R Kaiserman-Abramof (1970). "The small pyramidal neuron of the rat cerebral cortex. The perikaryon, dendrites and spines." *The American journal of anatomy* 127.4 (Apr. 1970), pp. 321–55.

Petralia, Ronald S., Nathalie Sans, Ya-Xian Wang, and Robert J. Wenthold (2005). "Ontogeny of postsynaptic density proteins at glutamatergic synapses". *Molecular and Cellular Neuroscience* 29.3 (2005), pp. 436–452.

Pevsner, Jonathan (2002). "Leonardo da Vinci's contributions to neuroscience". *Trends in Neurosciences* 25.4 (2002), pp. 217–220.

Price, C J, P Kim, and L A Raymond (1999). "D1 dopamine receptor-induced cyclic AMP-dependent protein kinase phosphorylation and potentiation of striatal glutamate receptors." *Journal of neurochemistry* 73.6 (Dec. 1999), pp. 2441–6.

Prieto, M J, M Castanho, A Coutinho, A Ortiz, F J Aranda, and J C Gómez-Fernández (1994). "Fluorescence study of a derivatized diacylglycerol incorporated in model membranes." *Chemistry and physics of lipids* 69.1 (Jan. 1994), pp. 75–85.

Pruunsild, Priit, Anna Kazantseva, Tamara Aid, Kaia Palm, and Tõnis Timmusk (2007). "Dissecting the human BDNF locus: bidirectional transcription, complex splicing, and multiple promoters." *Genomics* 90.3 (Sept. 2007), pp. 397–406.

Rao, Christopher V, Denise M Wolf, and Adam P Arkin (2002). "Control, exploitation and tolerance of intracellular noise." *Nature* 420.6912 (Nov. 2002), pp. 231–7.

Ren, Si-Qiang, Jing-Zhi Yan, Xiao-Yan Zhang, Yun-Fei Bu, Wei-Wei Pan, Wen Yao, Tian Tian, and Wei Lu (2013). "PKCλ is critical in AMPA receptor phosphorylation and synaptic incorporation during LTP." *The EMBO journal* 32.10 (May 2013), pp. 1365–80.

Resasco, Diana C, Fei Gao, Frank Morgan, Igor L Novak, James C Schaff, and Boris M Slepchenko. "Virtual Cel:l computational tools for modeling in cell biology." *Wiley interdisciplinary reviews. Systems biology and medicine* 4.2 (), pp. 129–40.

Ritter, Petra, Michael Schirner, Anthony R McIntosh, and Viktor K Jirsa (2013). "The virtual brain integrates computational modeling and multimodal neuroimaging." *Brain connectivity* 3.2 (Jan. 2013), pp. 121–45.

Roche, Katherine W, Richard J O'Brien, Andrew L Mammen, Jeffrey Bernhardt, and Richard L Huganir (1996). "Characterization of Multiple Phosphorylation Sites on the AMPA Receptor GluR1 Subunit". *Neuron* 16.6 (1996), pp. 1179–1188.

Rosenmund, C. (1998). "The Tetrameric Structure of a Glutamate Receptor Channel". *Science* 280.5369 (June 1998), pp. 1596–1599.

Round, June L, Tamar Tomassian, Min Zhang, Viresh Patel, Stephen P Schoenberger, and M Carrie Miceli (2005). "Dlgh1 coordinates actin polymerization, synaptic T cell receptor and lipid raft aggregation, and effector function in T cells." *The Journal of experimental medicine* 201.3 (Feb. 2005), pp. 419–30.

Saarelainen, Tommi, Jouko A. Lukkarinen, Susanna Koponen, Olli H.J. Gröhn, Jukka Jolkkonen, Eija Koponen, Annakaisa Haapasalo, Leena Alhonen, Garry Wong, Jari Koistinaho, Risto A. Kauppinen, and Eero Castrén (2000). "Transgenic Mice Overexpressing Truncated trkB Neurotrophin Receptors in Neurons Show Increased Susceptibility to Cortical Injury after Focal Cerebral Ischemia". *Molecular and Cellular Neuroscience* 16.2 (2000), pp. 87–96.

Sanhueza, Magdalena, Charmian C McIntyre, and John E Lisman (2007). "Reversal of synaptic memory by Ca2+/calmodulin-dependent protein kinase II inhibitor." *The Journal of neuroscience : the official journal of the Society for Neuroscience* 27.19 (May 2007), pp. 5190–9.

Sanna, Pietro Paolo, Maurizio Cammalleri, Fulvia Berton, Cindy Simpson, Robert Lutjens, Floyd E Bloom, and Walter Francesconi (2002). "Phosphatidylinositol 3-kinase is required for the expression but not for the induction or the maintenance of long-term potentiation in the hippocampal CA1 region." *The Journal of neuroscience : the official journal of the Society for Neuroscience* 22.9 (May 2002), pp. 3359–65.

Sayer, R J, M J Friedlander, and S J Redman (1990). "The time course and amplitude of EPSPs evoked at synapses between pairs of CA3/CA1 neurons in the hippocampal slice." *The Journal of neuroscience : the official journal of the Society for Neuroscience* 10.3 (Mar. 1990), pp. 826–36.

Schaff, James C., Anu Lakshminarayana, and Lucian P. Smith (2013). *SBML Level 3 Package Specification - Spatial Processes*. 2013.

Schmidt, Hartmut and Jens Eilers (2009). "Spine neck geometry determines spino-dendritic cross-talk in the presence of mobile endogenous calcium binding proteins." *Journal of computational neuroscience* 27.2 (Oct. 2009), pp. 229–43.

Schomburg, Ida, Antje Chang, Oliver Hofmann, Christian Ebeling, Frank Ehrentreich, and Dietmar Schomburg (2002). "BRENDA: a resource for enzyme data and metabolic information." *Trends in biochemical sciences* 27.1 (Jan. 2002), pp. 54–6.

Selbie, L A, C Schmitz-Peiffer, Y Sheng, and T J Biden (1993). "Molecular cloning and characterization of PKC iota, an atypical isoform of protein kinase C derived from insulin-secreting cells." *The Journal of biological chemistry* 268.32 (Nov. 1993), pp. 24296–302.

Shahrezaei, Vahid and Peter S Swain (2008). "The stochastic nature of biochemical networks." *Current opinion in biotechnology* 19.4 (Aug. 2008), pp. 369–74.

Shaw, Andrey S and Erin L Filbert (2009). "Scaffold proteins and immune-cell signalling." *Nature reviews. Immunology* 9.1 (Jan. 2009), pp. 47–56.

Shaywitz, A J and M E Greenberg (1999). "CREB: a stimulus-induced transcription factor activated by a diverse array of extracellular signals." *Annual review of biochemistry* 68 (Jan. 1999), pp. 821–61.

Sherrington, Charles Scott (1906). *The integrative action of the nervous system*. 1906.

Shi, Song-Hai, Yasunori Hayashi, José A. Esteban, and Roberto Malinow (2001). "Subunit-Specific Rules Governing AMPA Receptor Trafficking to Synapses in Hippocampal Pyramidal Neurons". *Cell* 105.3 (2001), pp. 331–343.

Shinohara, Yoshiaki (2012). "Quantification of postsynaptic density proteins: glutamate receptor subunits and scaffolding proteins." *Hippocampus* 22.5 (May 2012), pp. 942–53.

Siekevitz, P (1972). *Biological membranes: the dynamics of their organization.* en. Jan. 1972.

Silva, A J, C F Stevens, S Tonegawa, and Y Wang (1992). "Deficient hippocampal long-term potentiation in alpha-calcium-calmodulin kinase II mutant mice." *Science (New York, N.Y.)* 257.5067 (July 1992), pp. 201–6.

Simons, K and E Ikonen (1997). "Functional rafts in cell membranes." *Nature* 387.6633 (June 1997), pp. 569–72.

Simons, Kai and Julio L Sampaio (2011). "Membrane organization and lipid rafts." *Cold Spring Harbor perspectives in biology* 3.10 (Oct. 2011), a004697.

Simons, Kai and Winchil L C Vaz (2004). "Model systems, lipid rafts, and cell membranes." en. *Annual review of biophysics and biomolecular structure* 33 (Jan. 2004), pp. 269–95.

Singer, S J and G L Nicolson (1972). "The fluid mosaic model of the structure of cell membranes." *Science (New York, N.Y.)* 175.4023 (Feb. 1972), pp. 720–31.

Smolen, Paul, Douglas A Baxter, and John H Byrne (2008). "Bistable MAP kinase activity: a plausible mechanism contributing to maintenance of late long-term potentiation." *American journal of physiology. Cell physiology* 294.2 (Mar. 2008), pp. C503–15.

Smoluchowski, M. von (1917). "Versuch einer mathematischen Theorie der Koagulationskinetik". *Zeitschrift fuer physikalische Chemie* 92 (1917).

Sobolevsky, Alexander I, Michael P Rosconi, and Eric Gouaux (2009). "X-ray structure, symmetry and mechanism of an AMPA-subtype glutamate receptor." *Nature* 462.7274 (Dec. 2009), pp. 745–56.

Sommer, Bernd, Martin Köhler, Rolf Sprengel, and Peter H. Seeburg (1991). "RNA editing in brain controls a determinant of ion flow in glutamate-gated channels". *Cell* 67.1 (1991), pp. 11–19.

Sosinsky, Gina E, John Crum, Ying Z Jones, Jason Lanman, Benjamin Smarr, Masako Terada, Maryann E Martone, Thomas J Deerinck, John E Johnson, and Mark H Ellisman (2008). "The combination of chemical fixation procedures with high pressure freezing and freeze substitution preserves highly labile tissue ultrastructure for electron tomography applications." *Journal of structural biology* 161.3 (Mar. 2008), pp. 359–71.

Sossin, Wayne S (2007). "Isoform specificity of protein kinase Cs in synaptic plasticity." *Learning & memory (Cold Spring Harbor, N.Y.)* 14.4 (Apr. 2007), pp. 236–46.

Spacek, J and K M Harris (1997). "Three-dimensional organization of smooth endoplasmic reticulum in hippocampal CA1 dendrites and dendritic spines of the immature and mature rat." *The Journal of neuroscience : the official journal of the Society for Neuroscience* 17.1 (Jan. 1997), pp. 190–203.

Spacek, J and M Hartmann (1983). "Three-dimensional analysis of dendritic spines. I. Quantitative observations related to dendritic spine and synaptic morphology in cerebral and cerebellar cortices." *Anatomy and embryology* 167.2 (Jan. 1983), pp. 289–310.

Squinto, Stephen P., Trevor N. Stitt, Thomas H. Aldrich, Samuel Davis, Stella M. Blanco, Czeslaw RadzieJewski, David J. Glass, Piotr Masiakowski, Mark E. Furth, David M. Valenzuela, Peter S. Distefano, and George D. Yancopoulos (1991). "trkB encodes a functional receptor for brain-derived neurotrophic factor and neurotrophin-3 but not nerve growth factor". *Cell* 65.5 (1991), pp. 885–893.

Stefan, Melanie I, Stuart J Edelstein, and Nicolas Le Novère (2008). "An allosteric model of calmodulin explains differential activation of PP2B and CaMKII." *Proc Natl Acad Sci U S A* 105.31 (Aug. 2008), pp. 10768–10773.

Stephens, L R, K T Hughes, and R F Irvine (1991). "Pathway of phosphatidylinositol(3,4,5)-trisphosphate synthesis in activated neutrophils." *Nature* 351.6321 (May 1991), pp. 33–9.

Stier, A. and E. Sackmann (1973). "Spin labels as enzyme substrates Heterogeneous lipid distribution in liver microsomal membranes". *Biochimica et Biophysica Acta (BBA) - Biomembranes* 311.3 (1973), pp. 400–408.

Stiles, J R, D Van Helden, T M Bartol, E E Salpeter, and M M Salpeter (1996). "Miniature endplate current rise times less than 100 microseconds from improved dual recordings can be modeled with passive acetylcholine diffusion from a synaptic vesicle." *Proceedings of the National Academy of Sciences of the United States of America* 93.12 (June 1996), pp. 5747–52.

Strack, S. (1998). "Autophosphorylation-dependent Targeting of Calcium/ Calmodulin-dependent Protein Kinase II by the NR2B Subunit of the N-Methyl- D-aspartate Receptor". *Journal of Biological Chemistry* 273.33 (Aug. 1998), pp. 20689–20692.

Strand, Andrew D, Zachary C Baquet, Aaron K Aragaki, Peter Holmans, Lichuan Yang, Carine Cleren, M Flint Beal, Lesley Jones, Charles Kooperberg, James M Olson, and Kevin R Jones (2007). "Expression

profiling of Huntington's disease models suggests that brain-derived neurotrophic factor depletion plays a major role in striatal degeneration." *The Journal of neuroscience : the official journal of the Society for Neuroscience* 27.43 (Oct. 2007), pp. 11758–68.

Stroh, Mark, Warren R Zipfel, Rebecca M Williams, Shu Chin Ma, Watt W Webb, and W Mark Saltzman (2004). "Multiphoton microscopy guides neurotrophin modification with poly(ethylene glycol) to enhance interstitial diffusion." *Nature materials* 3.7 (July 2004), pp. 489–94.

Sugiyama, Yoshiko, Izumi Kawabata, Kenji Sobue, and Shigeo Okabe (2005). "Determination of absolute protein numbers in single synapses by a GFP-based calibration technique." *Nature methods* 2.9 (Sept. 2005), pp. 677–84.

Suzuki, Atsushi, Kazunori Akimoto, and Shigeo Ohno (2003). "Protein kinase C lambda/iota (PKClambda/iota): a PKC isotype essential for the development of multicellular organisms." *Journal of biochemistry* 133.1 (Jan. 2003), pp. 9–16.

Svoboda, K, D W Tank, and W Denk (1996). "Direct measurement of coupling between dendritic spines and shafts." *Science (New York, N.Y.)* 272.5262 (May 1996), pp. 716–9.

Szirmai, Imre, György Buzsáki, and Anita Kamondi (2012). "120 years of hippocampal Schaffer collaterals." *Hippocampus* 22.7 (July 2012), pp. 1508–16.

Takasaki, Kevin T, Jun B Ding, and Bernardo L Sabatini (2013). "Live-Cell Superresolution Imaging by Pulsed STED Two-Photon Excitation Microscopy." *Biophysical journal* 104.4 (Feb. 2013), pp. 770–7.

Tao-Cheng, Jung-Hwa, Virginia T Crocker, Christine A Winters, Rita Azzam, John Chludzinski, and Thomas S Reese (2011). "Trafficking of AMPA receptors at plasma membranes of hippocampal neurons." *The Journal of neuroscience : the official journal of the Society for Neuroscience* 31.13 (Mar. 2011), pp. 4834–43.

Tardin, Catherine, Laurent Cognet, Cécile Bats, Brahim Lounis, and Daniel Choquet (2003). "Direct imaging of lateral movements of AMPA receptors inside synapses." en. *The EMBO journal* 22.18 (Sept. 2003), pp. 4656–65.

The UniProt Consortium (2012). "Reorganizing the protein space at the Universal Protein Resource (UniProt)." *Nucleic acids research* 40.Database issue (Jan. 2012), pp. D71–5.

Tolle, Dominic P and Nicolas Le Novère (2010). "Brownian diffusion of AMPA receptors is sufficient to explain fast onset of LTP." *BMC Syst Biol* 4 (2010), p. 25.

Toresson, Hå kan and Seth G N Grant (2005). "Dynamic distribution of endoplasmic reticulum in hippocampal neuron dendritic spines." *The European journal of neuroscience* 22.7 (Oct. 2005), pp. 1793–8.

Triller, Antoine and Daniel Choquet (2003). "Synaptic structure and diffusion dynamics of synaptic receptors." *Biology of the cell / under the auspices of the European Cell Biology Organization* 95.7 (Oct. 2003), pp. 465–76.

Tsui, Jennifer and Robert C Malenka (2006). "Substrate localization creates specificity in calcium/calmodulin-dependent protein kinase II signaling at synapses." *The Journal of biological chemistry* 281.19 (May 2006), pp. 13794–804.

Turing, A. M. (1952). "The Chemical Basis of Morphogenesis". *Philosophical Transactions of the Royal Society Biological Sciences* 237.641 (Aug. 1952), pp. 37–72.

Van Laere, J (1993). "[Vesalius and the nervous system]." *Verhandelingen - Koninklijke Academie voor Geneeskunde van België* 55.6 (Jan. 1993), pp. 533–76.

Vaz, W L and P F Almeida (1991). "Microscopic versus macroscopic diffusion in one-component fluid phase lipid bilayer membranes." *Biophysical journal* 60.6 (Dec. 1991), pp. 1553–4.

Volfovsky, N, H Parnas, M Segal, and E Korkotian (1999). "Geometry of dendritic spines affects calcium dynamics in hippocampal neurons: theory and experiments." *Journal of neurophysiology* 82.1 (July 1999), pp. 450–62.

Volterra, Vito (1927). *Variazioni e fluttuazioni del numero d'individui in specie animali conviventi*. 1927.

Wang, Jie and David A Richards (2012). "Segregation of PIP2 and PIP3 into distinct nanoscale regions within the plasma membrane." en. *Biology open* 1.9 (Sept. 2012), pp. 857–62.

Watanabe, M, Y Inoue, K Sakimura, and M Mishina (1992). "Developmental changes in distribution of NMDA receptor channel subunit mRNAs." *Neuroreport* 3.12 (Dec. 1992), pp. 1138–40.

Watanabe, M, M Mishina, and Y Inoue (1994). "Distinct spatiotemporal expressions of five NMDA receptor channel subunit mRNAs in the cerebellum." *The Journal of comparative neurology* 343.4 (May 1994), pp. 513–9.

Westerhoff, Hans V and Bernhard O Palsson (2004). "The evolution of molecular biology into systems biology." *Nature biotechnology* 22.10 (Oct. 2004), pp. 1249–52.

Whitlock, Jonathan R, Arnold J Heynen, Marshall G Shuler, and Mark F Bear (2006). "Learning induces long-term potentiation in the

hippocampus." *Science (New York, N.Y.)* 313.5790 (Aug. 2006), pp. 1093–7.

Whitman, M, C P Downes, M Keeler, T Keller, and L Cantley (1988). "Type I phosphatidylinositol kinase makes a novel inositol phospholipid, phosphatidylinositol-3-phosphate." *Nature* 332.6165 (Apr. 1988), pp. 644–6.

Widmer, H R, D R Kaplan, S J Rabin, K D Beck, F Hefti, and B Knüsel (1993). "Rapid phosphorylation of phospholipase C gamma 1 by brain-derived neurotrophic factor and neurotrophin-3 in cultures of embryonic rat cortical neurons." *Journal of neurochemistry* 60.6 (June 1993), pp. 2111–23.

Wils, Stefan and Erik De Schutter (2009). "STEPS: Modeling and Simulating Complex Reaction-Diffusion Systems with Python." *Frontiers in neuroinformatics* 3 (Jan. 2009), p. 15.

Wilson, C J and J C Linder (1983). "THREE-DIMENSIONAL RAT NEOSTRIATUM âĂŹ STRUCTURE OF DENDRITIC SPINES". (1983), pp. 383–398.

Windisch, J M, R Marksteiner, M E Lang, B Auer, and R Schneider (1995). "Brain-derived neurotrophic factor, neurotrophin-3, and neurotrophin-4 bind to a single leucine-rich motif of TrkB." *Biochemistry* 34.35 (Sept. 1995), pp. 11256–63.

Wolf, Denise M, Vijay V Vazirani, and Adam P Arkin (2005). "Diversity in times of adversity: probabilistic strategies in microbial survival games." *Journal of theoretical biology* 234.2 (May 2005), pp. 227–53.

Wooten, M W, M L Seibenhener, K B Neidigh, and M L Vandenplas (2000). "Mapping of atypical protein kinase C within the nerve growth factor signaling cascade: relationship to differentiation and survival of PC12 cells." *Molecular and cellular biology* 20.13 (July 2000), pp. 4494–504.

World Health Organization (2007). *Neurological Disorders: Public Health Challenges*. Geneva, Switzerland: WHO Press, 2007.

Xu, Chang, James Watras, and Leslie M Loew (2003). "Kinetic analysis of receptor-activated phosphoinositide turnover." *The Journal of cell biology* 161.4 (May 2003), pp. 779–91.

Yang, Ying and Nicole Calakos (2013). "Presynaptic long-term plasticity." *Frontiers in synaptic neuroscience* 5 (Jan. 2013), p. 8.

Yeo, Giles S H, Chiao-Chien Connie Hung, Justin Rochford, Julia Keogh, Juliette Gray, Shoba Sivaramakrishnan, Stephen O'Rahilly, and I Sadaf Farooqi (2004). "A de novo mutation affecting human TrkB associated with severe obesity and developmental delay." *Nature neuroscience* 7.11 (Nov. 2004), pp. 1187–9.

Yong, Choong, Hu Li, Xiao Hua, Jia Jia, and Bao Wen (2008). "Simulation of the regulation of EGFR endocytosis and EGFR-ERK signaling by endophilin-mediated RhoA-EGFR crosstalk". 582 (2008), pp. 2283–2290.

Young, M E, P A Carroad, and R L Bell (1980). "Estimation of diffusion coefficients of proteins". *Biotechnology and Bioengineering* 22 (1980), pp. 947–955.

Zador, A, C Koch, and T H Brown (1990). "Biophysical model of a Hebbian synapse." *Proceedings of the National Academy of Sciences of the United States of America* 87.17 (Sept. 1990), pp. 6718–22.

Zhang, Yan-Ping, Niklaus Holbro, and Thomas G Oertner (2008). "Optical induction of plasticity at single synapses reveals input-specific accumulation of alphaCaMKII." *Proceedings of the National Academy of Sciences of the United States of America* 105.33 (Aug. 2008), pp. 12039–44.

Zhou, Huan-Xiang, Germán Rivas, and Allen P Minton (2008). "Macromolecular crowding and confinement: biochemical, biophysical, and potential physiological consequences." *Annual review of biophysics* 37 (Jan. 2008), pp. 375–97.

Zhou, Xin-Fu, Luis F. Parada, Dan Soppet, and Robert A. Rush (1993). "Distribution of trkB tyrosine kinase immunoreactivity in the rat central nervous system". *Brain Research* 622.1 (1993), pp. 63–70.

Zuber, Benoît, Irina Nikonenko, Paul Klauser, Dominique Muller, and Jacques Dubochet (2005). "The mammalian central nervous synaptic cleft contains a high density of periodically organized complexes." *Proceedings of the National Academy of Sciences of the United States of America* 102.52 (Dec. 2005), pp. 19192–7.

Zucker, Robert S and Wade G Regehr (2002). *Short-term synaptic plasticity.* en. Jan. 2002.